NATIONAL AERONAUTICS AND SPACE ADMINISTRATION

MSC APOLLO 13 INVESTIGATION TEAM

PANEL 1

SPACECRAFT INCIDENT INVESTIGATION

VOLUME I

ANOMALY INVESTIGATION

JUNE 1970

MANNED SPACECRAFT CENTER
HOUSTON, TEXAS

MSC APOLLO 13 INVESTIGATION TEAM

FINAL REPORT

PANEL 1

SPACECRAFT INCIDENT INVESTIGATION

June 10, 1970

VOLUME I

ANOMALY INVESTIGATION

Donald D. Arabian
Chairman, Panel 1

CONTENTS

1.0 SUMMARY

There were two investigative aspects associated with the loss of the cryogenic oxygen tank pressure during the Apollo 13 flight. First, what was the cause of the flight failure of cryogenic oxygen tank 2. Second, what possible contributing factors during the ground history of the tank could have led to the ultimate failure in flight.

The first flight indication of a problem occurred when the quantity measurement in the tank went full scale about 9 hours before the incident. This condition in itself could not have contributed to ignition in the tank, since the energy in the circuit is restricted to about 7 millijoules.

Data from the electrical system provided the second indication of a problem when the fans in tank 2 were activated to reduce any stratification which might have been present in the supercritical oxygen in the tank. Several short-circuits were detected and have been isolated to the fan circuits of tank 2. The first short-circuit could have contained as much as 160 joules of energy, which is within the current-protection level of the fan circuits. Tests have shown that two orders of magnitude less energy than this is sufficient to ignite the polytetrafluoroethylene insulation on the fan circuits in the tank. Consequently, the evidence indicates that the insulation on the fan wiring was ignited by the energy in the short-circuit.

The burning in the tank then proceeded, causing the tank pressure to rise to a peak value of 1008 psi, about half of the predicted tank burst pressure at cryogenic temperature. At that time the relief valve opened, as expected, and decreased the pressure in the tank. The burning had progressed to the point by this time that all energized electrical circuits to tank 2 had shorted and opened.

The next indication of a problem occurred when accelerometer traces in the command module showed vibration excitation with the largest amplitude along the longitudinal axis. This was apparently at the time that the integrity of tank 2 was lost and the vacuum dome relief plug blew out. The loss of tank pressure is concluded to have been caused by the failure of the electrical conduit tube when the fire progressed into the conduit. Tests under simulated conditions support this point of view. The only place the wiring comes close to, or touches, the pressure vessel is in the electrical conduit tubing at the top of the tank. To fail the tank at any location other than the electrical conduit, without burning metal inside, does not appear reasonable, particularly if only insulation is burning in zero g.

Following the rupture of the conduit tubing, the tank 2 pressure remained above 880 psi to the point of data loss. If the tank pressure had decreased below 880 psi, the heaters would have come on automatically at that time. The heater circuits were energized during the data loss period. Consequently, the evidence supports the theory of a small opening in the tank venting into the bay which housed the cryogenic tanks. A fraction of a second after the conduit failed, the pressure immediately increased in the bay and blew the panel off. Thermal measurements show significant heating was present just before the panel separated which indicated there must have been an area burning exterior to the pressure vessel. A ruptured tank that was dumping cold fluid would have caused a chilling of the temperature sensors. The data indicate that tank 2 remained in the bay and photoanalysts using sophisticated methods, believe the photographs reveal that at least part of tank 2 remained intact.

Many aftereffects resulted from the loss of tank 2 pressure integrity. Most significant were the eventual loss of tank 1 pressure and the loss of electrical power from two of the three fuel cells when the shock of the panel separating caused the oxygen supply valves to close. More important, however, was the fact that the condition was undetected since a warning is given to the crew only when both hydrogen and oxygen valves to a fuel cell are closed. Oxygen system 1 developed a leak either as the result of shock when the panel separated, or from the dynamics of the particular events associated with the failure of tank 2 electrical conduit.

The cryogenic oxygen tank 2 could not be off loaded after the initial filling during the countdown demonstration test. The problem resulted from loose or misaligned plumbing components of the dog-leg portion of the tank fill path. Allowable manufacturing tolerances are such that the tank may not be detanked normally. A test has verified this fact. The condition of loose plumbing in the probe assembly, which existed in the tank before the detanking, was judged to be safe for flight in every aspect.

The inability to perform a normal detanking operation during the countdown demonstration test led to the use of a special detanking procedure. The special detanking procedures failed the tank heater thermal switches to the closed position. An incompatibility between the voltage output of ground power supply used for the heaters and the thermal switch capacity resulted in fusing the contacts when operating in this mode for the first time. This resulted in continuous heater-on times in excess of 8 hours, which went undetected prior to flight. This condition overheated the insulation, causing major electrical wire insulation degradation (splits and cracks). Several mechanisms could have moved the fan wiring and caused the shorted conditions which triggered the fire within the tank and finally caused the loss of all service module oxygen.

2.0 INTRODUCTION

The main substance of the investigation of the cryogenic oxygen tank 2 anomaly is contained in this report. Additional information concerning the tank 2 manufacturing and checkout history, the details of the analyses, and the results of the special tests conducted in support of the investigation will be forwarded under separate cover.

PRECEDING PAGE BLANK NOT FILMED

3.0 PERTINENT DATA

The significant system parameters for the period of interest are shown in figure 3-1. Bay 4 of the service module and the hardware mounted in this area are shown in figure 3-2.

Approximately 9 hours prior to the period of interest, the quantity gage in cryogenic oxygen tank 2 failed to full scale during a fan cycle.

At 55:53:20, the electrical fan circuits for cryogenic oxygen tank 2 were energized. Approximately 2 seconds later, a momentary short was indicated in the current from fuel cell 3. Within several seconds, two other momentary shorted conditions occurred.

The cryogenic oxygen tank 2 pressure increased from 880 to 1008 psi in approximately 90 seconds with a plateau at 40 seconds. The pressure then decreased to 995 psi in about 9 seconds. The fuel cell flow rates responded to the pressure profile.

The temperature in the tank rose rapidly during the final 25 seconds of the pressure rise, then the measurement failed. The quantity gage, which had previously failed, corrected itself and then failed again.

The command module accelerometers responded to a vibration disturbance about 420 milliseconds after the last pressure reading and to an impulse about 340 milliseconds later. Approximately 40 milliseconds later, all data from the spacecraft were lost for about 1.8 seconds. Following recovery of the data, the spacecraft had experienced a translation change of 0.4 ft/sec primarily in a plane normal to the cryogenic oxygen tank bay. Cryogenic oxygen tank 2 pressure read zero. The cryogenic oxygen tank 1 pressure was decaying rapidly, and its heaters were on. A main bus B undervoltage alarm and a computer restart were present. Several structural temperatures in bays 3 and 4 were reading up to 8° F higher than before the data loss.

The crew reported that they had heard and felt a sharp "bang," coincident with a computer restart and a master alarm associated with a main bus B undervoltage condition. Within 20 seconds, a quick check of the electrical parameters was made by the crew and all parameters appeared normal. However, the crew did report the following barberpole indications:

a. Service module reaction control system helium 1 on quads B and D

b. Service module reaction control system helium 2 on quad D

c. Service module reaction control system secondary propellant valves on quads A and C.

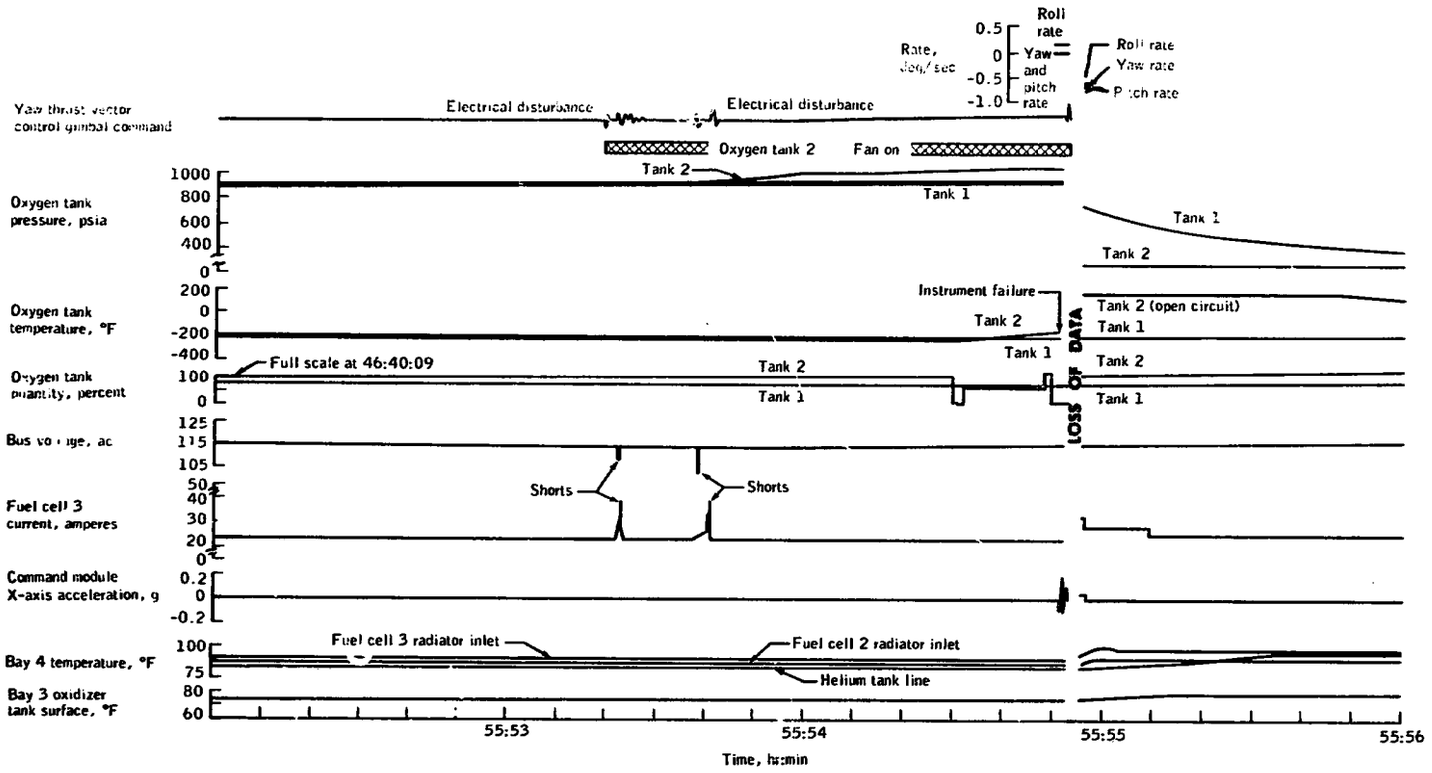

Figure 3-1.- Significant event timeline.

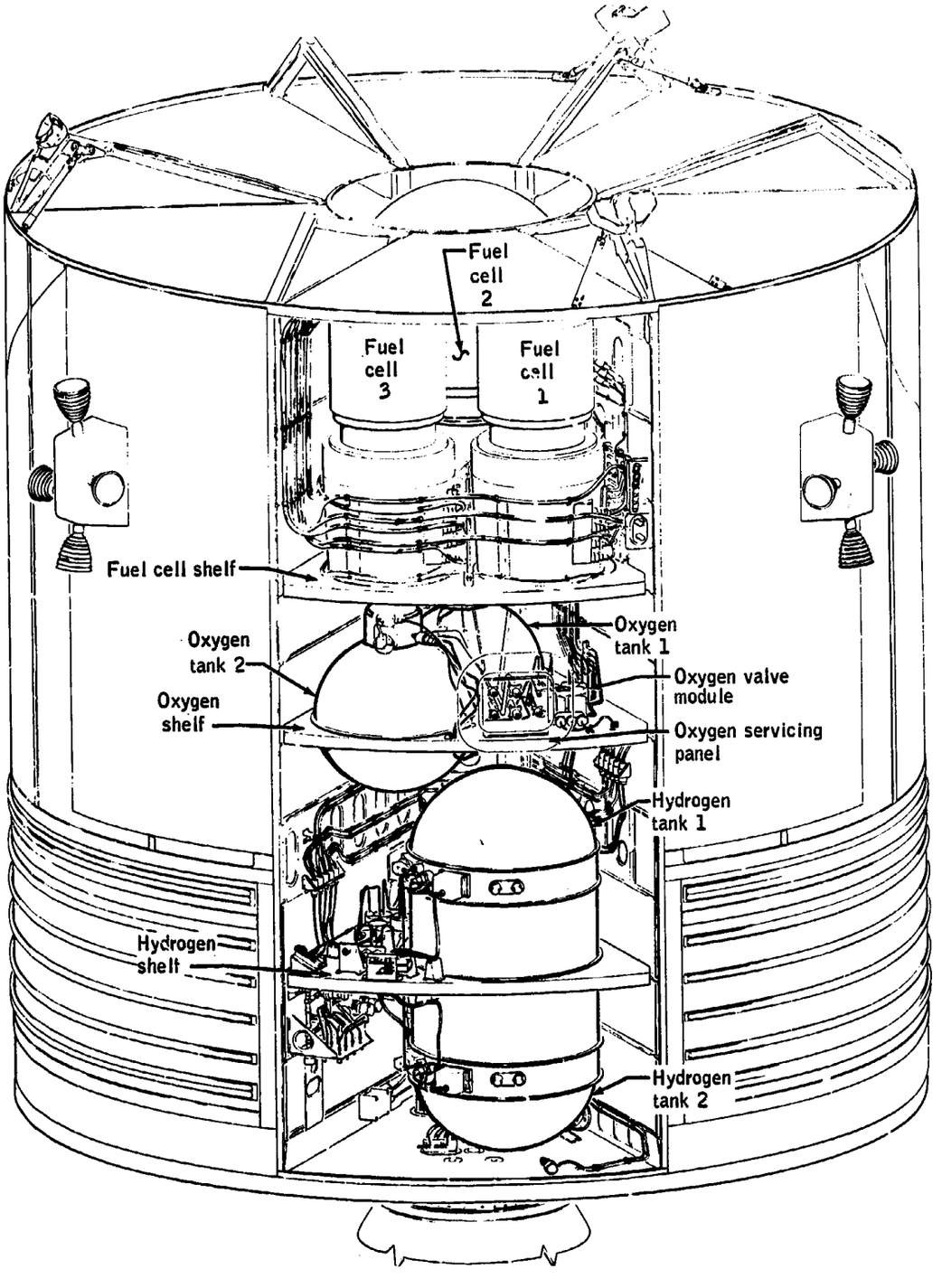

Figure 3-2.- Arrangement of fuel cells and cryogenic systems in bay 4.

About 2-1/2 minutes later, fuel cells 1 and 3 ceased generating electrical power. About 2 hours later, fuel cell 2 was turned off as a result of the pressure loss in cryogenic oxygen tank 1.

Photographs taken after service module separation showed that the bay 4 panel was missing and that one high-gain antenna horn was damaged.

4.0 DATA ANALYSIS

This section analyzes the significant events relative to the incident involving cryogenic oxygen tank 2 and identified in section 3.0.

4.1 QUANTITY GAGE

The first anomalous inflight condition associated with the cryogenic oxygen tank 2 occurred at 46:40:06 when the ac-powered destratification fans in both cryogenic oxygen tanks were turned on. Within about 3 seconds after fan activation, the quantity measurement for cryogenic oxygen tank 2 abruptly indicated full-scale high. This system indicates density of the cryogenic oxygen by measuring its dielectric constant, which is a function of density. This instrument is a capacitor which consists of two concentric aluminum tubes inside the tank (fig. 4-1).

Tests have shown that an open-circuit in the leads to the capacitor assembly or a short across the capacitor or its leads will drive the output to full scale. If this short-circuit is removed, the output signal drops abruptly from full scale to zero, and then in about a second, it settles out to the proper reading, as noted in the data of figure 4-2. This agrees with the flight data from the quantity probe. Tests also show that if the inner tube is shorted to ground, the output may oscillate in a random manner. Such an oscillation was noted several minutes after data recovery following the incident. It should be noted that with a short-circuit in the quantity gaging system inside the tank, the maximum current that could be drawn is 15 milliamperes.

4.2 ELECTRICAL SHORTS

The configuration of the electrical power system at the time of the incident is shown in figure 4-3, and the configuration of the electrical power to the cryogenic oxygen tanks is shown in figure 4-4. As shown in figure 4-5, three separate shorting events occurred following application of power to the fan circuits in cryogenic oxygen tank 2.

The ac bus 1 voltage dropped 1.2 volts and the dc current increased 1.6 amperes when the cryogenic oxygen tank 1 fans were turned on (fig. 4-5).

About 1.5 seconds later, when the cryogenic oxygen tank 2 fans were energized, the ac bus 2 voltage dropped 0.6 volt and the spacecraft current increased 1.6 amperes. The thrust vector control gimbal command

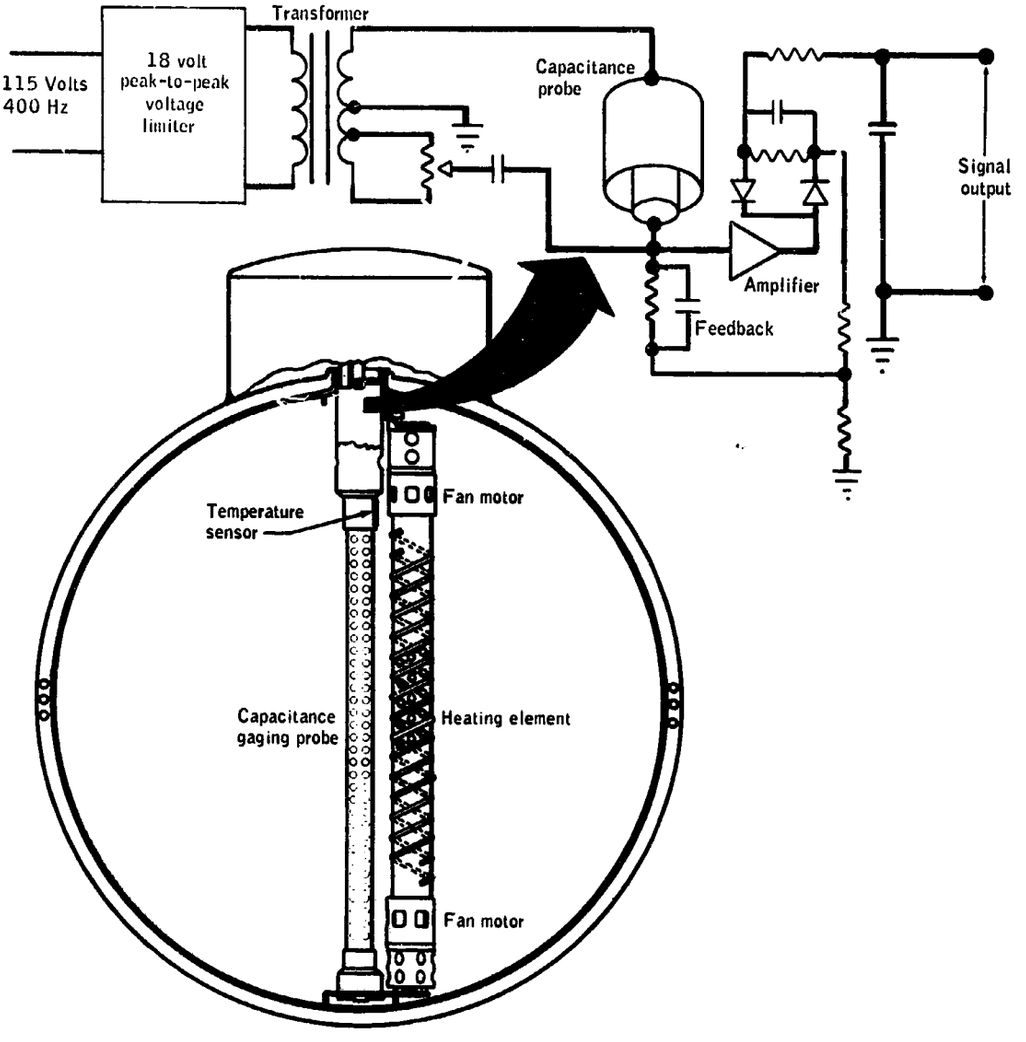

Figure 4-1.- Quantity gage.

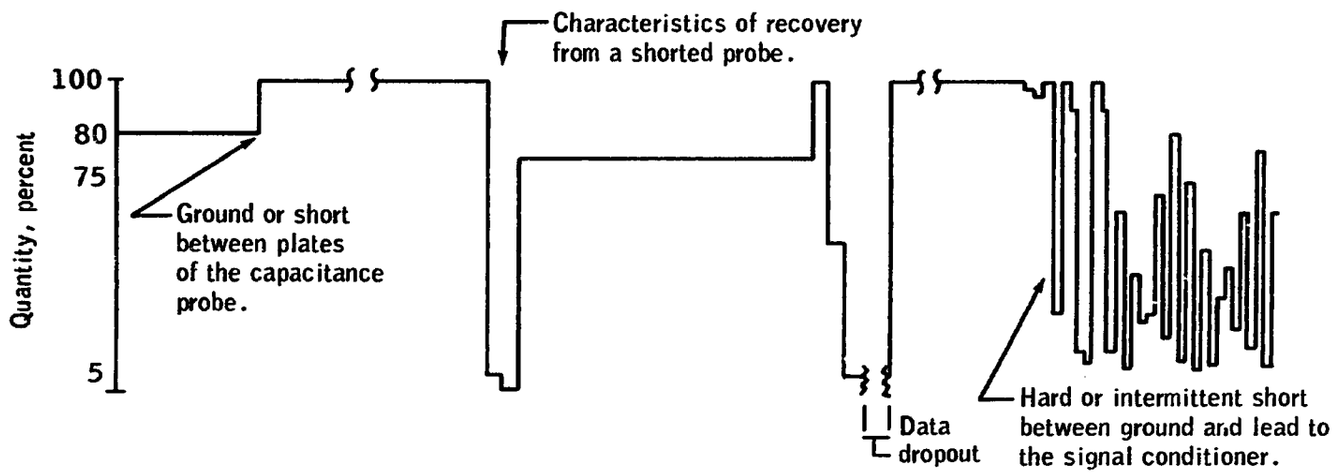

Figure 4-2.- Correlation of cryogenic oxygen tank 2 quantity flight data with measurement failure modes.

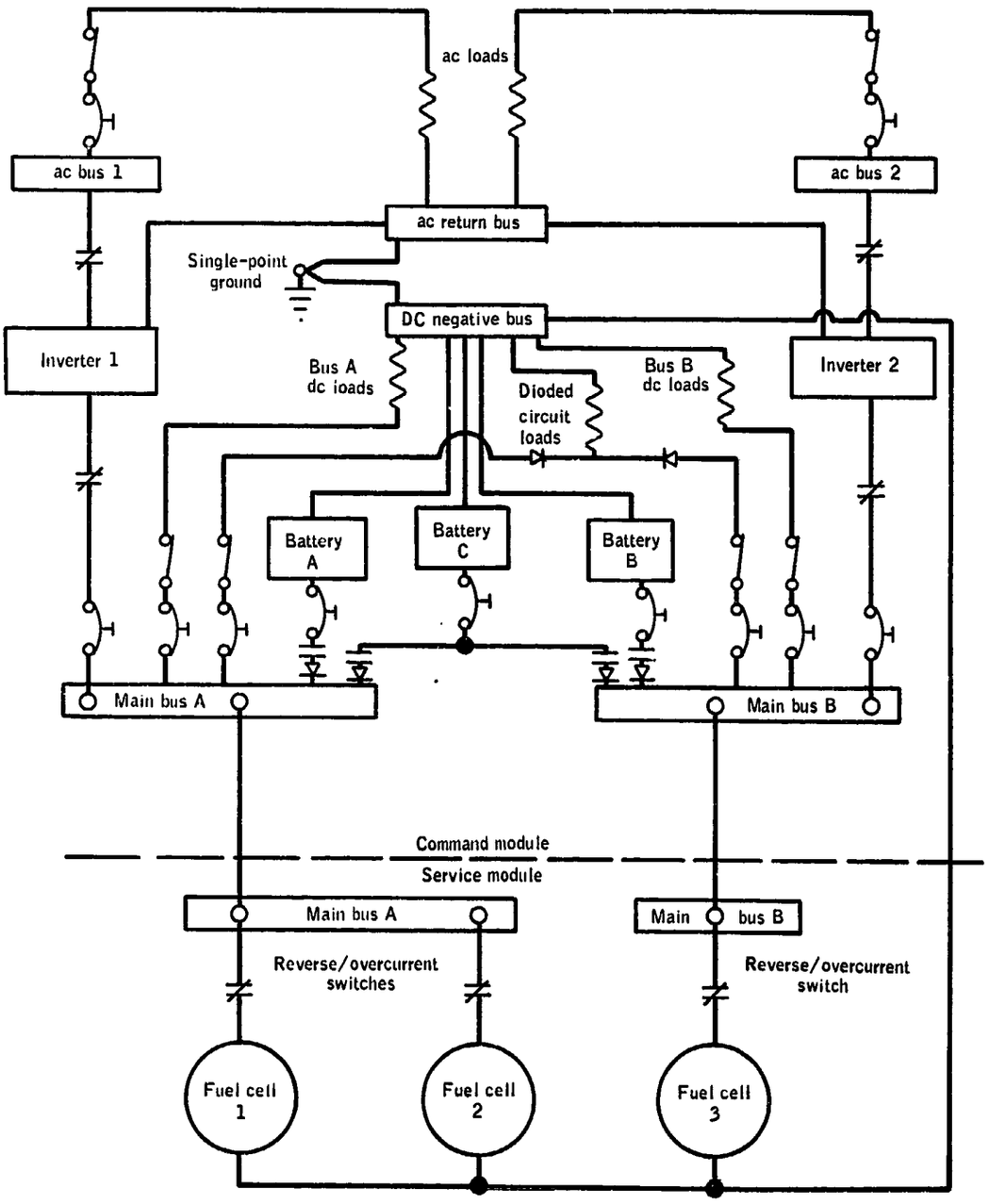

Figure 4-3.- Electrical power system schematic.

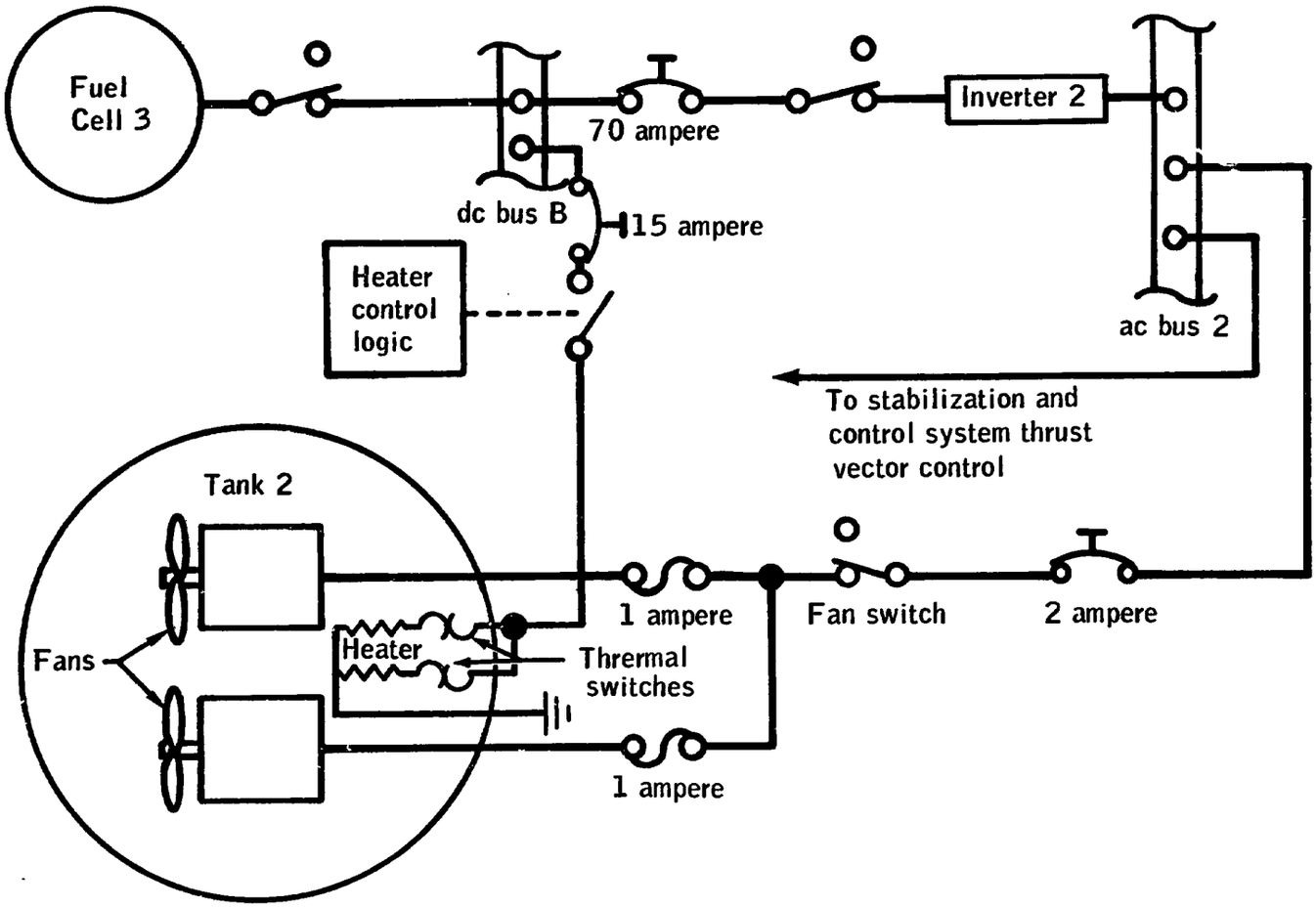

Figure 4-4.- Cryogenic oxygen tank 2 electrical configuration.

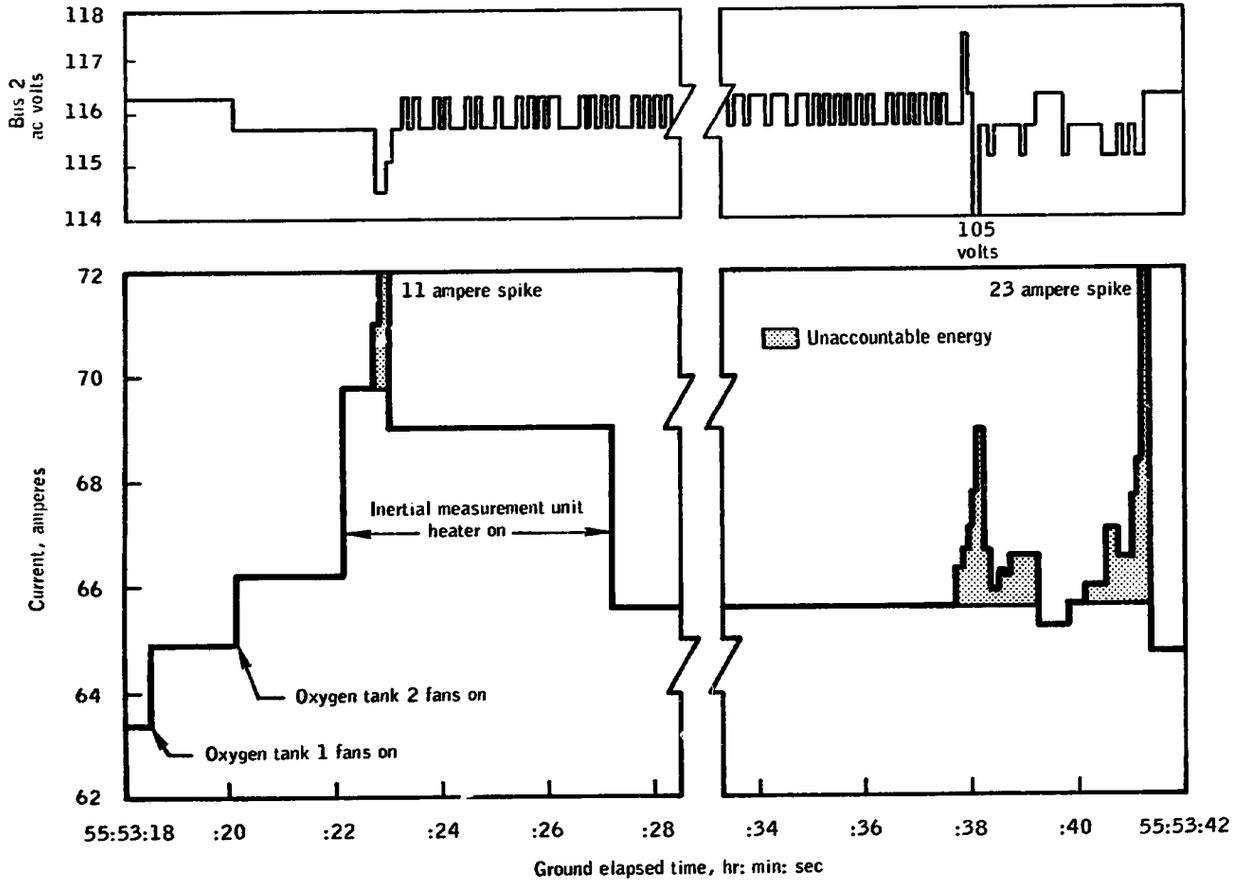

Figure 4-5.- Spacecraft current and ac voltage during period of interest.

data from the stabilization and control system indicated a corresponding voltage transient. Testing on the stabilization and control system has shown that a low voltage transient on ac bus 2 results in a transient on the gimbal command data. The ac bus 2 voltage decrease and the spacecraft current increase show that power was applied to the cryogenic oxygen tank 2 fans (fig. 4-5) but does not indicate whether the fan motors were running, since the stall and running currents are essentially the same.

The ac voltage decrease and the spacecraft current increase for the fans in each tank were normal and agree with data from previous cryogenic oxygen tank fan cycles. Also, the transient on the stabilization and control system data appeared during previous tank fans cycles.

The first indication of a short on ac bus 2 appeared about 2-1/2 seconds after activation of the cryogenic oxygen tank 2 fans. The ac bus 2 voltage dropped 1.2 volts, the fuel cell 3 current increased 11 amperes (fig. 4-5), and the stabilization and control system gimbal command data experienced a transient. Subsequent to the short, the spacecraft current data show a decrease of 0.8 ampere from the level just prior to the short. Also, the ac bus 2 voltage started to toggle-up 0.6 volt, or one data bit (fig. 4-5). These data indicate that a load was removed from ac bus 2 and that it was approximately one-half the load normally applied when the cryogenic oxygen tank 2 fans were turned on. This indicates that a short in one of the two fan motor circuits in cryogenic oxygen tank 2 caused its fuses to blow.

The second indication of shorting occurred about 15 seconds later when phase A of ac bus 2 voltage increased 1.8 volts. Since the inverter attempts to maintain a constant average 3-phase voltage, this increase in phase A indicates a decrease on phase B or C of the ac bus 2 caused by an increased load.

Approximately 200 milliseconds later, the ac bus 2 voltage momentarily decreased 11 volts (fig. 4-5), and the total spacecraft current increased 3.5 amperes, indicating an increased load. After the momentary decrease, the ac bus 2 voltage reading was 0.6 volt less than the previous indication. This could be an indication that a single phase short on phase B or C was removed by blowing a fuse.

About 20 seconds after the first short, the third ac bus 2 short occurred. Fuel cell 3 current increased 23 amperes, and the stabilization and control system data again indicated a transient (fig. 3-1). Subsequently, the total spacecraft current level decreased to the same level as it was prior to turning on the cryogenic oxygen tank 2 fans. This indicates that power to the remaining cryogenic oxygen tank 2 fan was removed by blowing its fuses due to this short. Also, the ac bus 2 voltage increased to the same level as that prior to turning the tank 2 fans on (fig. 4-5).

The electrical energy that could not be accounted for by normal spacecraft loads (fig. 4-5) is attributed to the shorts. Calculations were made of the maximum energy levels that could have been transmitted through the circuit during these shorted conditions and that would still meet the constraints imposed by the flight data resolution and sampling times, inverter performance, fuse clearing time, and dc and ac bus voltage sensor performance. Inverter performance and fuse clearing time tests were performed to provide data for the energy calculations. The energy calculations are summarized in table 4-I.

The spacecraft current data show that the heaters were not on prior to the data loss. The heaters were set for automatic operation and the cryogenic oxygen tank 2 pressure switch was open, thereby preventing application of power to the heaters in either tank. In the automatic mode, the heaters in both tanks are energized simultaneously when the pressure switches for tanks 1 and 2 are closed (fig. 4-6). When data were reacquired after the incident, the spacecraft current indicated that heaters in one of the cryogenic oxygen tanks had automatically been energized. For this to occur, the cryogenic oxygen tank 2 pressure must have dropped below the switch actuation point during the data loss. The tank 1 pressure was already below the switch actuation point. The cryogenic oxygen tank 1 heaters came on because they were the only operative heaters when manually actuated later. The heaters use the same power circuitry to the tanks during manual and automatic operation.

At about the time of the shock to the spacecraft, a master alarm and a main bus B undervoltage light were noted coincident with a computer restart. The voltage must decrease to below about 18 volts for at least 15 microseconds before a computer restart will occur. This event would indicate a hard short on both main buses because the computer receives its power, through diodes, from both buses. An undervoltage light on main bus B only would be most probable because only one fuel cell supplies its power, while bus A power is supplied by two fuel cells. The main bus voltage must be below 26 volts for longer than 70 milliseconds for an undervoltage indication to occur. The most likely cause of such a low voltage for that length of time is a short on the wiring to the tank pressure switches that control the heaters (fig. 4-6), resulting from the cryogenic oxygen tank failure. This circuit receives power from both buses through 10-ampere fuses located in the service module. The short must have occurred after closure of the pressure switches which provide power to drive the motor switch, since the motor switch must close in order to apply power to the tank heaters in the automatic heater control mode. Cryogenic oxygen tank 2 heaters did not come on because the circuits were open.

TABLE 4-I.- DELTA ENERGY CALCULATIONS

AC current, amperes	AC level, volts	Watts	DC amperes	Time constraints	Total fault energy joules
Single phase short					
0.2	115	23	1	13.6 sec	313
1.5	111	167	9	(2) 200 ms	33
2.0	110	220	12	(2) 200 ms	44
2.5	109	273	14	(2) 200 ms	55
3.0	107	321	17	(1) 120 ms	39
4.0	105	420	23	(1) 31 ms	13
5.0	102	510	28	(1) 20 ms	10
7.0	95	666	36	(1) 10 ms	7
9.0	75	675	37	(1) 8 ms	5
12.0	4	48	13	(1) 4 ms	0.2
Two phase short					
0.1	115	11.5	1	13.6 sec	313
1.5	111	167	14	(2) 200 ms	67
2.0	110	220	19	(2) 200 ms	88
2.5	109	273	23	(2) 200 ms	109
3.0	107	321	28	(1) 120 ms	77
4.0	104	416	36	(1) 31 ms	26
5.0	101	505	45	(1) 20 ms	20
7.0	80	560	58	(1) 10 ms	11
9.0	45	400	44	(1) 8 ms	6
Three phase short					
0.07	115	7.7	1	13.6 sec	313
1.5	111	167	22	(2) 200 ms	100
2.0	110	220	31	(2) 200 ms	132
2.5	109	273	39	(2) 200 ms	164
3.0	107	321	47	(4) 70 ms	23
4.0	104	416	65	(1) 31 ms	39
5.0	101	505	84	(1) 20 ms	31
7.0	90	630	105	(1) 10 ms	19
9.0	10	90	25	(1) 8 ms	2

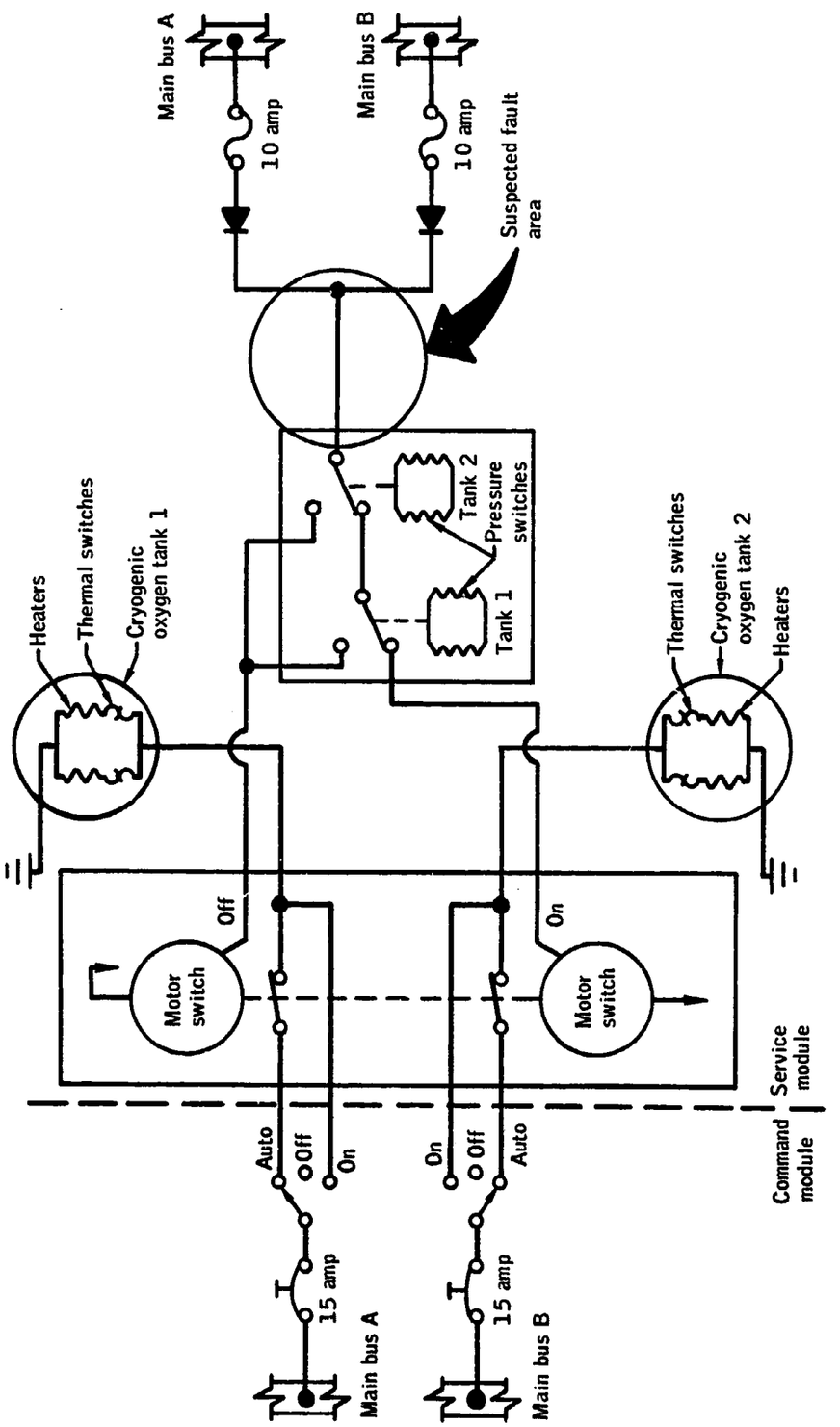

Figure 4-6.- Heater control circuitry

4.3 CRYOGENIC OXYGEN TANK 2 PRESSURE TRANSIENT

The interface of the cryogenic oxygen tank 2 with the oxygen system is shown in figure 4-7.

The internal components of the tank and location of the wiring are shown in figure 4-8. The oxygen temperature is measured from within the tank as shown. Tank pressure is measured external to the tank in the valve module (fig. 4-9) and is sampled once per second. The pressure switch which controls the automatic heater circuits is attached to the valve module.

The electrical data show that power was applied to both fan motors in cryogenic oxygen tank 2. It seems probable that one, and possibly both, fan motors came on, but this cannot be determined conclusively from the pressure data. Further, the electrical data confirm that the oxygen tank heaters were not energized.

The time history of cryogenic oxygen tank 2 pressure variations during the last fan cycle can be divided into three regions (fig. 4-10). The first region is the pressure rise which began just after the fans were turned on and lasted for 40 seconds, when a distinct change in the pressure rise rate occurred.

The second region covers a 45-second time interval from the pressure plateau to the peak pressure of 1008 psia. The third region is characterized by about a 14-psia pressure drop over a 9-second period, after which data were lost. A detailed discussion of the last 800 milliseconds before data loss is presented in section 4.7.

4.3.1 Tank Pressure Data Analysis

Since the pressure transducer is located in a flow line and not on the tank itself, an investigation was conducted to insure that the pressure data are, in fact, a valid indication of pressure in the oxygen tank.

Tests on the sensor in the system show that the sensor will respond from zero to full scale in 5 milliseconds to a step input. The system, including the plumbing, has a response of less than 30 milliseconds.

The transducer is located in the valve module (fig. 4-9), along with the relief valve, and is about 20 feet of line length from the tank cavity (fig. 4-7). The pressure measurement has been verified as representative of the actual pressure in the tank in two tests under dynamic conditions

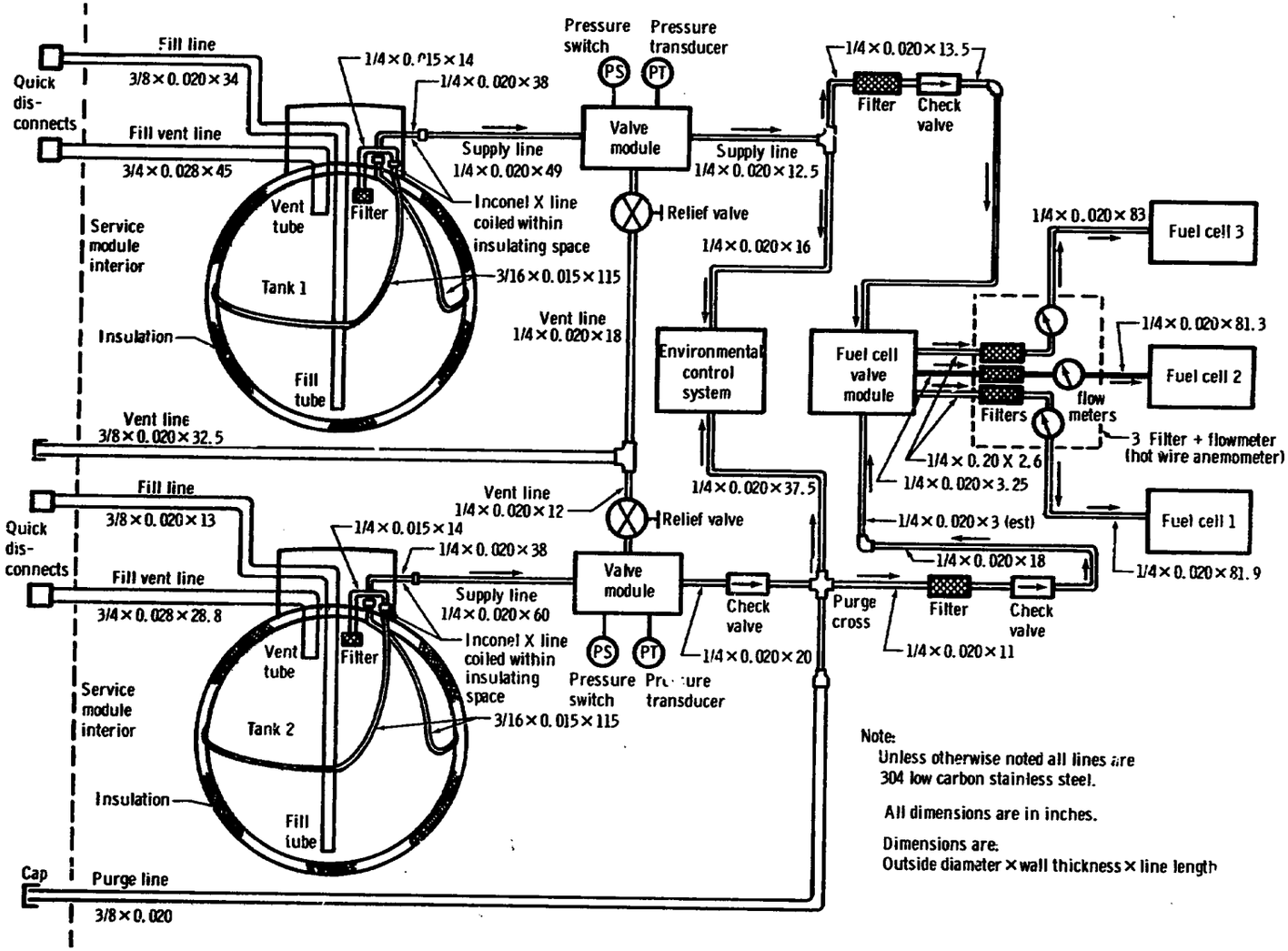

Figure 4-7. - Oxygen system.

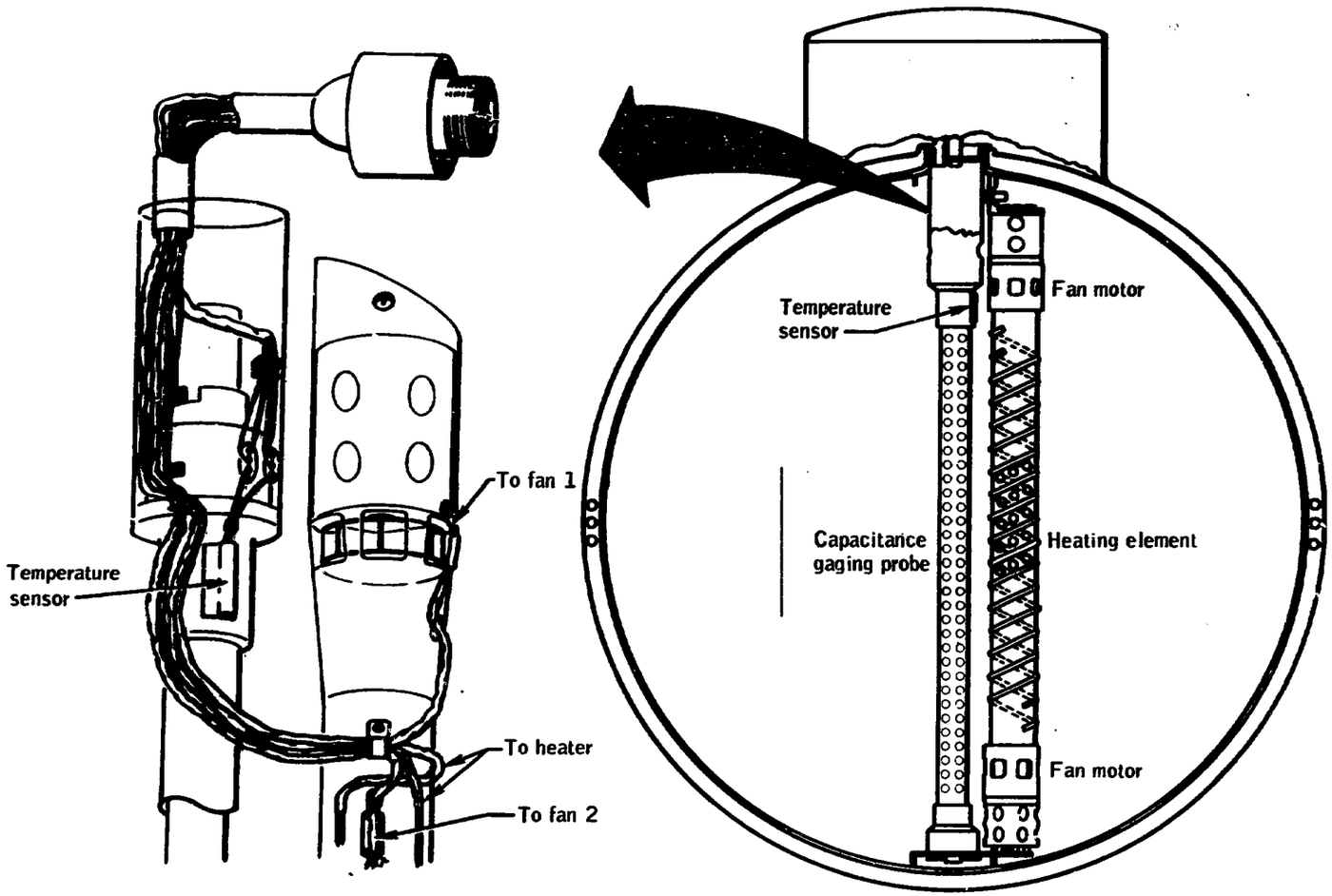

Figure 4-8.- Arrangement of components and wiring within oxygen tank.

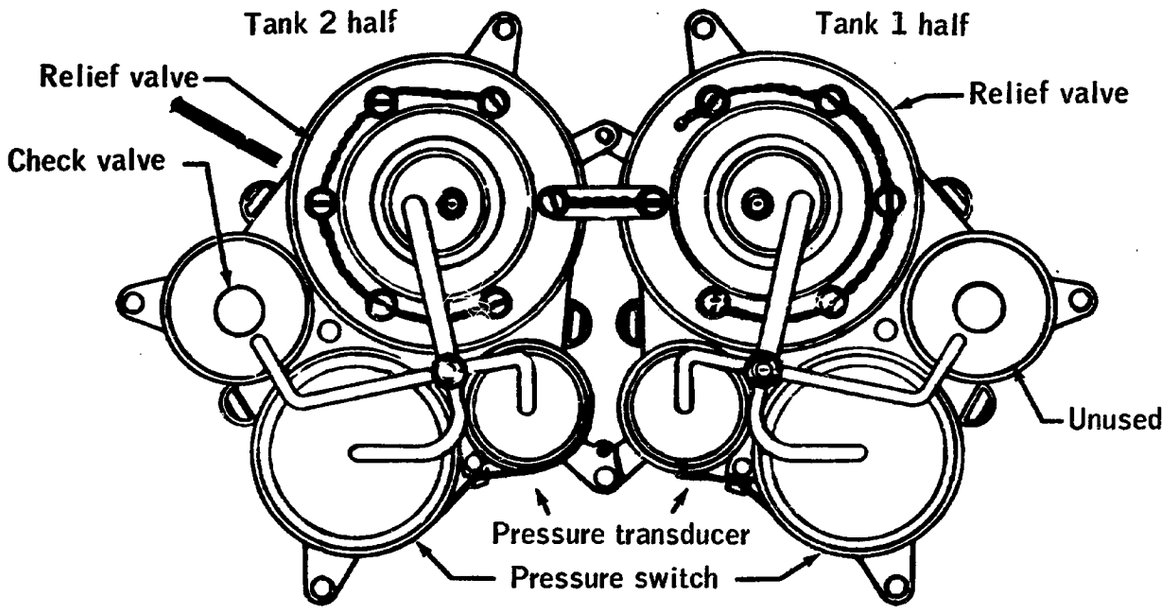

Figure 4-9.- Cryogenic oxygen valve module.

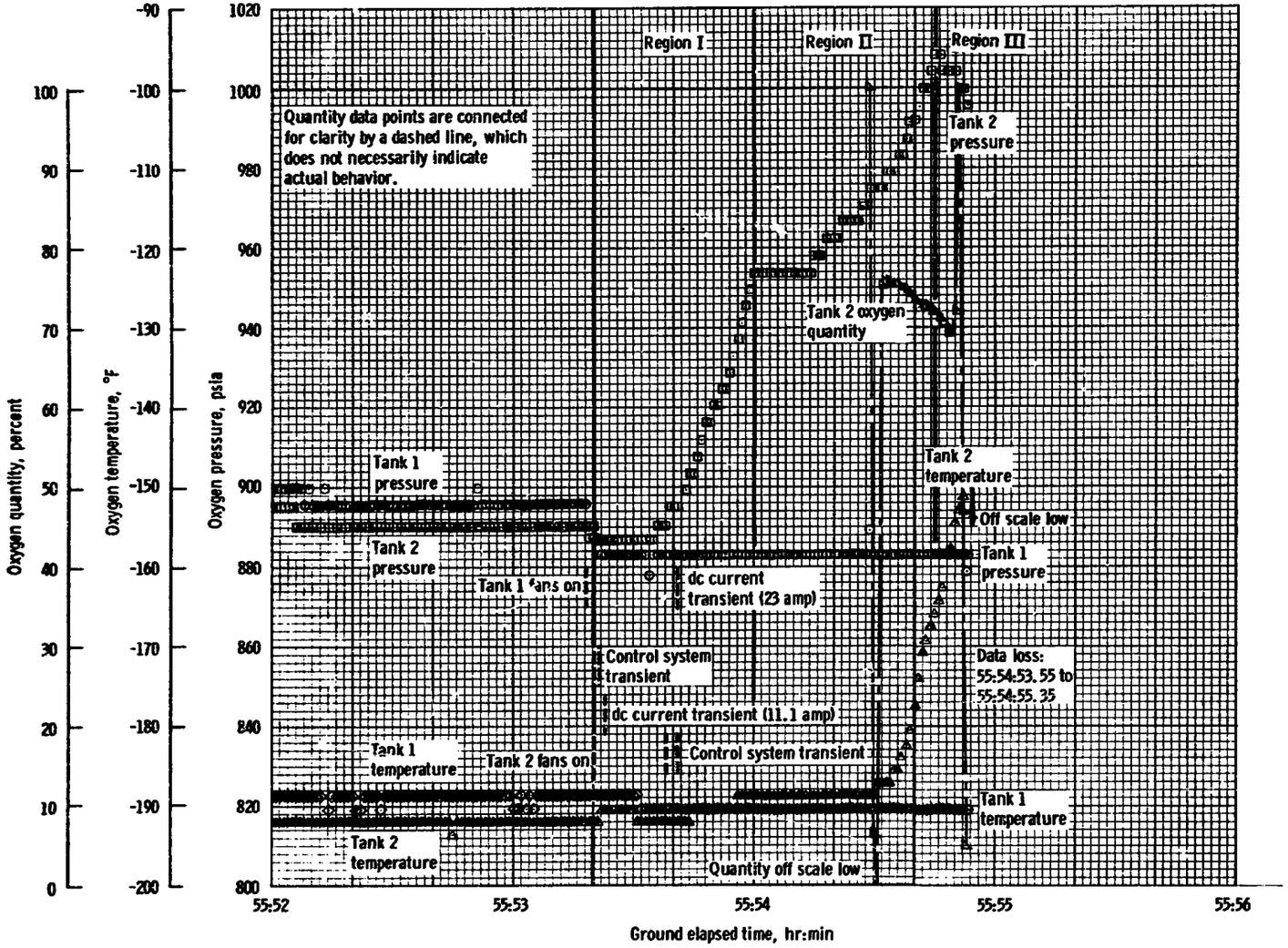

Figure 4-10.- Pressures, temperatures, and quantities during period of interest.

with flow through the relief valve using simulated flight system hardware. With high pressure gas, the measurement given by the transducer was within 18 psi of the actual tank pressure. With cryogenic oxygen, the transducer reading was within 9 psi of the actual tank pressure.

Another validation of the pressure transducer under dynamic pressure conditions consisted of integrating the flow rate change to the fuel cell (fig. 4-11). This calculation substantiated the tank pressure peak as about 1008 psia. Throughout the mission, both tank pressures were reading as expected, further substantiating their validity.

The pressure rise rates shown in figure 4-10 can be described analytically by various thermodynamic processes. All thermodynamic calculations on pressure rise, heat input, mass flow, etc. were performed using data on the "real gas" properties. In the supercritical region, deviations from ideal gas relationships can be extremely large.

The maximum energy input to satisfy the observed pressure rise is a constant density heating process. This condition is shown by the upper curve of figure 4-12. A second process, which establishes the minimum energy input, is an isentropic compression of the fluid. This compression is represented by all the energy input being confined to a small bubble, which has no mass. The resulting thermodynamic state is one of higher pressure in the tank. The result of this process is depicted by the lower curve of figure 4-12.

In actuality, the energy input into the tank lies somewhere between the maximum and minimum energy input curves shown in the figure. The process is modeled by a hot oxygen bubble of constant uniform temperature, growing at a rate sufficient to isentropically compress the surrounding cryogenic oxygen. This formulation accounts for mass transfer both to the hot mass (to increase the volume) and from the hot mass (tank outflow). This mass transfer requires a larger energy input to sustain the pressure rise. The center curve of figure 4-12 shows a comparison of this model with the maximum and minimum energy models. The results (fig. 4-13) are dependent upon the temperature of the hot mass. Note that while the energy input increases by approximately 300 percent, the hot mass volume changes only 10 percent. Therefore the energy source is confined to a small region within the tank, and is essentially independent of the temperature of the burning material.

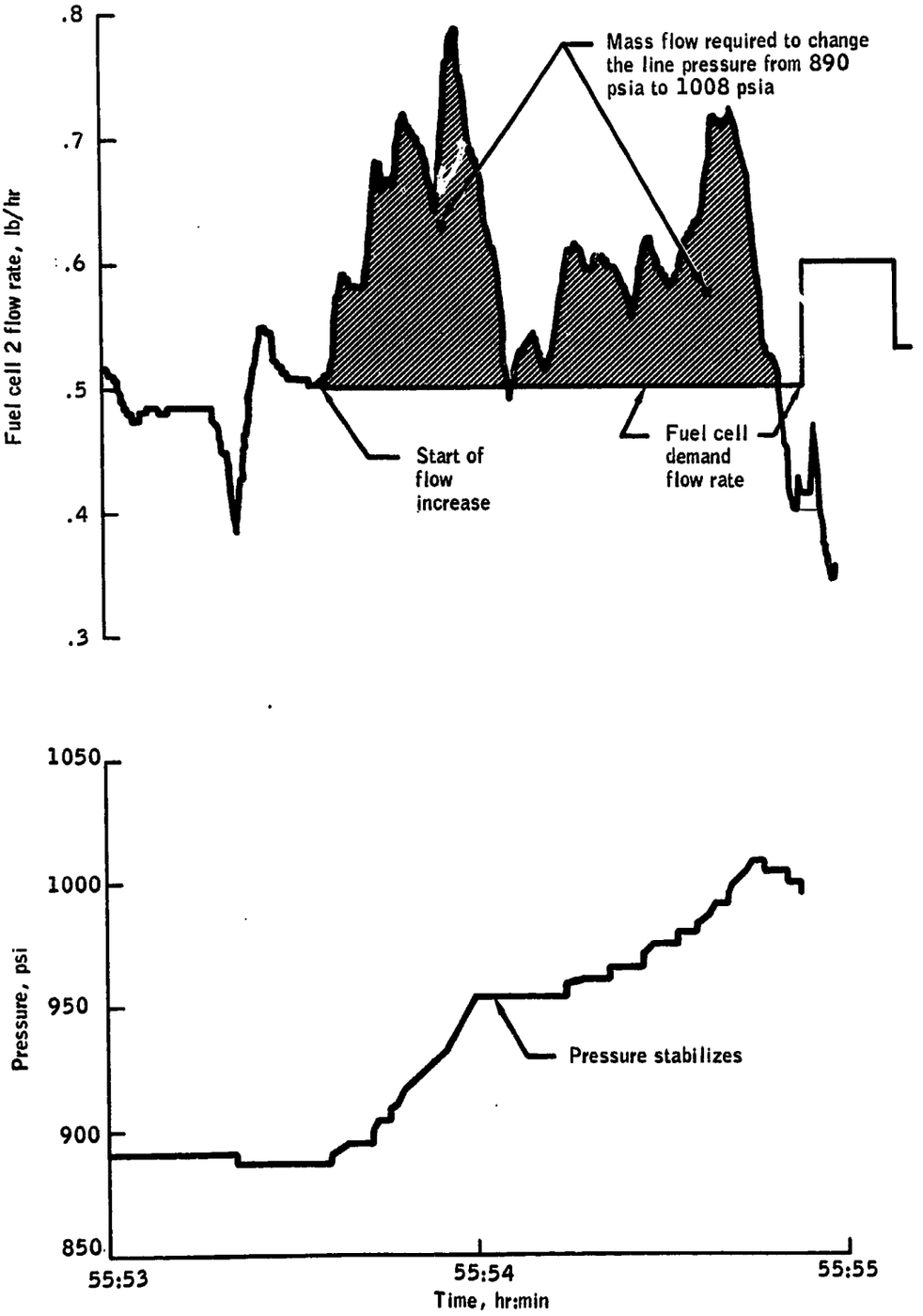

Figure 4-11.- Effect of oxygen pressure on fuel cell flow rates.

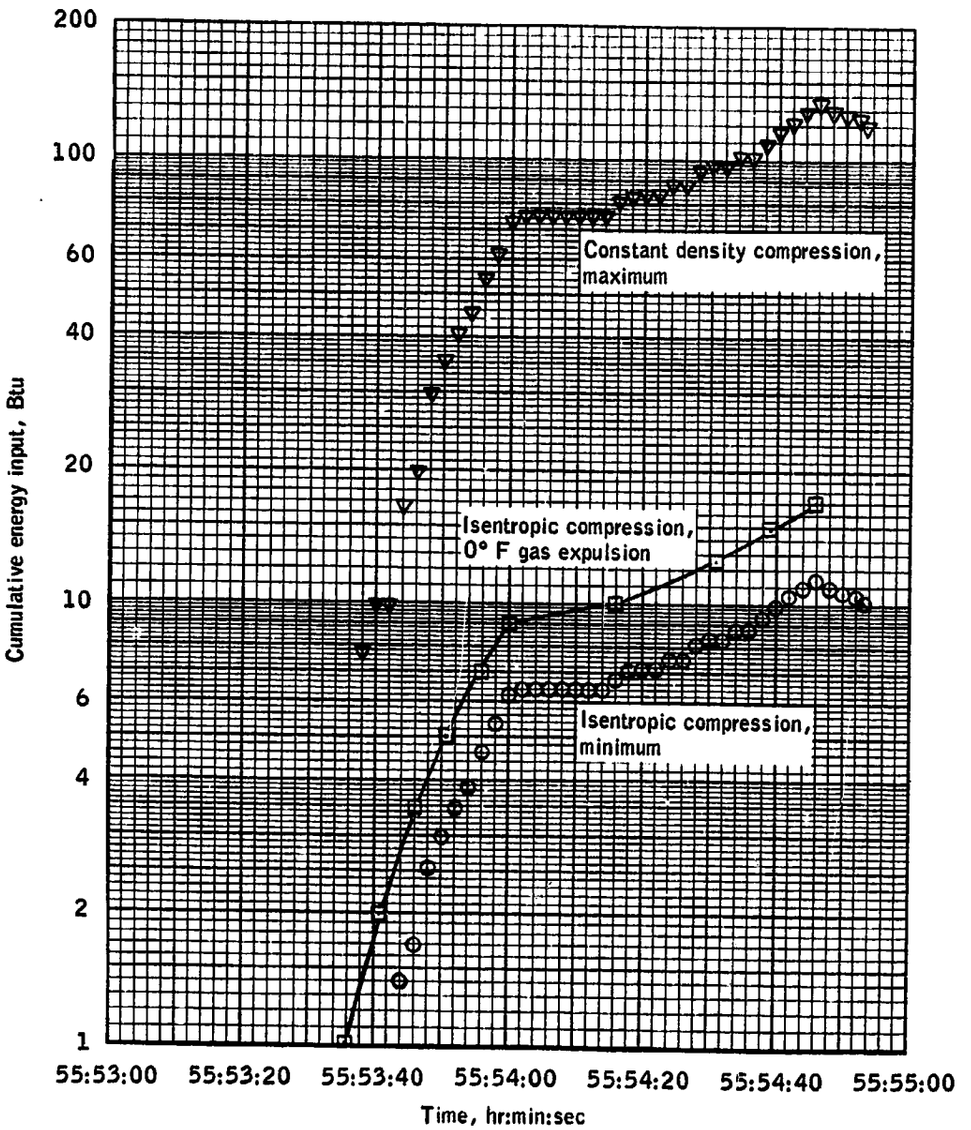

Figure 4-12.- Oxygen tank 2 energy addition.

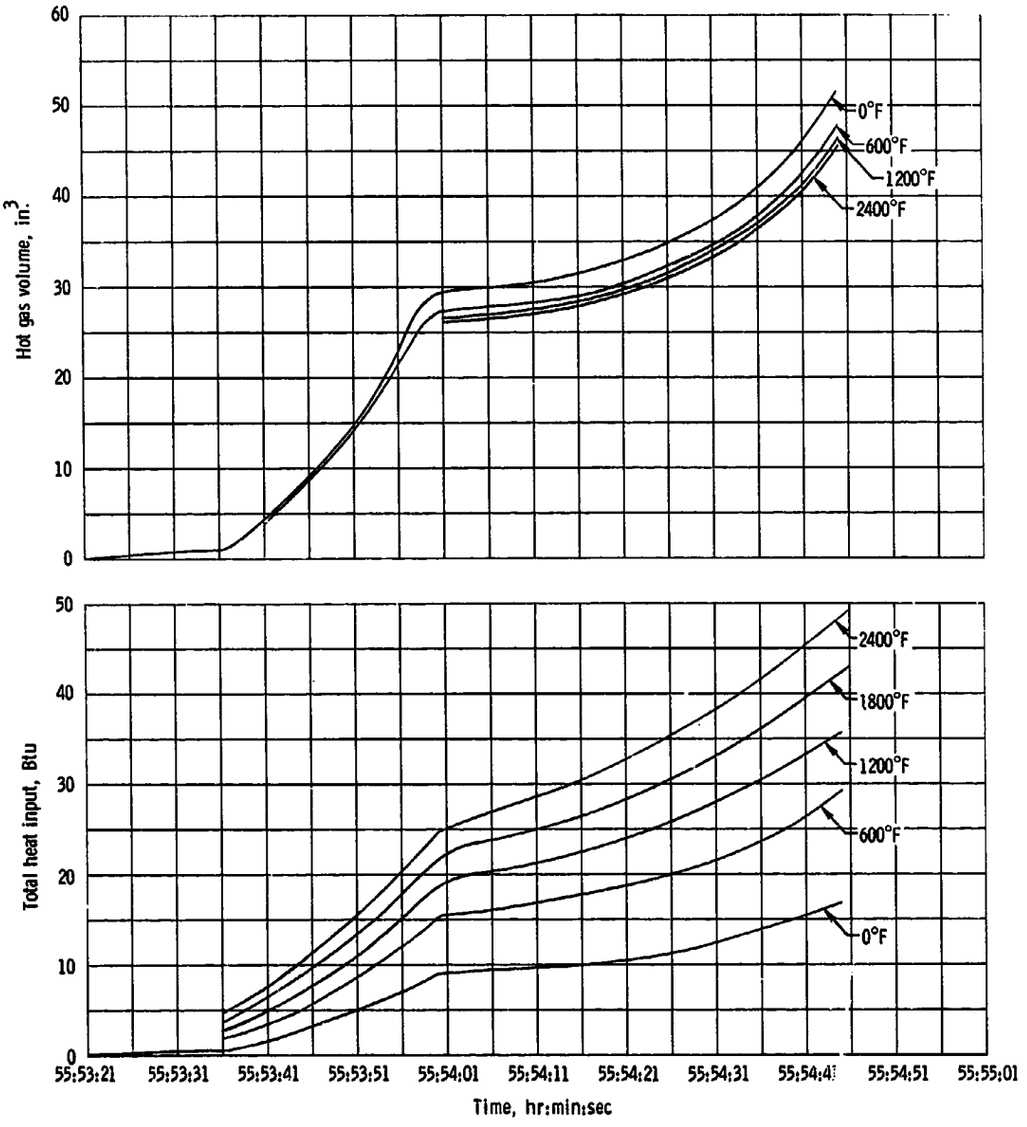

Figure 4-13. - Computed total heat input and hot gas volume.

4.3.2 Region I and II Analysis

There are only two plausible mechanisms for the slope changes on the pressure-time curve during regions I and II: a change in the mass outflow characteristics or a change in the energy input characteristics. Several analyses were performed in an attempt to relate changes in mass outflow characteristics to the pressure curve. These studies show that the only reasonable explanation for the observed pressure characteristics is a rapidly changing combustion rate within the tank.

4.3.3 Region III Analysis

Region III is the portion of the pressure-time curve that is decreasing quite rapidly, from 1008 psia to 996 psia in about 9 seconds. The analysis of the events in this time period must necessarily include a discussion of the relief valve characteristics. The acceptance test of this relief valve showed the valve started to open at 1004 psia and was fully open at 1005 psia. The relief valve flow capability, which has been established by test, is much greater than the flow rate required to produce the observed pressure decay in region III (fig. 4-14). In figure 4-15, note that the relief valve has the capability to relieve the pressure more rapidly than observed, even considering that the energy input is increasing exponentially.

There are at least two possible ways to explain the observed pressure response. One is a partial restriction of the flow and the other is a change in the combustion rate within the tank. There are several conditions which could lead to partial restriction of the flow, but the simplest of these is a restriction in the relief valve itself.

A change in the combustion rate could easily account for the slower-than-expected pressure decay after the relief valve opened. In order to properly account for the increase in combustion rate, it is necessary to consider about the last 2 seconds of region II. At this point, the pressure is 1004 psia, the relief valve crack pressure. When the relief valve opens, the velocity at the filter (inside the oxygen tank) increases. It is hypothesized that this increase in velocity provides both a convective force field and additional oxygen to the combustion source. When the relief valve opens fully the local velocity increases to a maximum. A further postulation is that this yields a maximum burning rate which raises the pressure to 1008 psia. The relief valve flow then decreases the pressure, although the combustion rate remains high. A heat input rate of approximately 2 Btu/sec will raise the pressure from 1004 psia to 1008 psia with the relief valve open. A constant heat rate of approximately 1-1/4 Btu/sec will match the observed pressure decay in region III (fig. 4-15). This energy input rate is about two and one-half times larger than the exponential rate of region II.

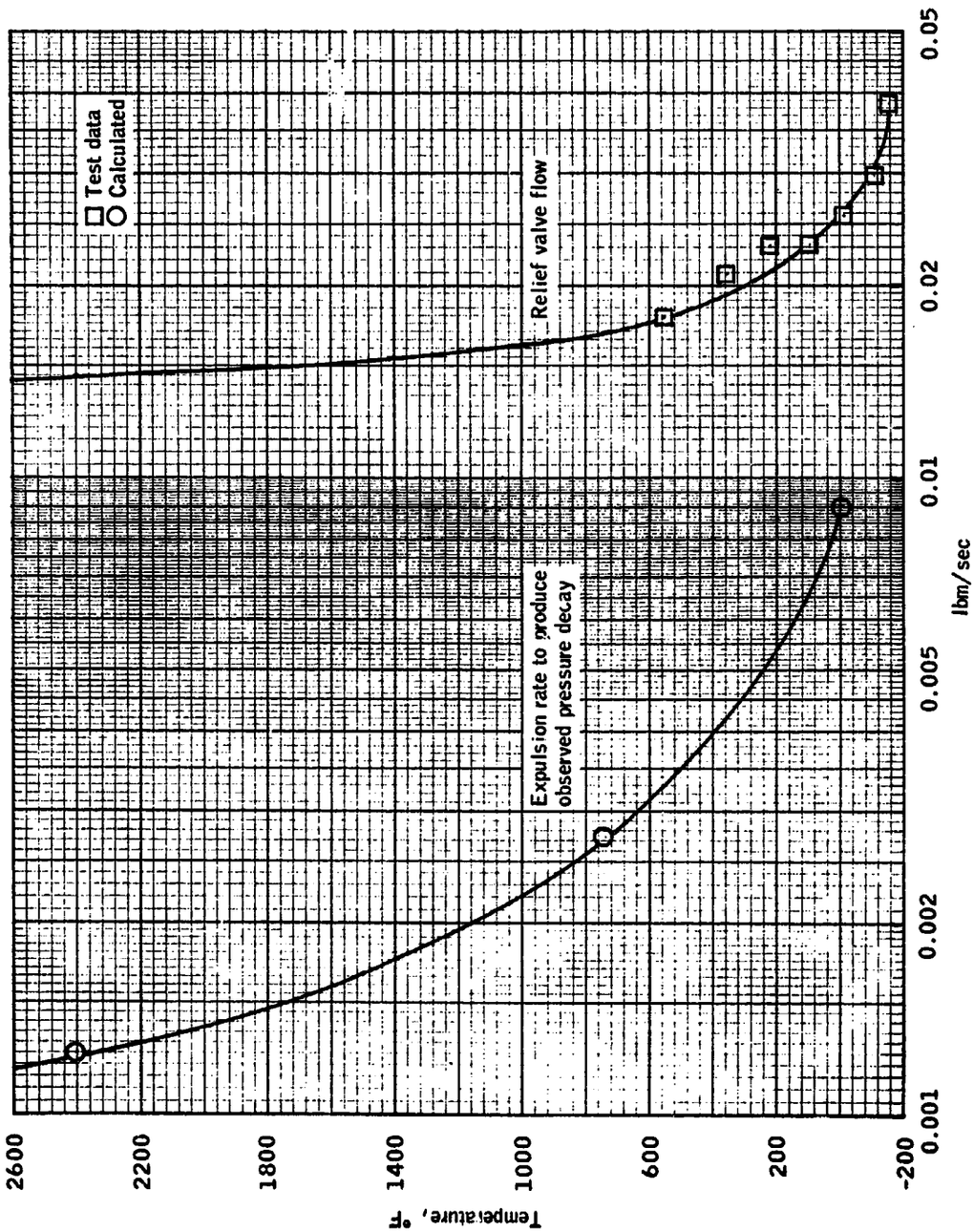

Figure 4-14.- Region III flow comparison.

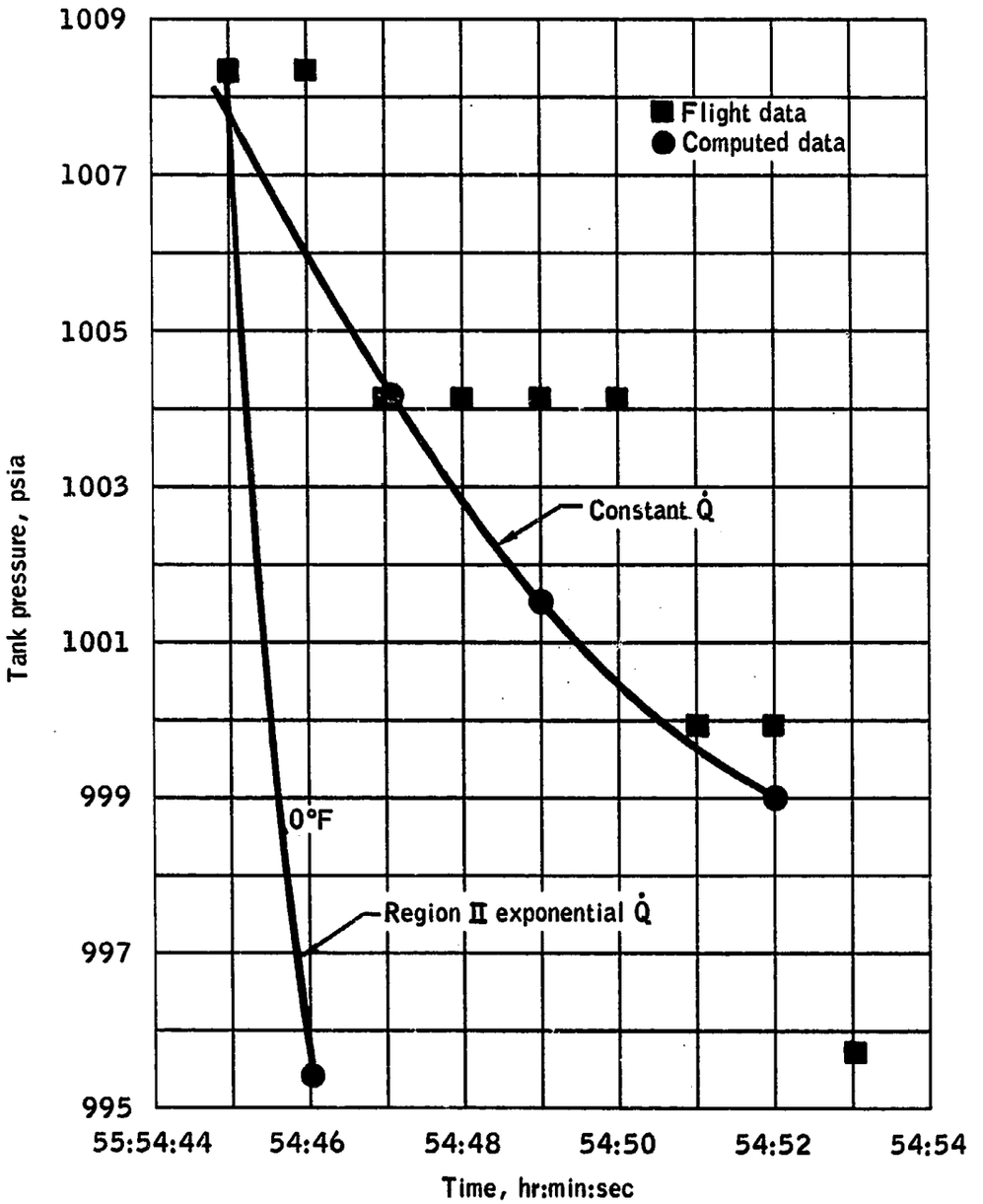

Figure 4-15.- Relief valve response in region III.

When data were recovered after the incident, the cryogenic oxygen tank 2 pressure indication was at the lower limit, which means that either the pressure at the transducer was, in fact, zero or that the measurement had failed electrically. The pressure reading would go to zero if the feedline failed or the pressure in the tank was zero.

4.3.4 Cryogenic Oxygen Tank 1 Pressure Decay

An analysis was conducted to determine what hardware damage was required to explain the loss of oxygen from cryogenic oxygen tank 1. Figure 4-16 compares the cryogenic oxygen tank 1 pressure decay with the pressure decay rate computed, assuming choked flow. Also, cross-plotted on this figure are the integrated flow-rate curve and the quantity gage data. This latter curve tends to substantiate the analytical approach. The analysis yields an effective flow area of approximately 0.005 in^2. This area is of the same order as the line on the pressure switch; a flow area this small could also result from a crimp in any of the lines from cryogenic oxygen tank 1.

4.4 CRYOGENIC OXYGEN TANK 2 TEMPERATURE

While the pressure was rising sharply in cryogenic oxygen tank 2, changes occurred in the temperature indication (fig. 4-10). The temperature data are obtained from a sensor located on the quantity probe assembly (fig. 4-8) within the tank. The temperature increased about 2° F during the first pressure rise (region I). A temperature increase of this magnitude is in accord with that expected due to the pressure rise alone.

The significant aspect of the temperature data is the rapid rise rate commencing approximately 24 seconds prior to loss of data (fig. 4-10). Several analyses were performed to interpret the data. The results indicated that a temperature range of 600° to 2900° F could produce the observed response. This wide temperature span is a result of the geometric configurations which are possible. The significant results from these analyses confirmed that the combustion source was near the sensor during the period of rapid temperature rise. Just prior to the loss of data, the temperature dropped to zero, indicating an open circuit failure in the measurement circuit.

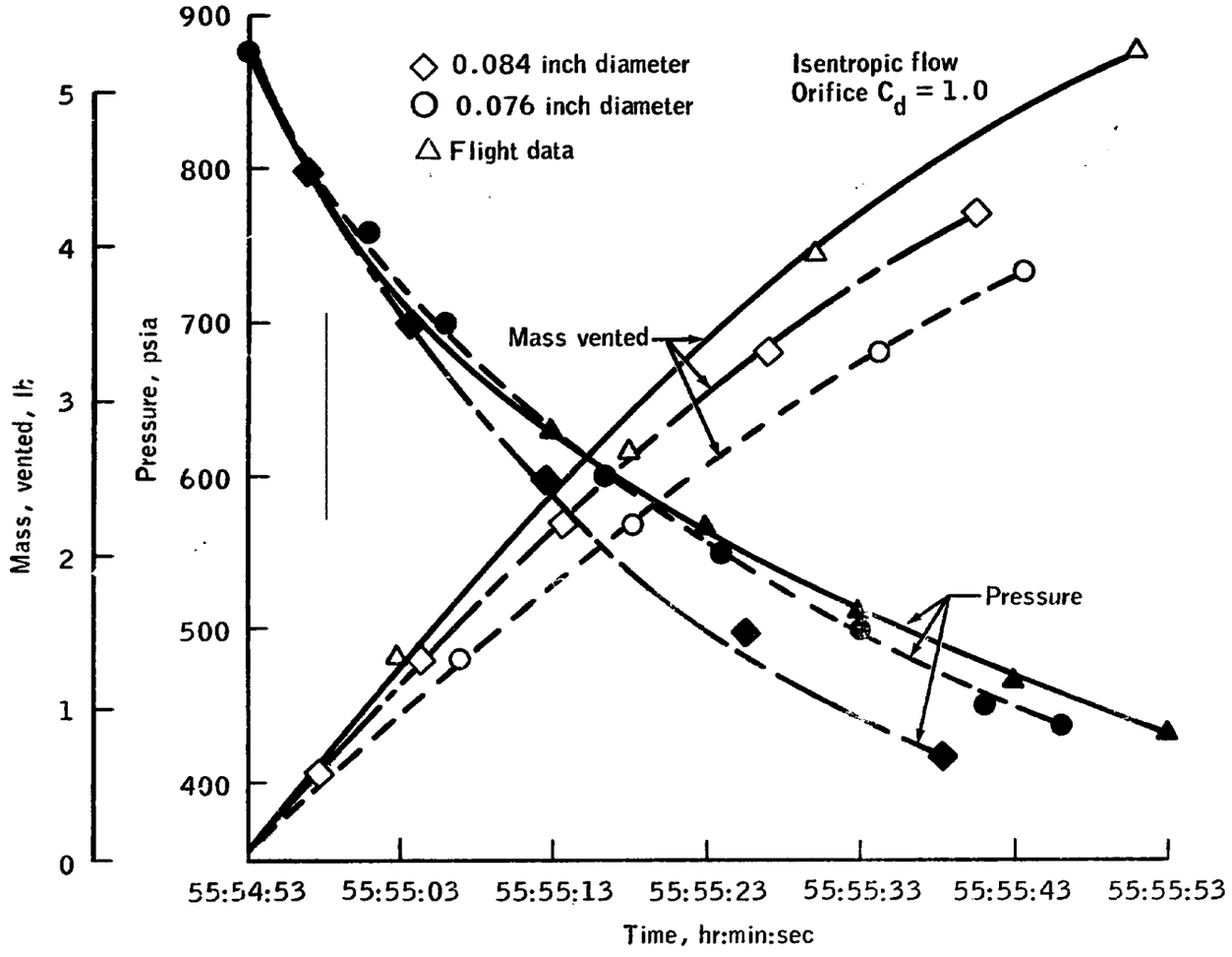

Figure 4-16.- Pressure decay rate comparison

4.5 PHOTOGRAPHIC ANALYSIS

4.5.1 Photographic Data

The photographic data used in this analysis included onboard photography of the service module taken by the crew after the service module was separated from the command module. The onboard photography was of marginal quality and included the following:

a. Twenty-six frames of 70-mm (magazine N) SO 368 Ektachrome MS color film, using the Hasselblad hand-held camera with the 250-mm lens

b. Forty-three frames of 70-mm (magazine R) 3400 Panatomic X black and white film, using the Hasselblad hand-held camera with the 80-mm lens

c. Nineteen frames of 16-mm (magazine FF) SO 368 Ektachrome MS color film, using the hand-held motion picture camera with the 75-mm lens.

The average distance from the Hasselblad cameras to the service module for the onboard photography was about 410 feet for magazine R and about 880 feet for magazine N, resulting in an image scale of 1:1500 and 1:1077, respectively. Of the frames showing the service module, orientation was such that the majority do not show bay 4, and at no time are the sun angle and camera view simultaneously directed into bay 4.

In an effort to draw detail out of the high density in the area of the normal location of the cryogenic oxygen tank 2 in bay 4, two black and white frames (AS13-59-8500 and -8501) and three color frames (AS13-58-8462, -8464, and -8465) were subjected to photographic processing enhancement for specific details. These same frames were also subjected to electronic scanning with an image digital construction technique similar to that used on the Surveyor lunar surface photography. Assisting the Photographic Technology Laboratory at the Manned Spacecraft Center were the Jet Propulsion Laboratory, McDonnell-Douglas Corporation, LogEtronics Incorporated, Ciba Corporation, and Data Corporation with their specialized techniques, facilities, and experienced personnel. After exhausting all means of enhancement from the masters, the original film was taken to Data Corporation, Dayton, Ohio, to be scanned with their high-intensity, 1-micron probe and digitally reconstructed to bring out the detail for analysis.

Without the benefit of sharp, well-lighted views of the bay 4 area, such as are available in the preflight closeout photographs, it was necessary to obtain all the available information from each of the better frames and then to combine the findings. This approach was also used in examining the transparencies and prints of individual frames at each stage of enlargement and enhancement.

In addition, the contact and enlarged transparencies, combined with the digitized enhancements, showed where the Mylar/Kapton was blocking, or shadowing, to hide certain component areas. The information was reconstructed into a scale model, which confirmed the presence of hard point components presenting different reflective surface, such as the oxygen and hydrogen tank surfaces, as well as the influence of the Mylar/Kapton highlights and blacks.

4.5.2 Onboard Photography Analysis

Figure 4-17a shows cryogenic oxygen tank 2 as it appeared at the time of bay 4 closeout and figure 4-17b identifies the features shown.

Figure 4-18a shows frame 8464 of the 70-mm color film taken through the window of the lunar module. Figure 4-18b identifies the principal features. Figure 4-19a shows frame 8501 of the 70-mm black and white film and the principal features are identified in figure 4-19b.

Figure 4-20 shows the 1/6 scale model with fuel cells tipped, Mylar and Kapton insulation extended, skin panel removed as in frame 8464, but with a bright metal oxygen tank having a clean Inconel-type surface. Figure 4-21 shows the 1/6 scale model the same as in figure 4-20 except with cryogenic oxygen tank 2 discolored brown. Figure 4-22 shows the same 1/6 scale model except with oxygen tank 2 removed.

Figure 4-18 and 4-19 are representative of the best onboard photography analyzed by stereo plotter, monocular photographic interpretation, enlarging and enhancement, electronic scanning and digitizing, and by model simulation. The results indicate the following:

a. The fuel cells (1 and 3) are tipped slightly forward (outboard) so the rear of the fuel cell shelf apparently was raised.

b. The insulation blanket was removed from the underside of the fuel cell shelf near radial beam 3 and above oxygen tank 2, since the color of the bare shelf is visible.

c. Mylar and Kapton insulation blown, torn, and/or partially burned free from its initial fastening, now congest some areas of the bay and extend outside the service module from several places along the edges of shelves and beams.

d. The oxygen tank 2 appears to be present and discolored. Because of the blackness of the non-illuminated remaining interior, aluminized Mylar and Kapton, and the discoloration of the oxygen tank 2, the blend

of brown and black does not show on photographic prints and is only discernible by subtle color change in the enhanced transparencies of frame 8465 which provides the most direct look into the unlighted area of the oxygen tank in bay 4.

e. The electrical cable to cryogenic oxygen tank 2 is identified by its length and point of attachment to the oxygen shelf. The tank attachment free end extends upwards and outwards from the shelf (fig. 4-19).

f. Reflections from the end domes, body, and some connections on the hydrogen tank indicate it is apparently externally sound and in proper position.

g. A portion of the bay 4 panel remained attached at the forward end by radial beam 3, and the lower access panel remained attached to the service module at the aft end of beam 3.

h. One of the four reflectors and feeder horns for the high-gain antenna was damaged. The attitude of the antenna, with the damaged reflector nearest the service module, had changed since the incident because the gimbals are free to rotate whenever the power is turned off.

i. The oxygen service panel appeared in its normal position, but with considerable loosened Mylar and Kapton in the area.

j. A brown stain was observed on the outside surface of the service propulsion system engine nozzle extension, near the plus Z axis, and in line with the vent path from the vent annulus around the nozzle.

4.5.3 Ground Photography

Three of the observatories tracking the spacecraft took photographs of a nebulosity or cloud that appeared shortly after the incident.

Such a cloud, having a maximum measured diameter of 25 nautical miles, appeared on a photograph from the Manned Spacecraft Center 16-inch telescope at approximately 56 hours.

Analysis of a photograph taken through the telescope at Mount Kobau Observatory, British Columbia, at 58 hours 27 minutes, about 2-1/2 hours after the incident, indicated that approximately 20 pounds of oxygen would be required to form the observed cloud. The characteristics of cloud shape and axes alignment indicate that it was not formed by an instantaneous release of oxygen.

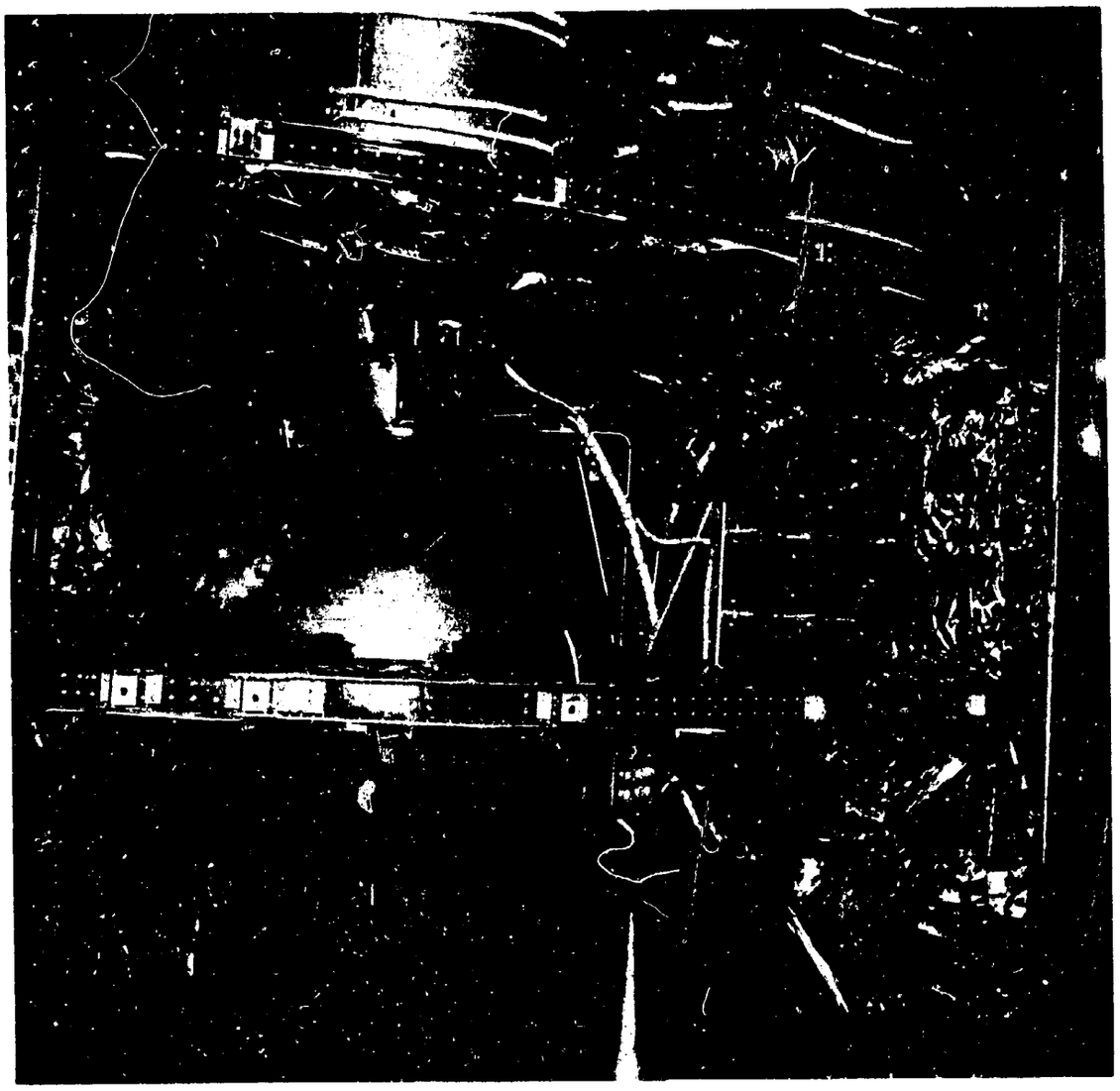

(a) Cryogenic oxygen tank 2.

Figure 4-17.- Bay 4 closeout photography.

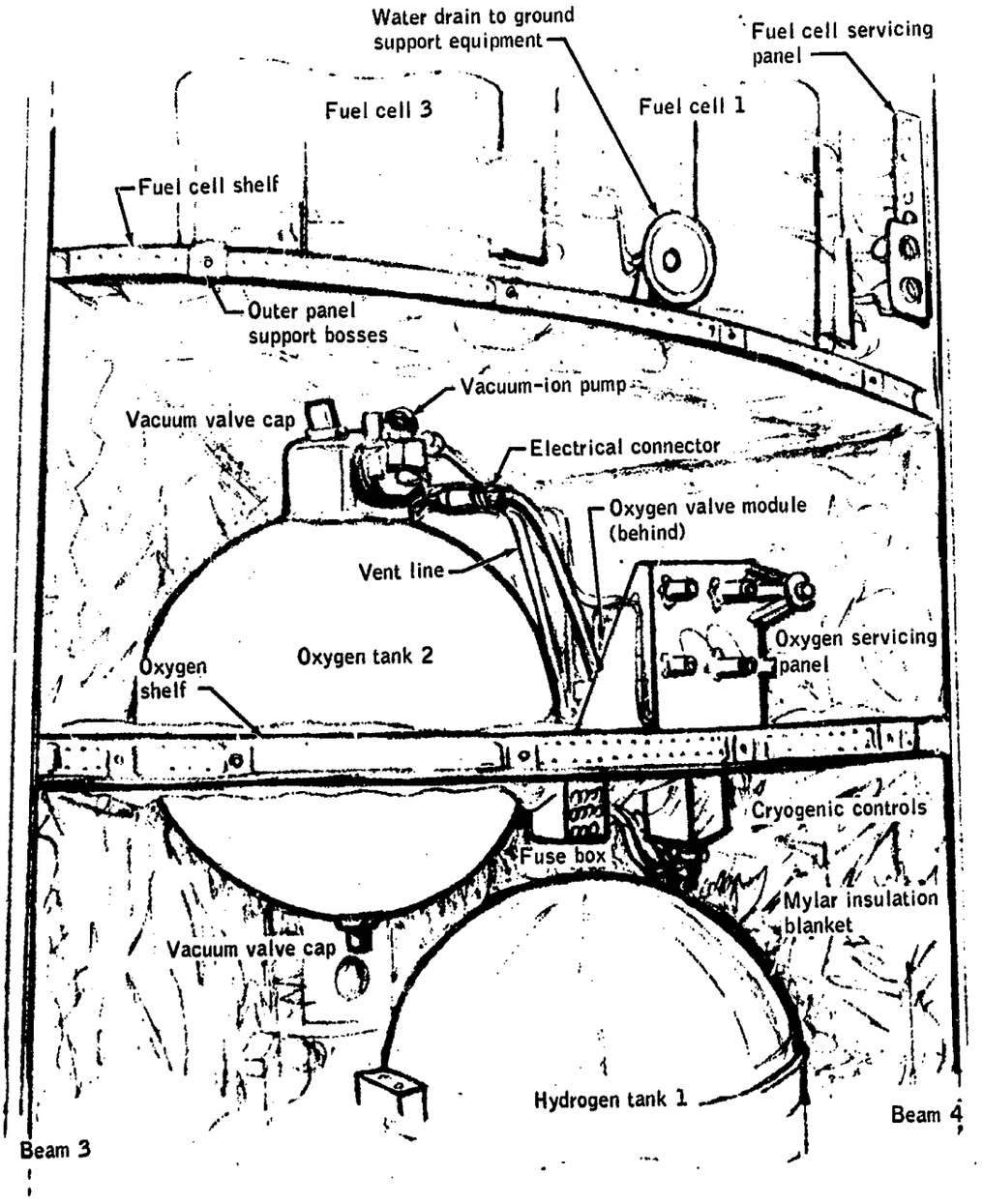

(b) Identification of features in figure 4-17a.

Figure 4-17.- Concluded.

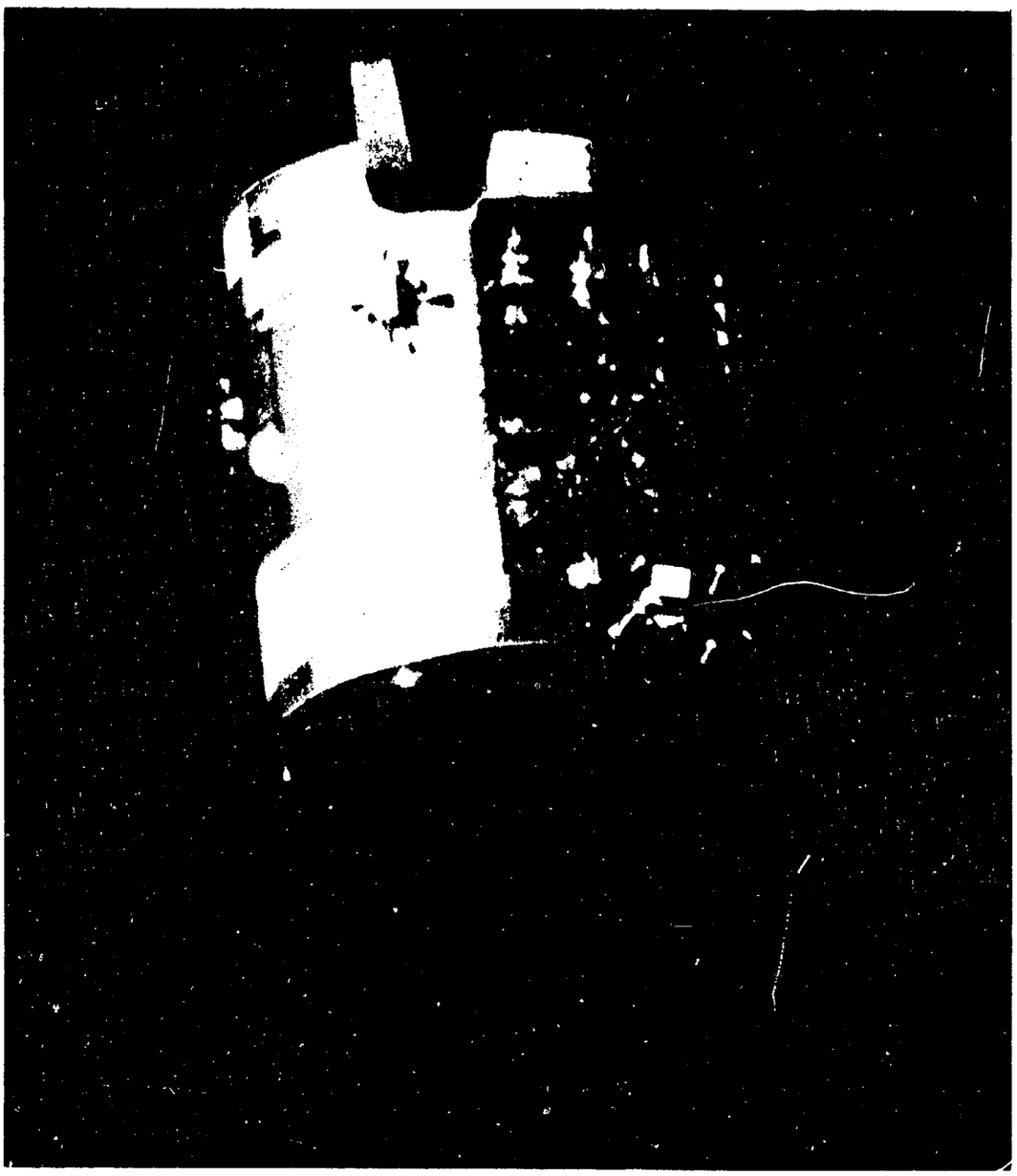

(a) Onboard camera view.

Figure 4-18.- 70-mm color film frame 8464.

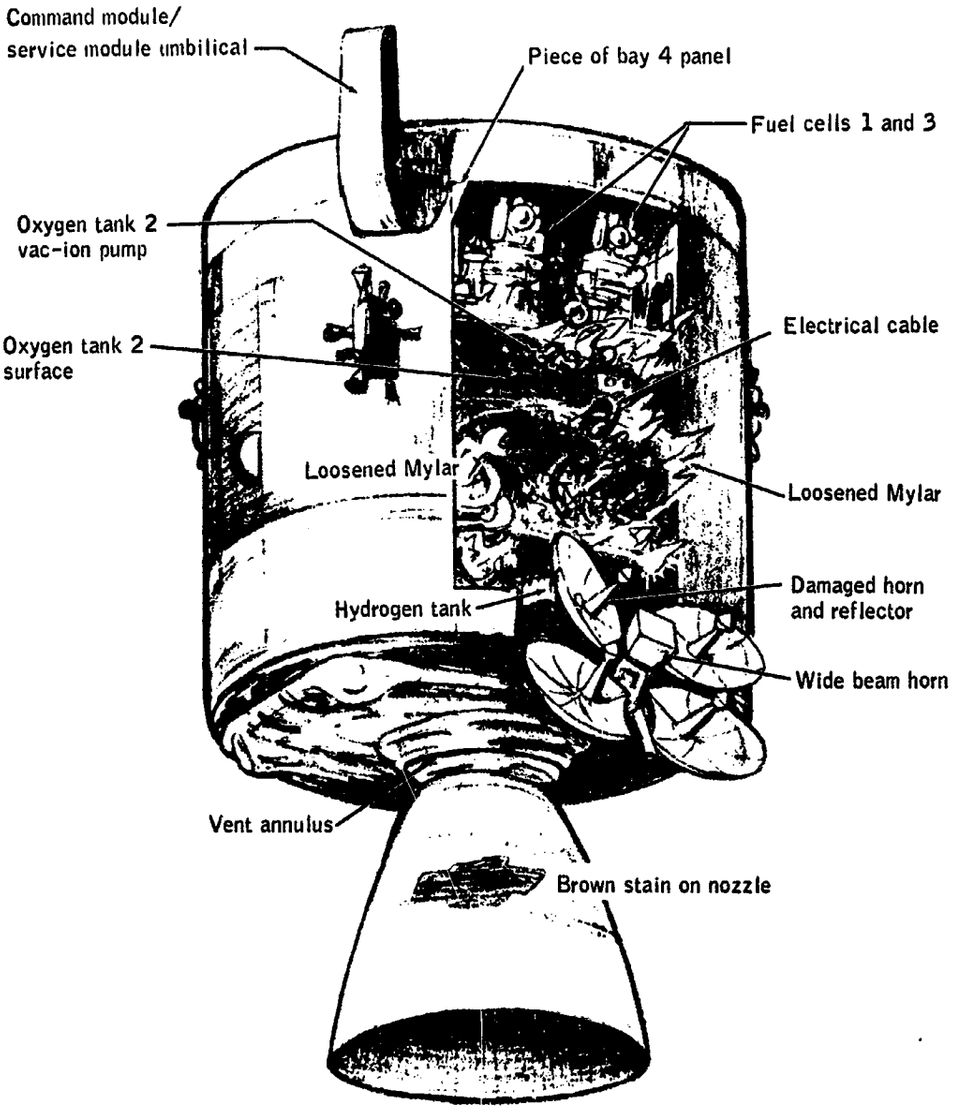

(b) Identification of features in figure 4-18a.

Figure 4-18.- Concluded.

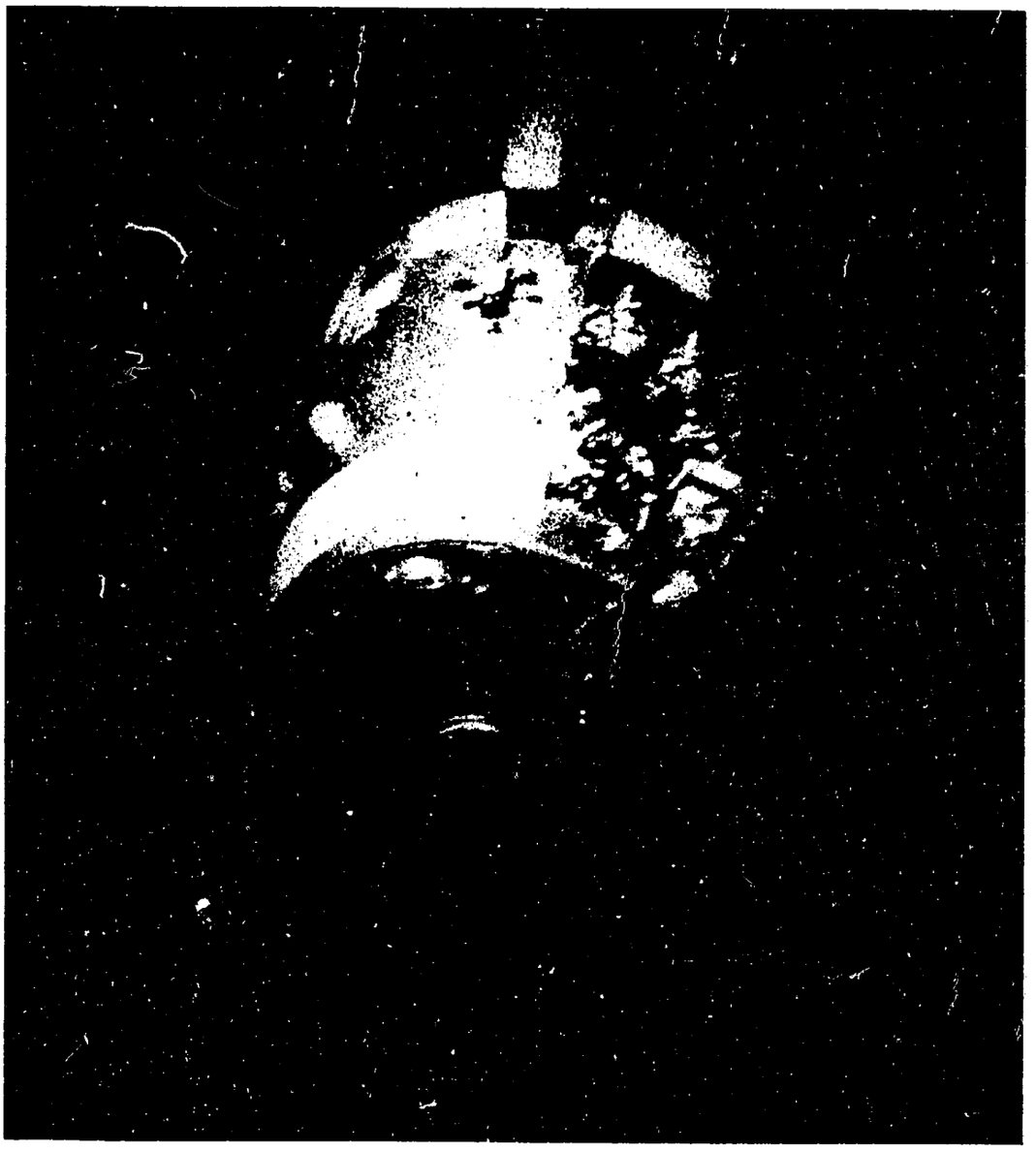

(a) Onboard camera view.

Figure 4-19.- 70-mm black and white film frame 8501.

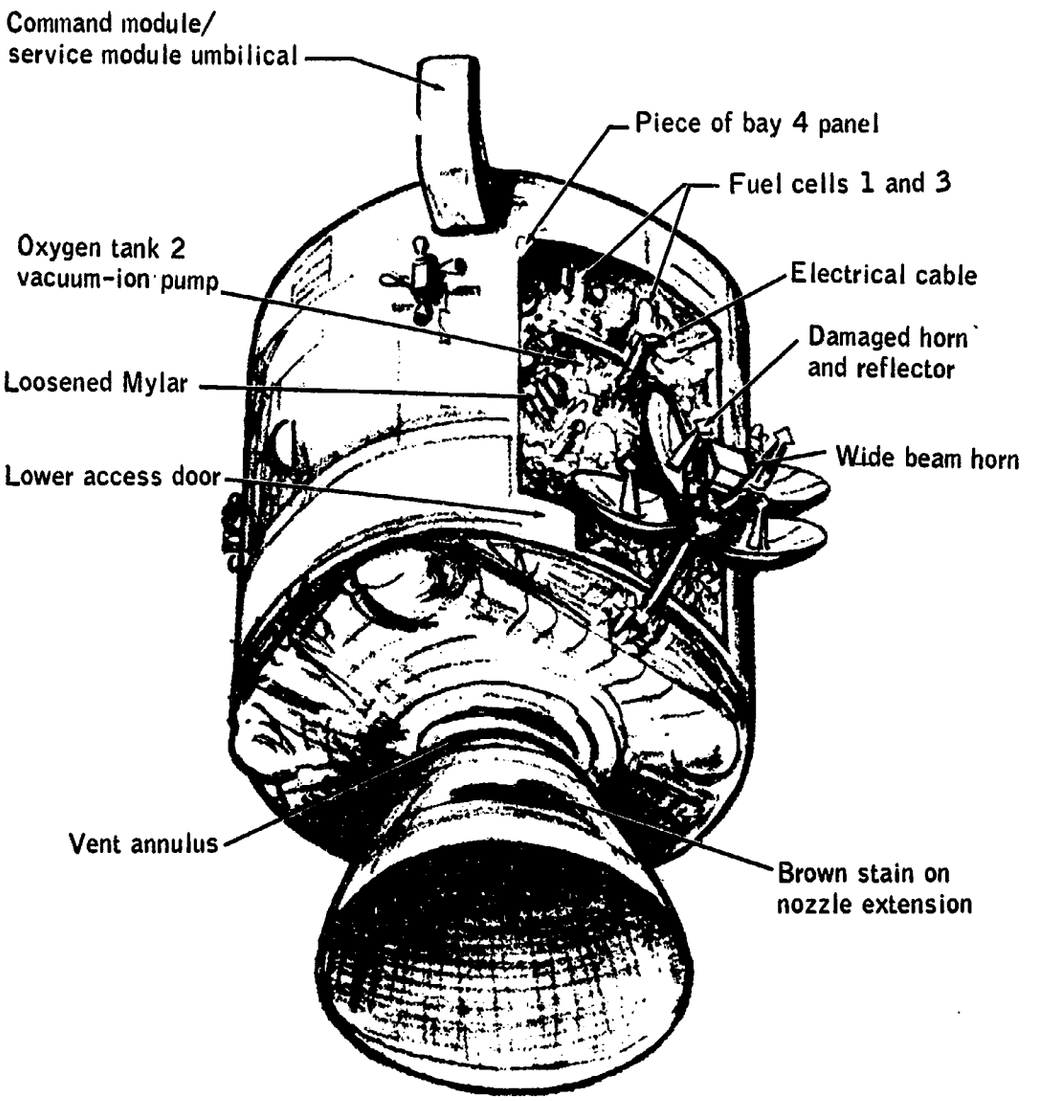

(b) Identification of features in figure 4-19a.

Figure 4-19.- Concluded.

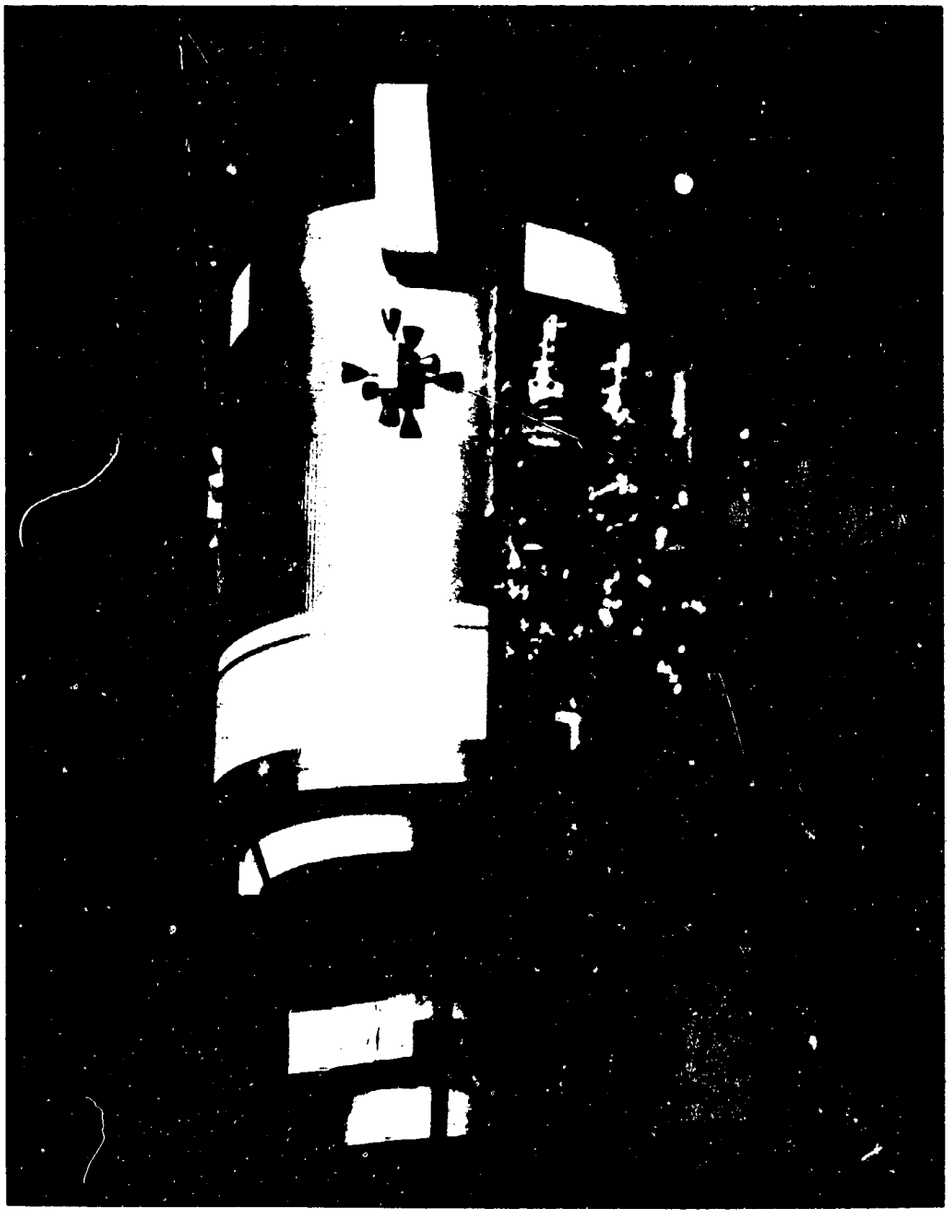

Figure 4-20.- Model with lighting similar to onboard frame 8464.

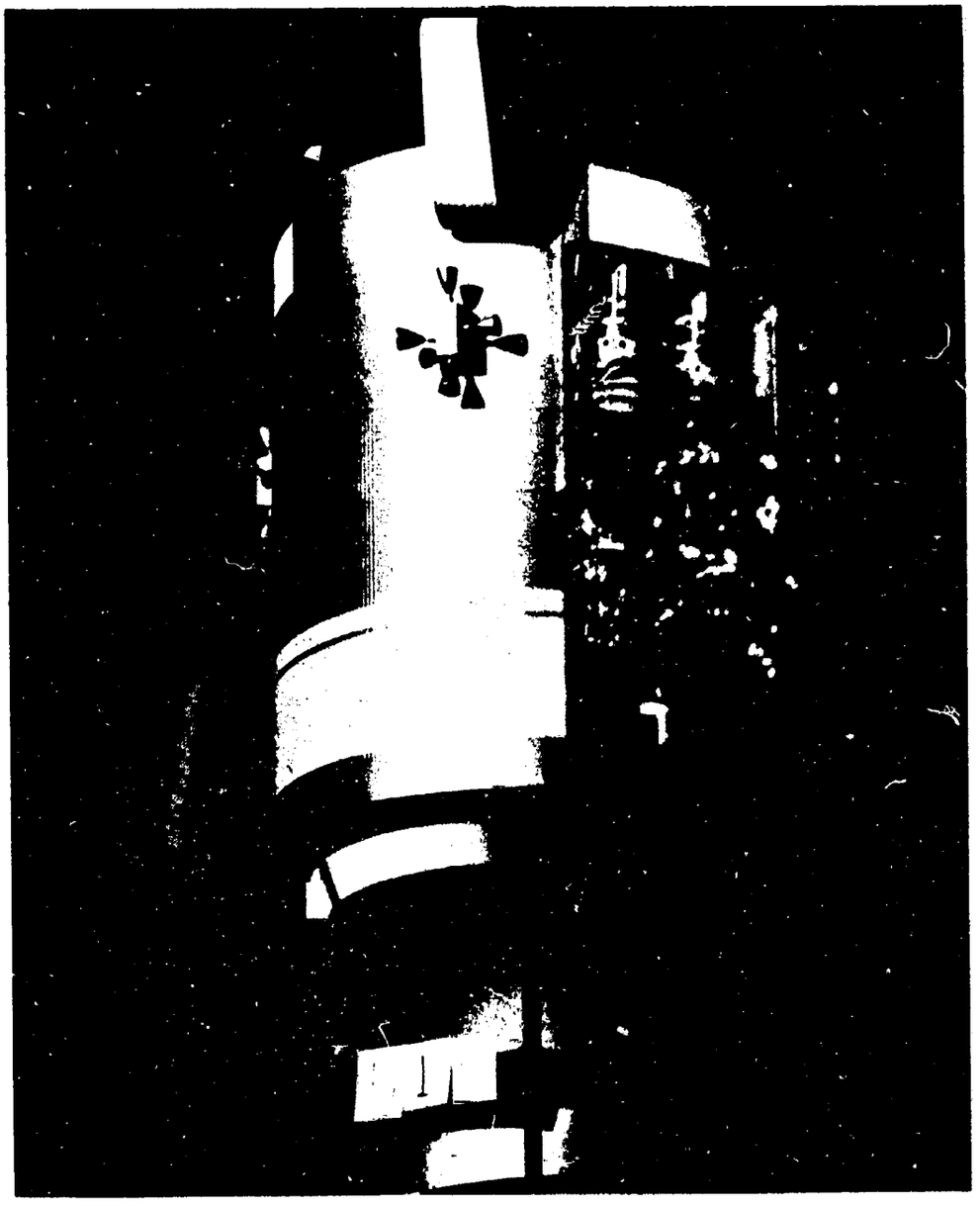

(a) Lighting similar to onboard frame 8464.

Figure 4-21.- Model with Inconel tank surface discolored.

(b) Bay 4 illuminated.

Figure 4-21.- Concluded.

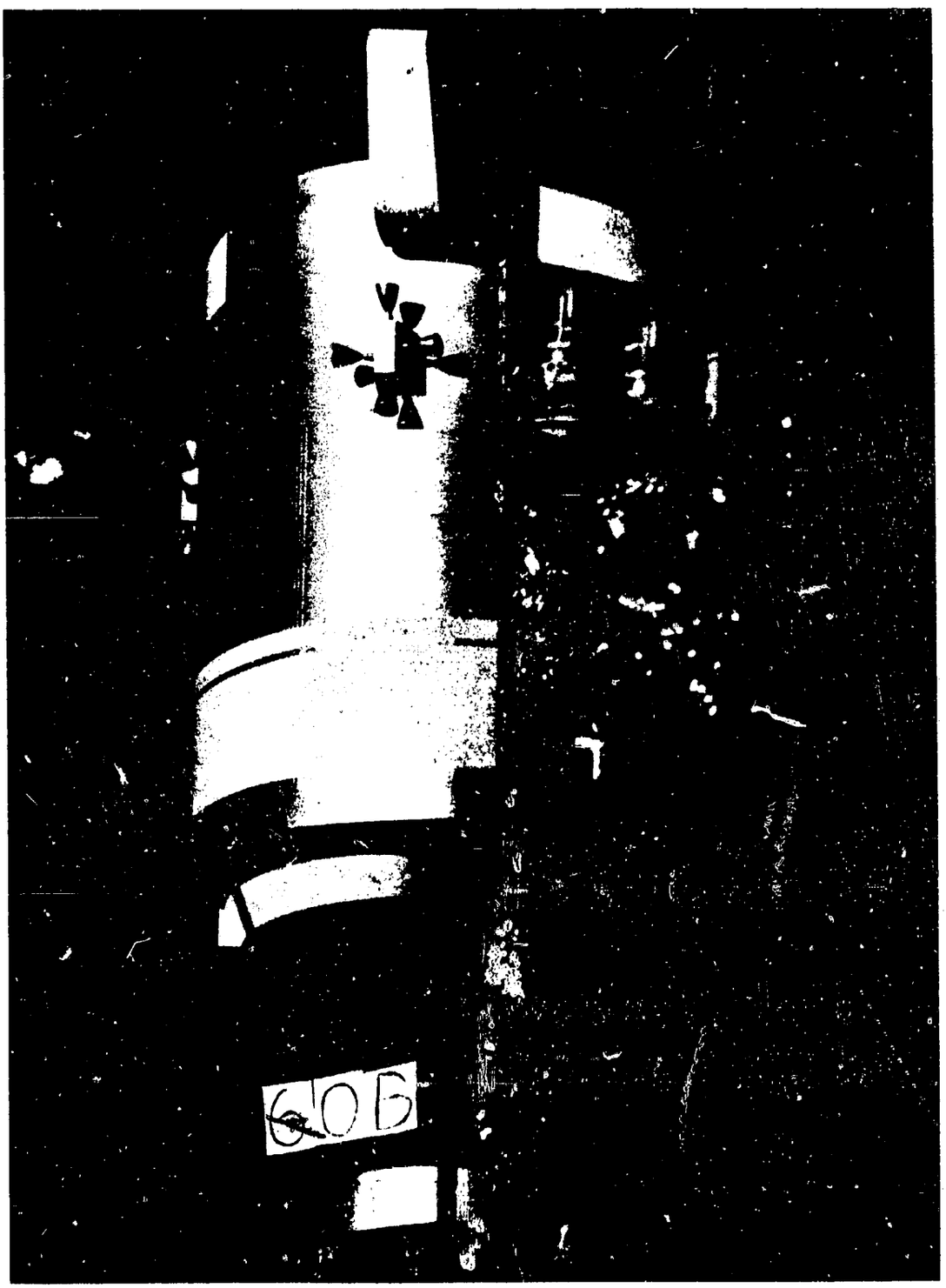

Figure 4-22.- Model without oxygen tank 2 and lighting similar to onboard frame 9464.

4.6 SERVICE MODULE BAY 4 PANEL SEPARATION

This section discusses the sequence of events immediately preceding, during, and immediately following the separation of the outer shell panel from bay 4 of the service module. A description of the associated structure and its failure mode is presented first, followed by a discussion of the cryogenic oxygen tank 2 structure and how it might fail. Next, the events occurring during the last second of data prior to the incident are discussed.

4.6.1 Bay 4 Structural Description

Bay 4 of the service module with the exterior shell panel removed, is shown in figure 3-2. The exterior shell panel is bonded aluminum honeycomb 1-inch thick; the exterior facesheet is 2024-T81 (0.020-inch thick over most of the panel with a triangular section of 0.016-inch thickness at the upper end), the interior facesheet is 7178-T6 (0.010-inch thick), and the perforated core is 5052-H39 (3/16 by 0.0007-inch, 2.2 lb/ft^3).

The panel has several small doors, for servicing the tanks and fuel cells located in bay 4, and one large door located in the lower left-hand corner of the panel as viewed from the service module exterior. The panel is fastened at the periphery by 1/4-inch bolts (NAS 1134C) on approximately 2-inch spacing and to the three shelves (fuel cell, oxygen, and hydrogen) by bolts at each shelf.

Bay 4 is enclosed at the top by the 1-inch thick aluminum honeycomb service module forward bulkhead and at the bottom by the 3-inch thick aluminum honeycomb aft bulkhead. Radial beams 3 and 4 bound the left and right sides of bay 4, respectively, as viewed from the service module exterior. Bay 4 is open to the center tunnel except for three areas. One 0.032-inch sheet extends 18 inches from the forward bulkhead and one 0.020-inch sheet extends between stations X_a 933 and X_a 942. The inner radial beam caps are laterally supported.

Three shelves are made of aluminum honeycomb and have the following construction:

a. Fuel cell - Two inches thick with 7178-T6 facesheets chemically milled to 0.020 and 0.035 inch. The core is 3/16 by 0.0015 inch.

b. Oxygen - Two inches thick with 7075-T6 facesheets of 0.030 to 0.060 inch. The core is 3/16 by 0.003 inch.

c. Hydrogen - One and one-half inches thick with 7075-T6 facesheets of 0.015 inch. The core is 3/16 by 0.0015 inch.

Insulation consisting of 28 layers of 0.15-mil aluminized Mylar sandwiched between two layers of 0.50-mil aluminized Kapton is attached to specific bay 4 surfaces with Velcro patches. The insulation is located on the tunnel section of the fuel cell bay, on the beams, and shelves of the cryogenic bays, and on the panel from the aft bulkhead to the fuel cell shelf.

4.6.2 Bay 4 Panel Structural Behavior

The bay 4 panel may be structurally idealized as a cylindrical shell segment supported elastically at its boundaries. The radial beams provide support in the axial and radial directions along the meridians of the panel. Tangential support along those boundaries is provided by the adjacent shell panels which are supported by the forward and aft bulkheads. The forward and aft bulkheads provide radial and circumferential support.

The panel and radial beams have 5/16 and 9/32 inch attachment holes, respectively, with large tolerances to allow removal and reinstallation of the panel when the spacecraft is on the launch pad. The maximum free movement at a single bolt would be 0.0975 inch considering the maximum dimensions of the hole in the panel and radial beam and the minimum bolt diameter.

Two simplified limiting cases may be used to describe the basic structural behavior of the panel. The first considers the panel as a flat plate supported on all edges. In this case the panel transfers loads to the boundary by bending. The second case considers the panel as a pure membrane which transfers loads into attachments by in-plane extension. The photographs of the service module show failure at the attachments along all the boundaries except for a small piece of structure (approximately 6 by 4 inches) in the upper left-hand corner (viewed from the exterior). If the panel behaved as a flat plate and failed cleanly at the attachments, the bolts would fail in tension at approximately 5100 pounds per bolt. This load on the bolt would require a shear load in the adjacent core of 785 pounds/inch which is greater than 3 times the core-failure load. Since no facesheet nor core is evident along the edge, the structure did not behave as the simplified model of a flat plate.

Because of the evidence which suggested primarily membrane behavior, simplified representations of the structure were used to investigate its behavior. Structural analyses were performed for numerous pressure distribution as well as for temperature gradients for both hot and cold inner facesheets. The results show that the peak pressure must exceed 20 psi and that temperature gradients of interest result in small edge loads. The static allowables for failure with a failure mode of shear tearout are shown in figure 4-23.

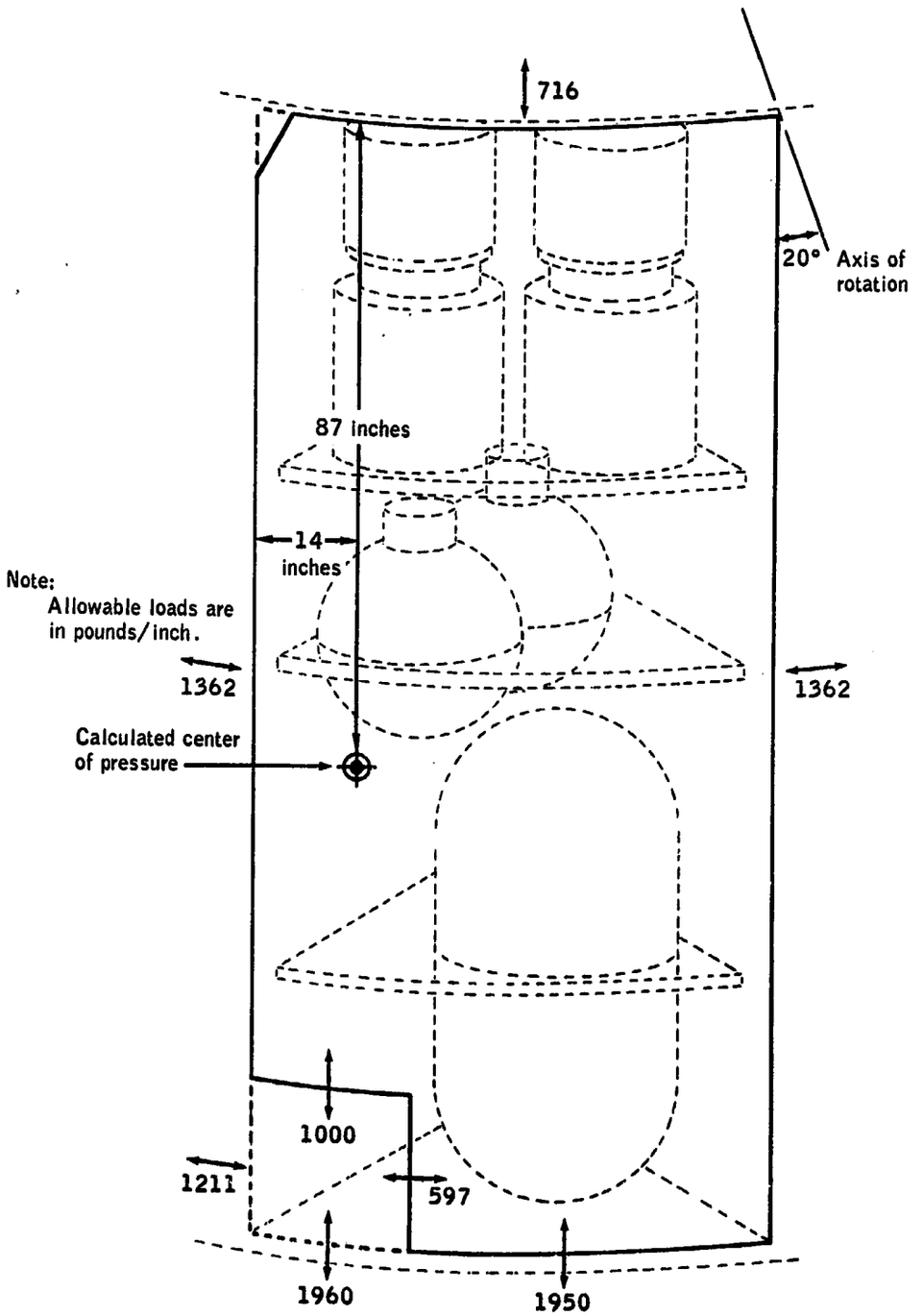

Figure 4-23.- Joint design allowables and axis of rotation.

4.6.3 Cryogenic Oxygen Tank 2 Structure

The cryogenic oxygen tank is fabricated from Inconel 718 and is composed of two hemispheres assembled by fusion welding. A sketch of the tank is shown in figure 4-24. The basic wall thickness of 0.059 inch with increasing thickness at the welds and boss areas. The inside radius is 12.528 inches. The limit design pressure (maximum operating pressure) is 1025 psi, proof pressure is 1367 psi, and design burst pressure at ambient temperature is 1538 psi. Structural analyses have predicted a positive margin at design conditions; burst tests using liquid nitrogen demonstrated burst strengths in excess of 2200 psi. Preflight fracture mechanics analysis of cryogenic oxygen tank 2 predicted that no flaw propagation would occur until a pressure of 1050 psi was reached and that the failure mode at pressures less than 1240 would be leakage.

4.6.4 Cryogenic Oxygen Tank 2 Fracture Mechanics

Figures 4-25 and 4-26 show the fracture mechanics data of the cryogenic oxygen tank. For the base material and the weld, as well as for heat-affected zone materials, the mode of failure is leakage at pressures up to those above proof pressure.

Cryogenic oxygen tank 2 was operating well within the fracture mechanics limits for sustained flaw growth; hence, neither leakage nor rapid fracture would be expected due to propagation of pre-existing flaws under the influence of pressure alone. Test data indicate that the addition of polytetrafluoroethylene combustion products to oxygen, and the immediate exposure of the mixture to a moderately stressed flaw, generated no detectable evidence of rapid sustained-load flaw growth.

Localized heating of the tank material is the probable mode of the loss of tank pressure integrity and is supported by all known test analyses and by telemetry data. Considering that only polytetrafluoroethylene was burning in the tank, then the only place where the polytetrafluoroethylene comes close to, or touches, the pressure vessel wall is in the electrical conduit. Tests of burning insulation in the electrical conduit shows that in a few seconds the generated heat fails the tube. Following the tube failure, the pressure in the annulus region would rapidly rise until the exterior shell burst disk (approximately 3 square inches) would rupture at approximately 80 psia.

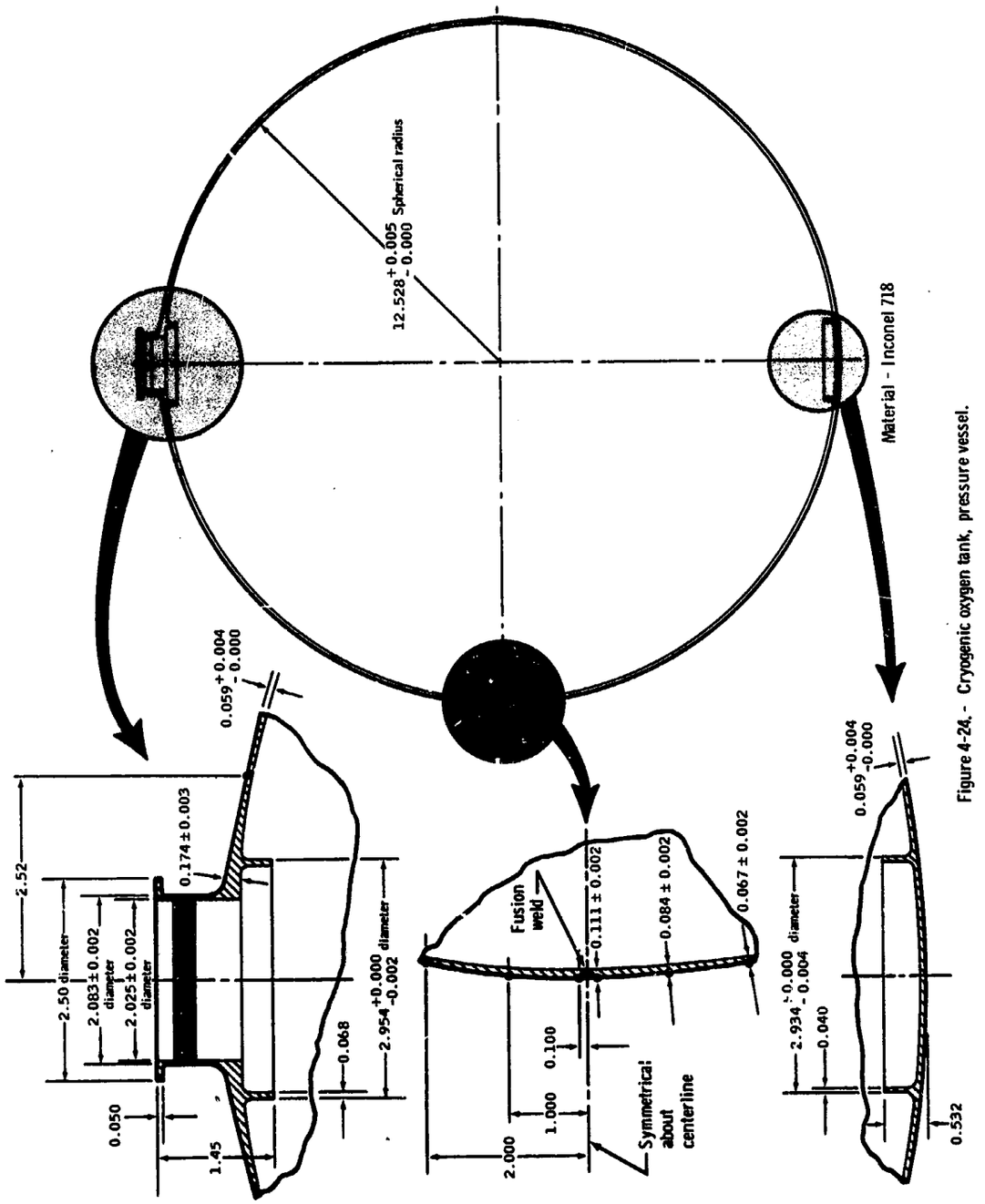

Figure 4-24. - Cryogenic oxygen tank, pressure vessel.

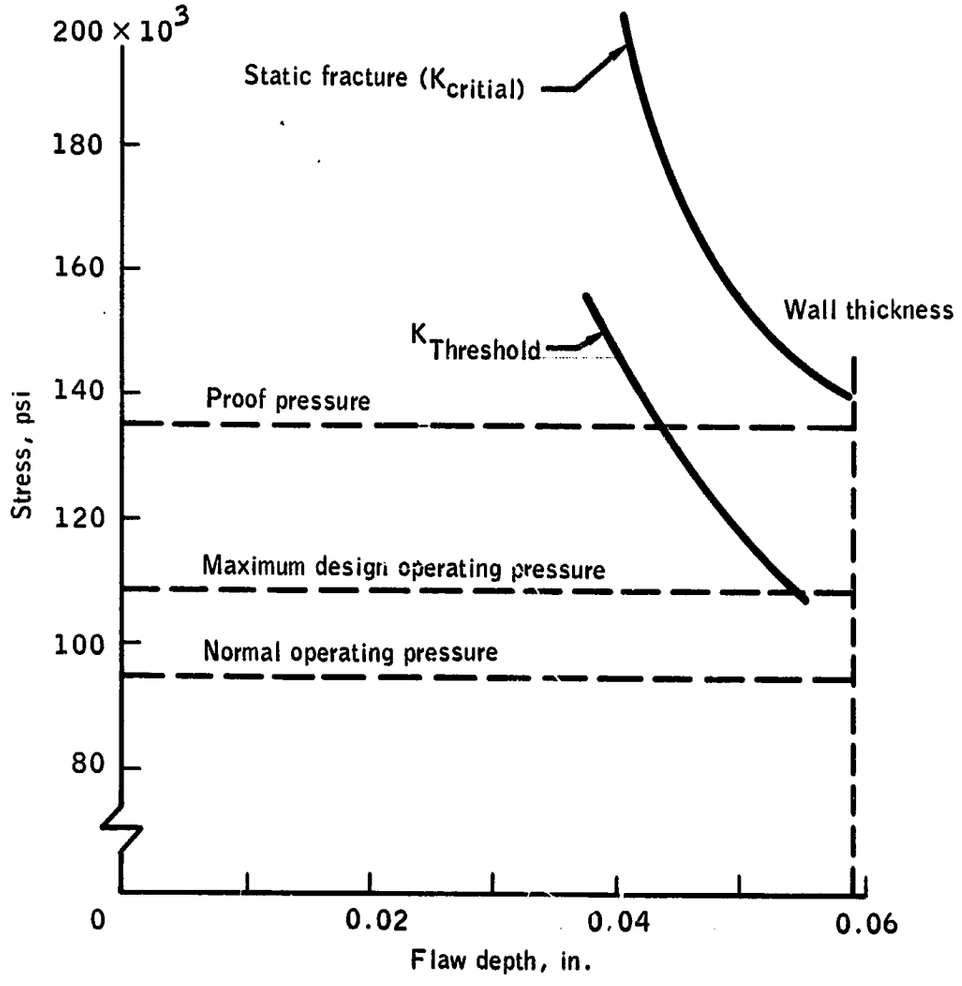

Figure 4-25.- Fracture mechanics data for cryogenic oxygen tank base material at -190° F.

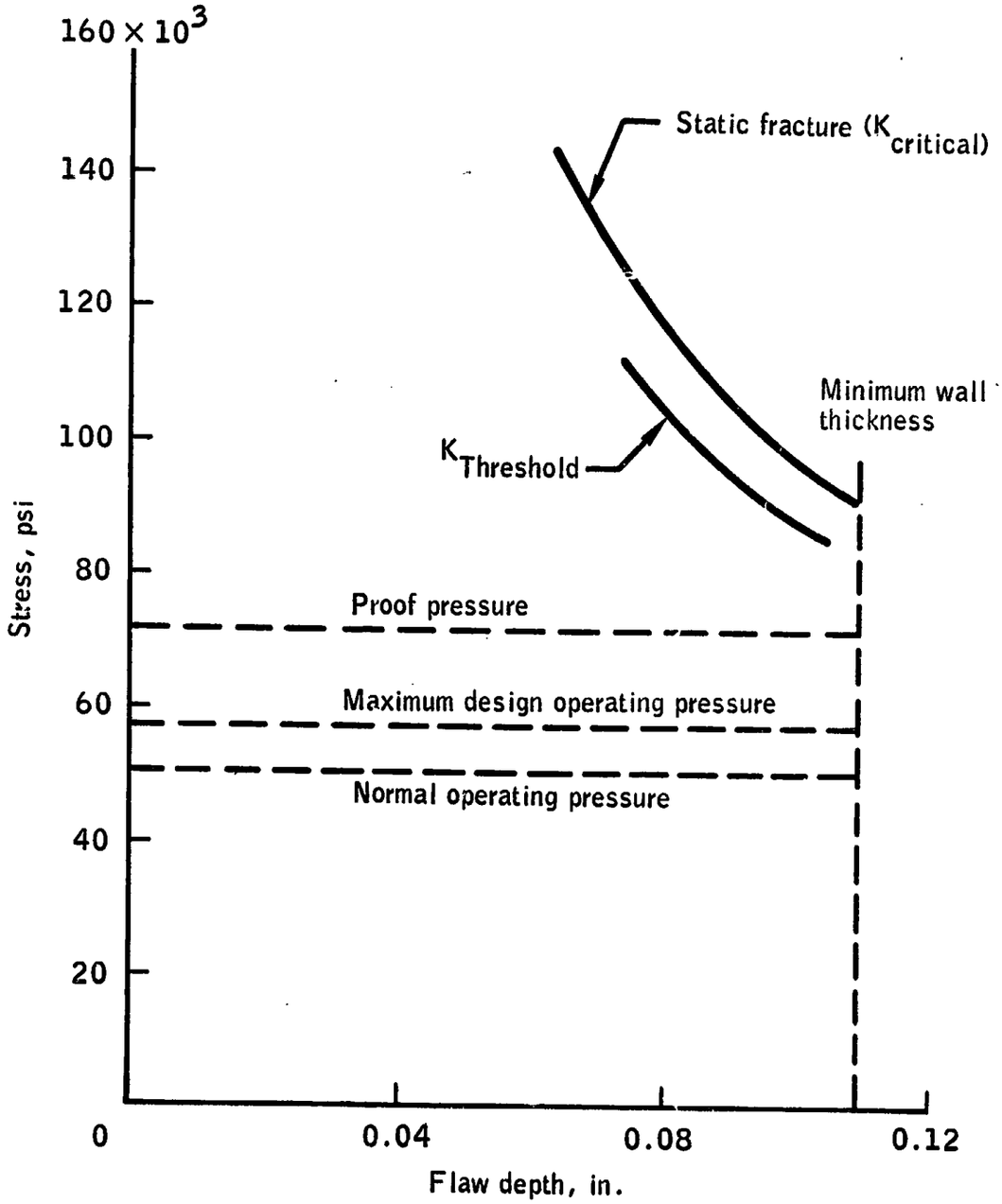

Figure 4-26.- Fracture mechanics data for cryogenic oxygen tank weld and heat affected zones at -190° F.

4.6.5 Significant Structural Events

The following interpretation and judgement of the most probable sequence of events are based on all applicable data in the 0.80-second time period prior to the loss of data (figs. 4-27 and 4-28).

At 55:54:52.763 the last pressure data from tank 2 were recorded as 996 psia and the pressure was rapidly decreasing. The fuel cell flowmeters were responding accordingly. Beyond the last pressure point, the pressure can be interpreted from fuel cell flow rates (fig. 4-28). Note the flow rates gradually decreased and then started to increase slightly. This can be interpreted to mean that the relief valve closed or that the burning rate increased.

The data at the following times are interpreted to be the first loss of pressure system integrity, and the vibration experienced during this time period is interpreted to be due to venting of the tank through the vacuum annulus.

a. At 55:54:53.182 command module accelerations in the X, Y, and Z axes indicated response of less than 0.5g, 0.1g, and 0.25g peak to peak, respectively, with an estimated frequency of 15 to 25 hertz.

b. At 55:54:53.204 the stabilization and control thrust vector control command in pitch and yaw indicates an oscillation of approximately 18 to 20 hertz, which is increasing with time. The results of full-scale testing of the docked command and service modules and lunar module to determine guidance and navigation transfer function were reviewed, as were the analytical mode shapes. These data revealed a mode at 18.76 hertz which exhibited the characteristic of motion in the area of the oxygen tank and rotational displacement at the rate gyros. Assuming 1 percent critical damping, the minimum harmonic forcing function was calculated to be 325 pounds at 18.76 hertz. The analysis shows that a forced vibration was present during this period.

c. At 55:54:53.271 the flow rate to the fuel cells reached a peak value. Based on the last pressure reading and the integration of the flow rates, the oxygen tank pressure at this time is estimated to have been less than 996 psia.

d. The next data from the fuel cell flow rate show a decrease, and may be interpreted as a change in the venting area from the initial indication of a leak. However, changes in the hydrogen flow meters at the same time place doubt on the meaning of the dropoff. Such a decrease could come from increased oxygen flow because of expulsion of the wiring from the controlling area or an extension of the original leak area due to increasing temperature.

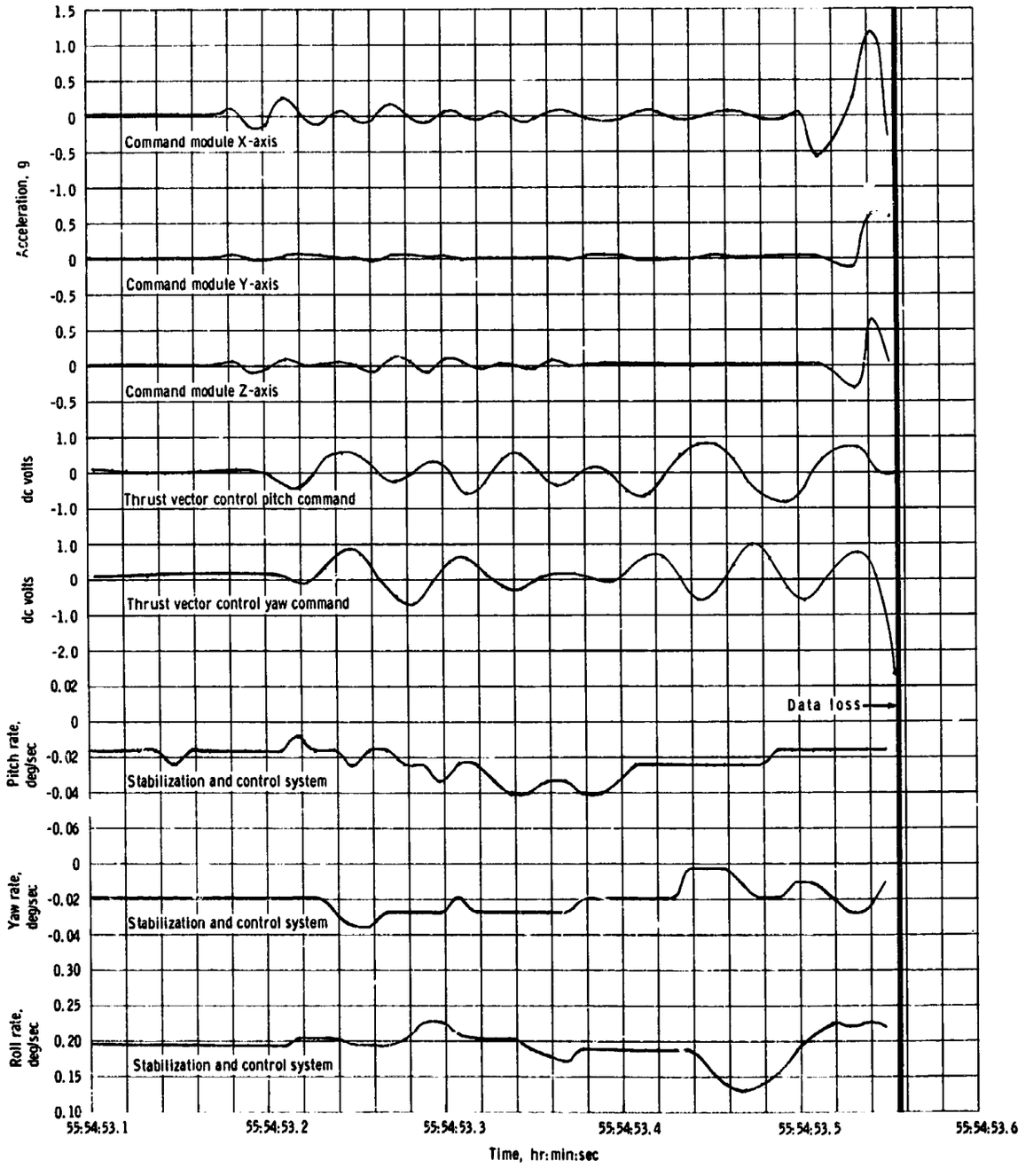

Figure 4-27. - Significant data immediately prior to data loss.

FOLDOUT FRAME 1

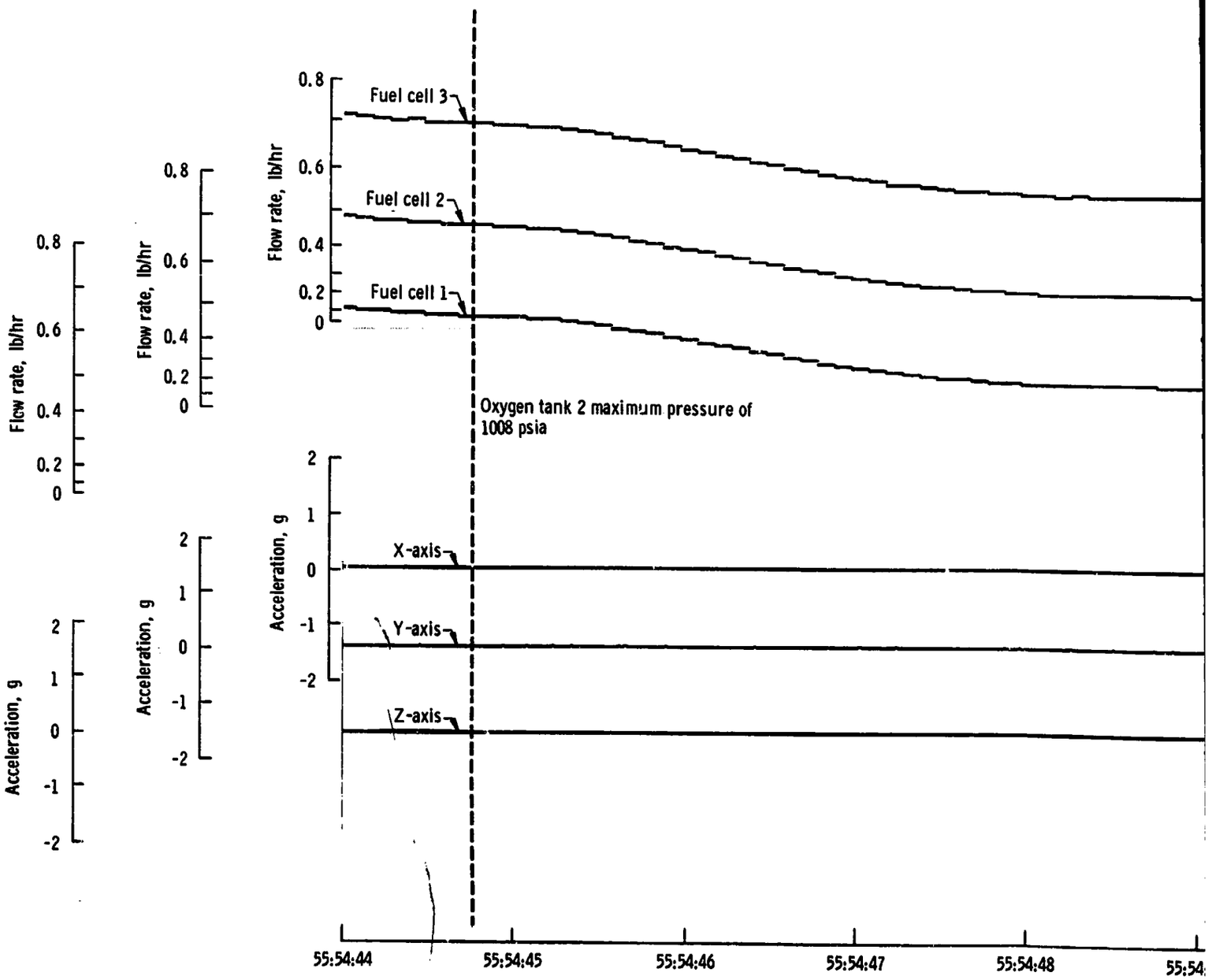

FOLDOUT FRAME 2

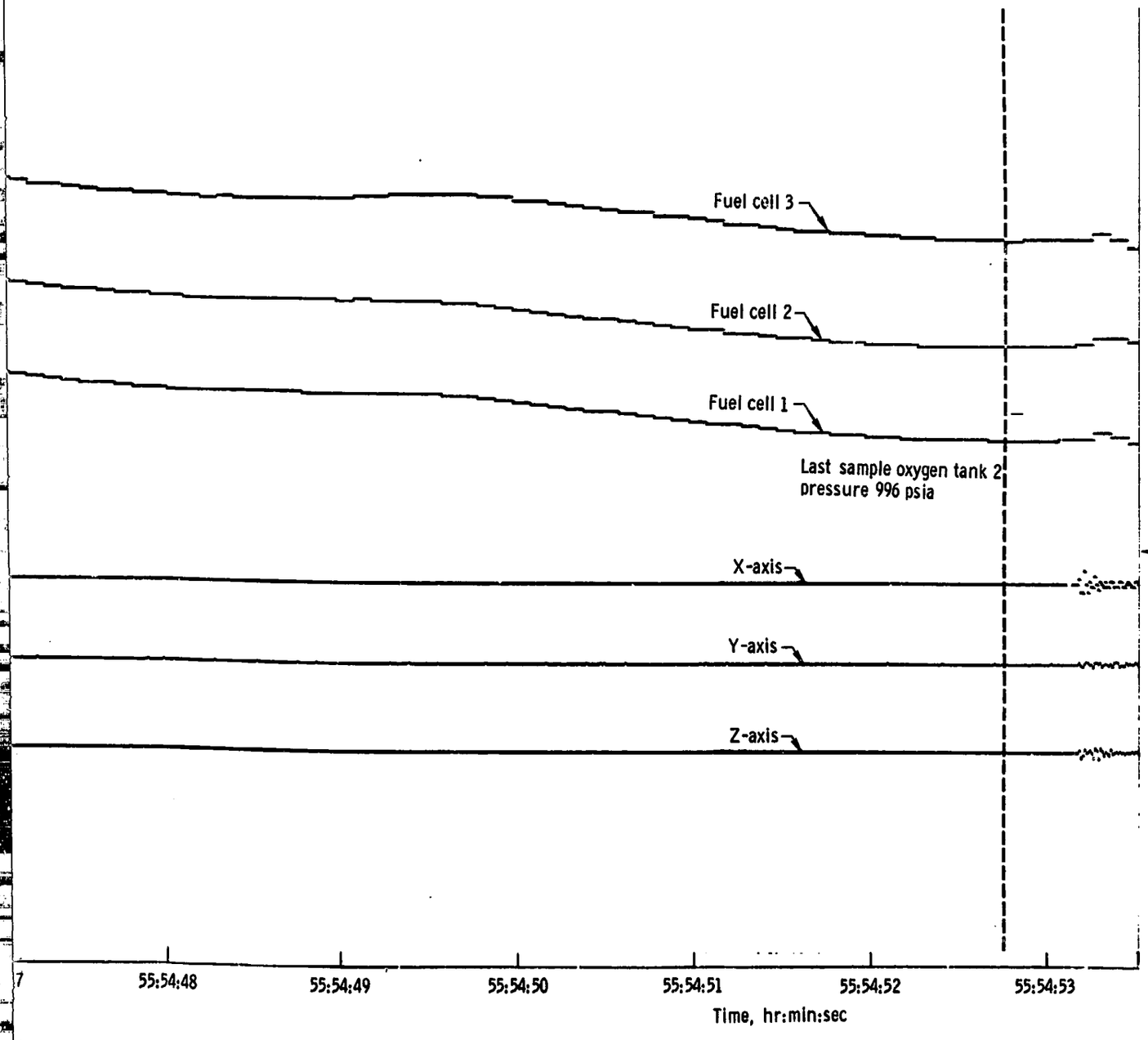

FOLDOUT FRAME 3

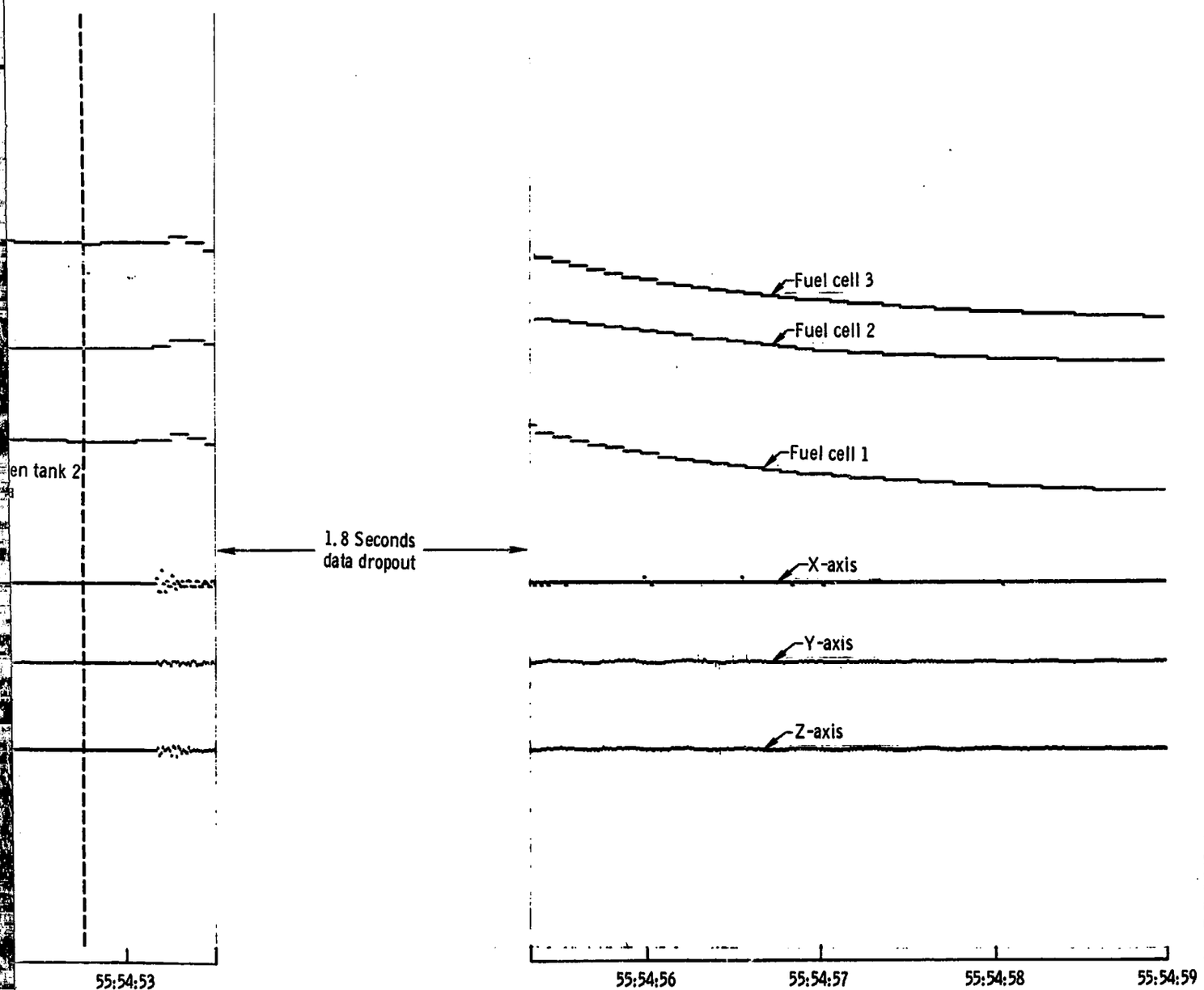

Figure 4-28. - Accelerations and fuel cell flow rates during period of incident.

Based on spacecraft current data measured at 55:54:53.472, the heaters did not come on and tank 2 pressure was above 878 psia, the heater-on point.

At 55:54:53.511, the command module X-axis accelerometer indicated minus 0.56g (fig. 4-27). This is interpreted as the start of the rapid pressurization of the bay. The Y and Z axis accelerometers responded 20 milliseconds later.

At 55:54:53.555, the data loss began. Based upon the damage noted in the photographs, this is interpreted as an impact by the separated bay 4 panel on the antenna.

a. The panel was subjected to a rapid overpressurization. To be consistent with the structural mechanics, the available strength, and the observed evidence, the peak pressures are estimated to have exceeded 20 psi.

b. An analysis of the kinematics and dynamics of the panel was performed. It was assumed that the panel failed very quickly and that contact of the panel and the high-gain antenna was limited to the damage observed to only one of the antenna dishes. The position of the antenna is shown in figure 4-29. The results of this analysis determined a required axis of rotation of the panel (fig. 4-23). Assuming a constant location of the line of action of the applied force, an approximate center of pressure can be located.

c. The foregoing analysis is consistent with the available strength (fig. 4-23). The axis of rotation required to satisfy the kinematics of panel separation, the available strength, and the photographic evidence support the origin of failure on the left side of the panel as viewed from the exterior. The response of the Y and Z axes accelerometers noted at 55:54:53.531 is consistent with a minus Y and minus Z force applied over 15 to 20 milliseconds. Analysis of the vehicle dynamics indicates a 900 to 1500 lb-sec impulse was experienced by the spacecraft. Such an impulse would require an initial total force greater than 60 000 pounds. The variation in strength with a failure mode of shear tearout in the panel is shown for loads applied perpendicular to the boundary. The allowable load applied parallel to the boundary is bounded by shear of the fastener at approximately 2200 lb/in.

Evidence of pressure and heat in the bay is indicated from the response of the temperature measurements discussed in section 4.7. The response of a measurement located on the outboard side of the oxidizer storage tank in bay 3 confirms failure of the web of radial beam 3. Damage to the beam caused the shifting of the fuel cell shelf.

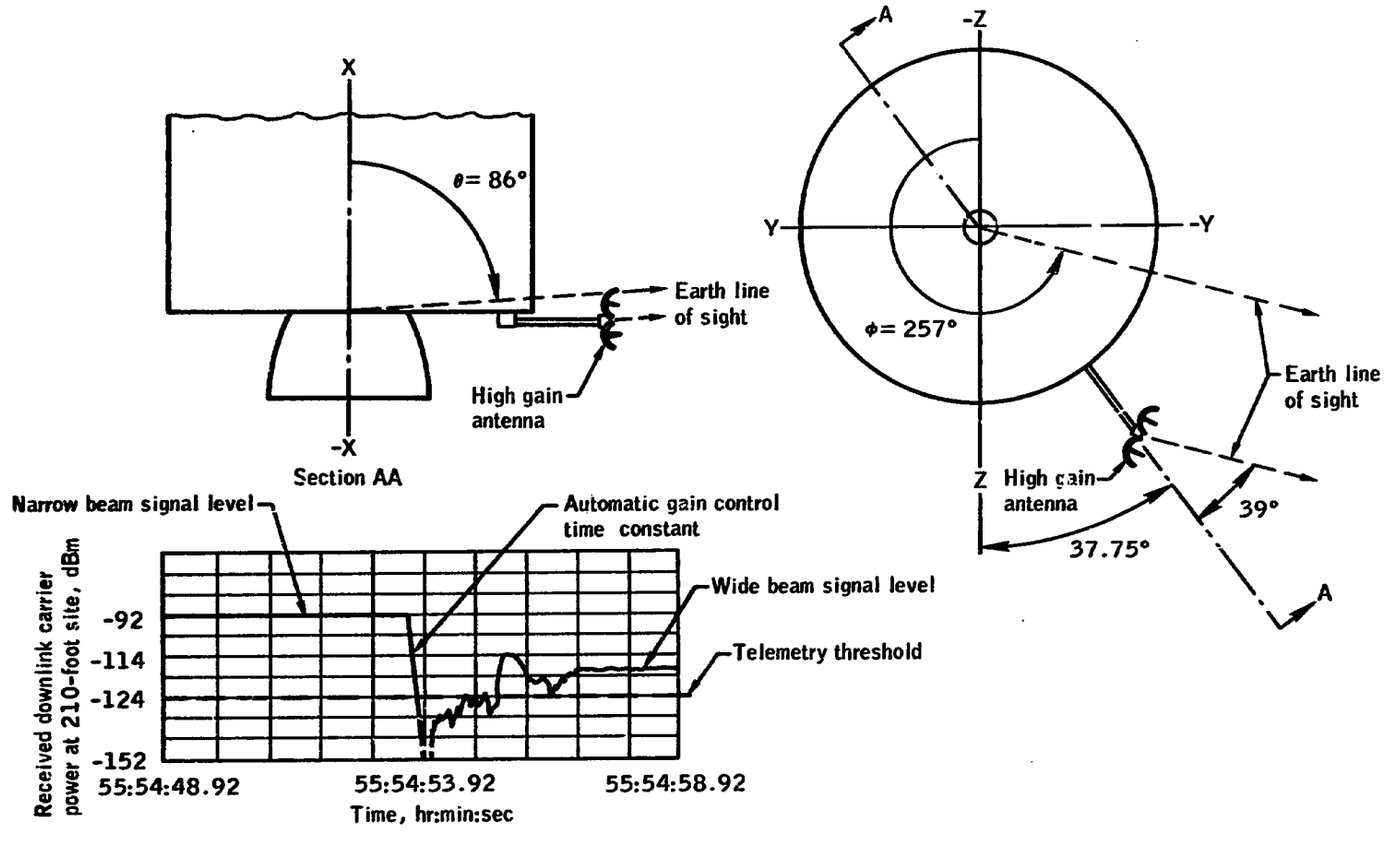

Figure 4-29.- Antenna configuration at the time of the incident.

Separation of the panel induced high shock loads to the service module as the attachments failed along the boundary and at the bay 4 shelves. This shock closed the reactant valves in the fuel cell oxygen system, as well as several reaction control propellant isolation valves.

Either the tank 2 feedline or the pressure transducer wiring or plumbing was severed during the loss of data. This explains the zero reading of low scale on tank 2 when data were recovered at 55:54:55.763. Figure 4-30 shows the plumbing and wiring on the oxygen shelf which were functional following data recovery. The figure also shows the location of the electrical leads to tank 1. After the event, the quantity and temperature sensing systems, heaters, and fans operated. The operation of these circuits and the location of the wire bundle of tank 1 with respect to tank 2 suggests there was no electrical damage associated with the loss of tank 2 pressure. Further, the motor-operated switch box through which all heater power goes for both tanks was still perative.

4.7 THERMAL EFFECTS ON SERVICE MODULE

Prior to the incident, all temperature transducers responded as expected. At the time of the incident the following measurements (fig. 4-31) indicated abnormal temperature responses:

(a) Bay 3 oxidizer storage tank surface

(b) Service propulsion helium supply line on bay 3 side of beam 3 at the inner edge of the beam

(c) Bay 3 reaction control quad C helium tank

(d) Fuel cell radiator glycol outlet lines on beam 4 in bay 4

(e) Fuel cell radiator glycol inlet lines or beam 4 in bay 4.

The bay 3 oxidizer tank surface temperature increased from 73.4° to 77.7° F in about 20 seconds (fig. 4-32). The temperature then decreased to 60° F about 2-1/4 hours later. Data received during the two command and service module power-up cycles at 101:55.54 and 123:05:25 showed 60° and 65.3° F, respectively. The rise rate of bay 3 service propulsion system oxidizer surface temperature is indicative of direct heating in the vicinity of the transducer, which is attached to the tank skin and covered with 30 layers of insulation.

Heat inputs to the bay 3 service propulsion tank surface transducer depend on the thermal integrity of the multilayer insulation blanket covering the transducer. To obtain the noted response requires severely degraded insulation, probably because of burning of the insulation or pressurization of the bay with hot gas.

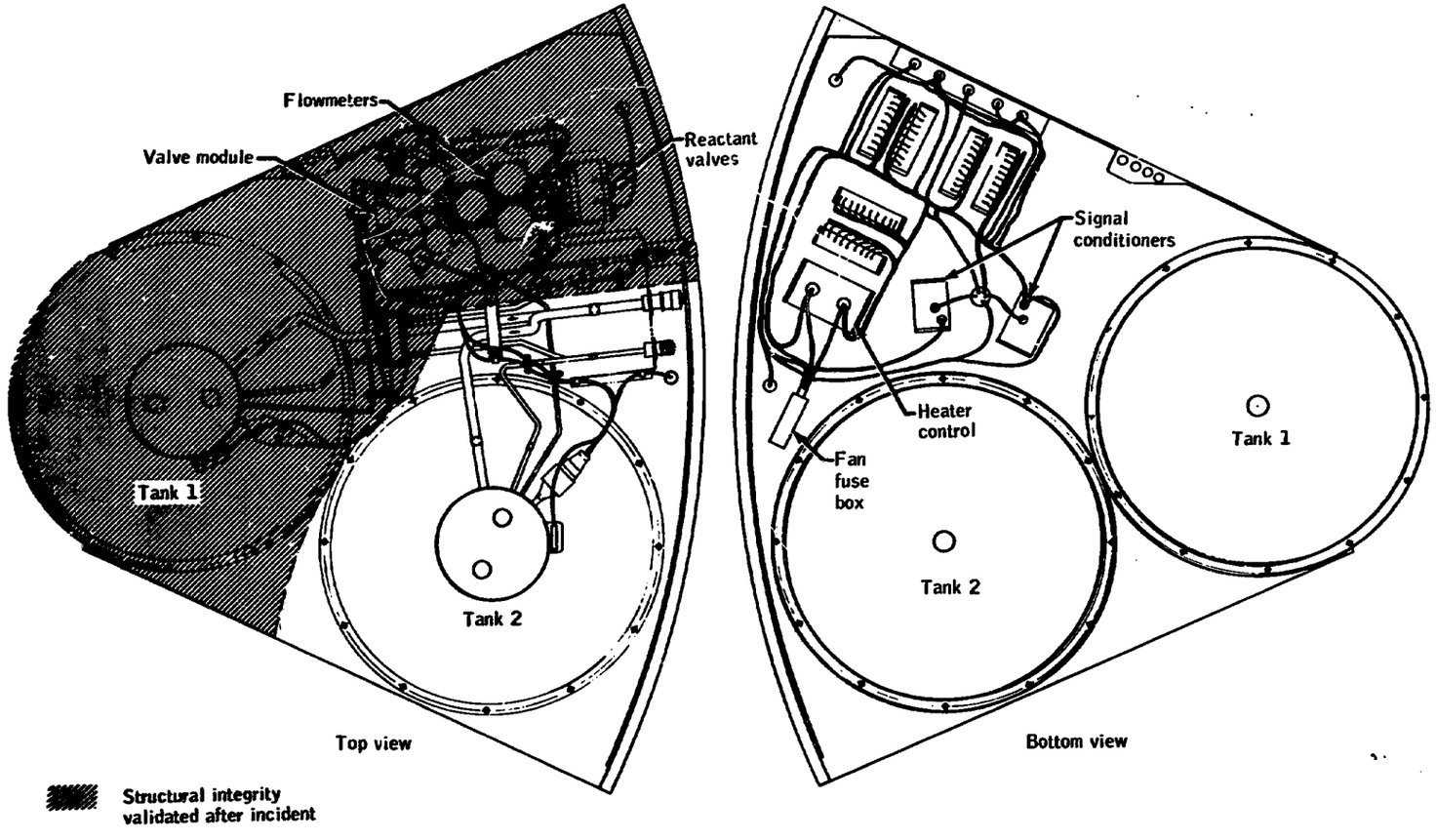

Figure 4-30.- Oxygen shelf plumbing and wiring layout.

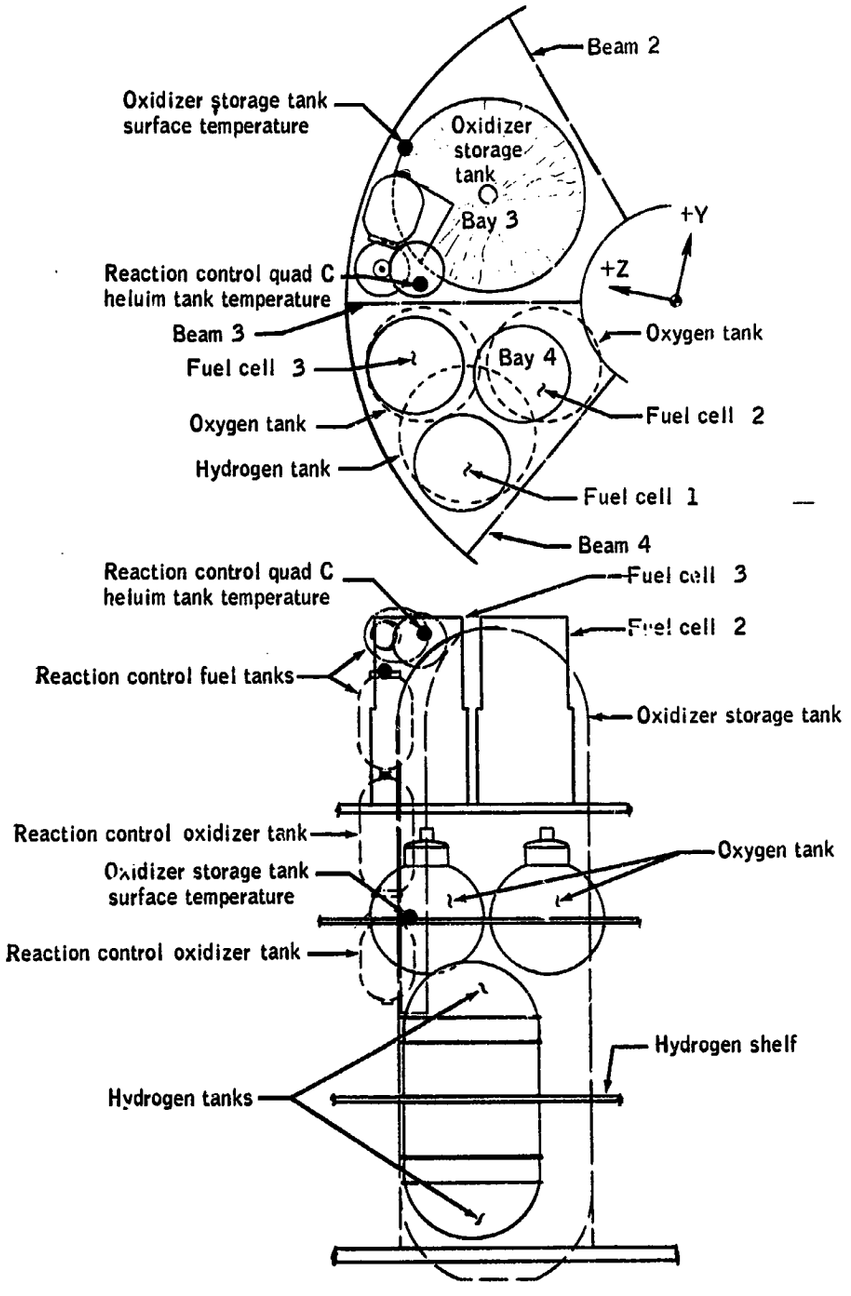

(a) View normal to beam 3.

Figure 4-31.- Temperature sensor locations.

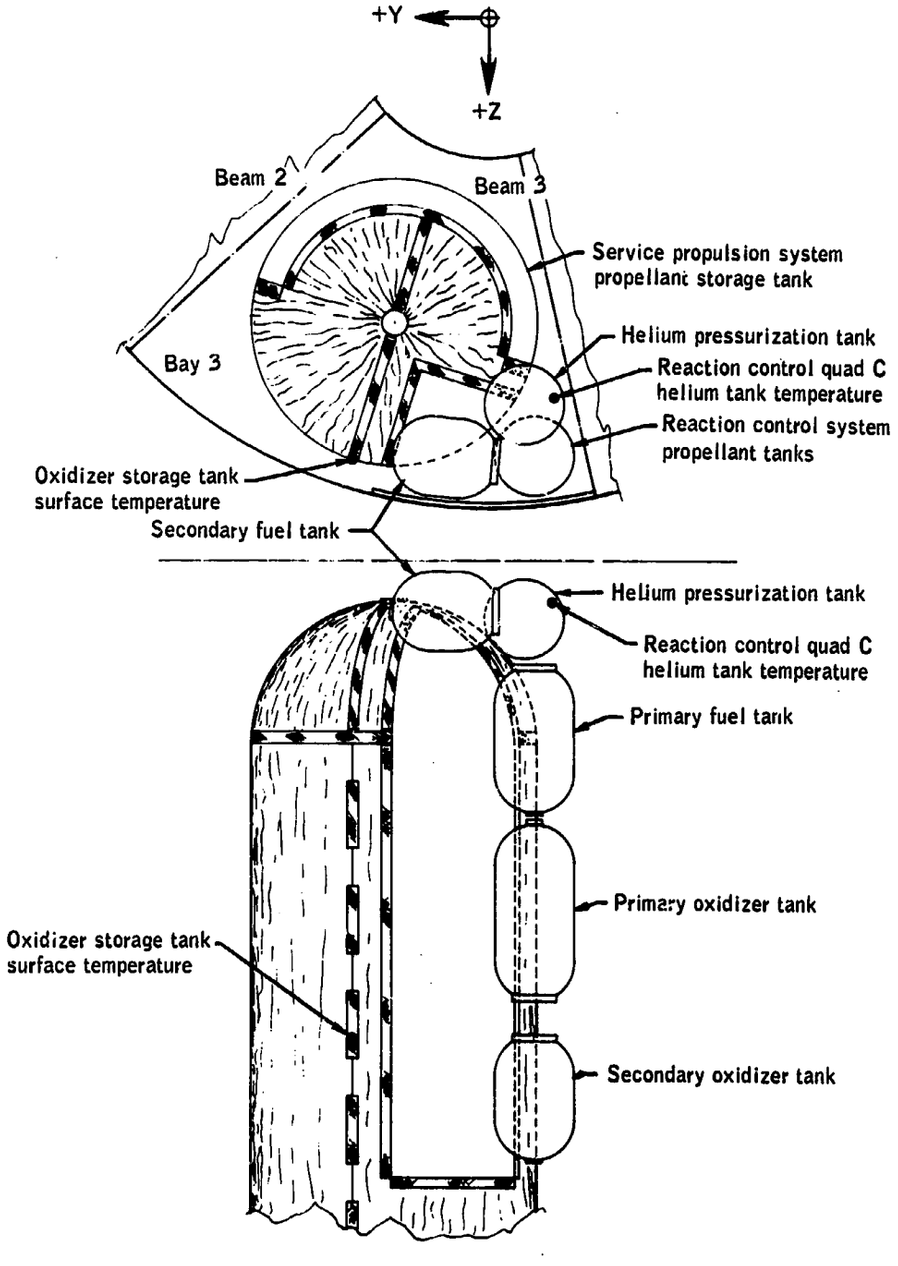

(b) View looking inboard of bay 3.

Figure 4-31.- Continued.

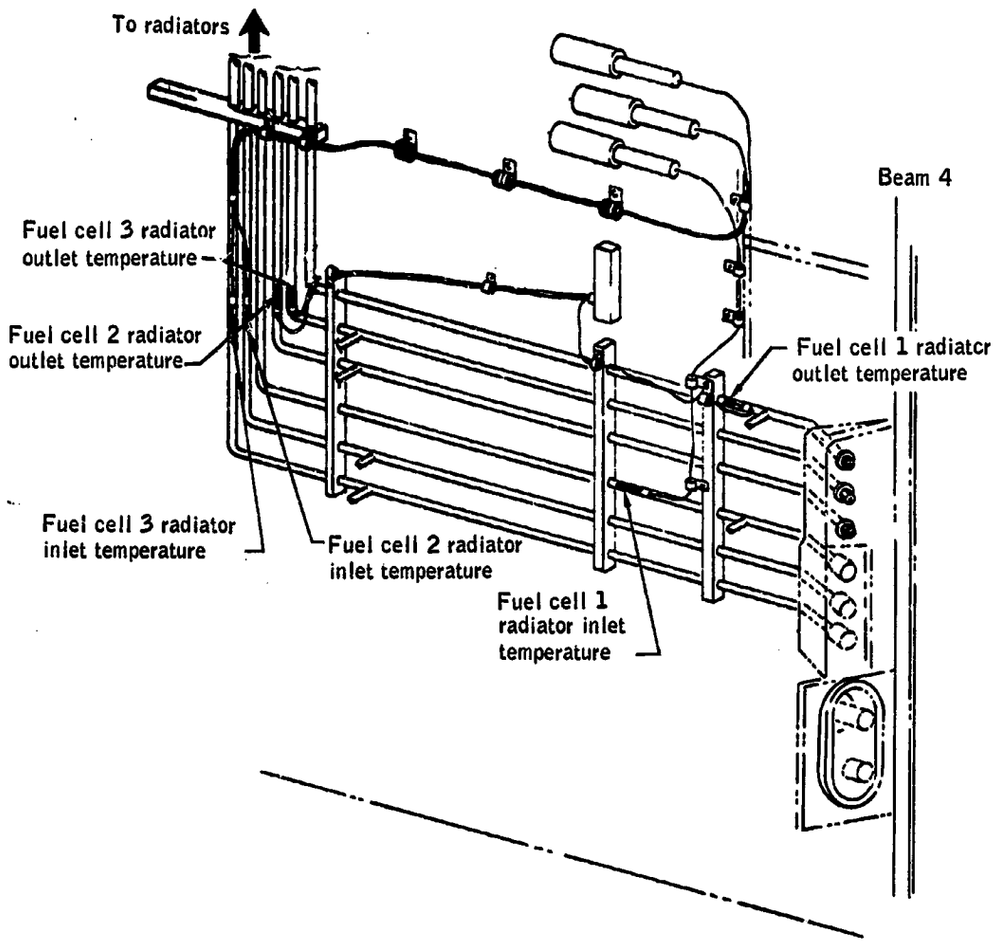

(c) View looking inboard of fuel cell shelf.

Figure 4-31.- Concluded.

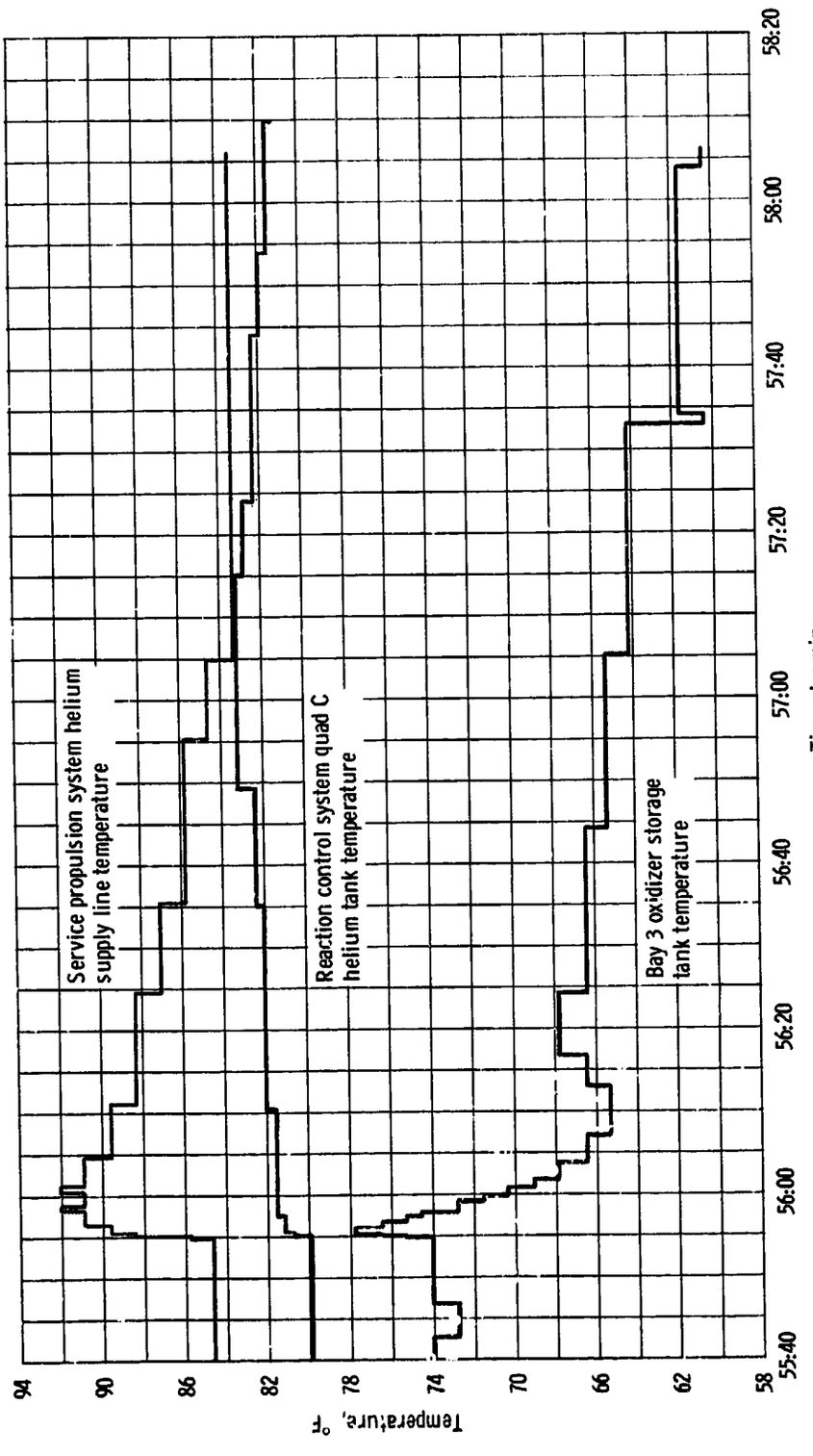

Figure 4-32. - Bay 3 and 4 structural temperatures.

The service propulsion helium line temperature (fig. 4-32) increased from 84.6° to 89° F in about 37 seconds. In 2 more minutes, the temperature had increased to 92.2° F. A gradual cooling trend followed, and 10 minutes later, the temperature had decreased to 83.4° F. During the two command and service module power-up cycles at 101:55:54 and 123:05:19, the helium line temperatures were 72.1° and 65.9° F, respectively. The initial rise rate is again indicative of direct heating in the vicinity of the transducer. However, unlike the oxidizer tank surface temperature, the gradual decrease in helium line temperature, after the initial rise, is indicative of a cool-down response to radiant heat loss. The helium line cooled gradually because of the lower temperature levels with the fuel cells shut down and the bay 4 panel missing.

Bay 3 reaction control quad C helium tank temperature (fig. 4-29) rose from 79.7° to 81° F in about 10 seconds. The temperature continued to rise to approximately 83° F about 5 minutes later, then it gradually decreased to 81.6° F.

Although all fuel cell radiator glycol inlet and outlet temperatures showed perturbations, the fuel cell 3 radiator inlet temperatures exhibited the largest response. The temperature increased from 93.1° to 97.4° F in 3 seconds or less. This represents the highest response rate noted from any of the transducers at the time of the incident. The data for fuel cell 3 radiator inlet temperature, and for other transducers, are shown in figure 4-33. A correlation of these data has been performed and it is concluded that these transducers could have been exposed to a sudden change in temperature environment prior to the data loss. An extrapolation can be made which would support the response noted at the time of the heat pulse (fig. 4-33), but it would depend on the heat input function. Tests performed with the temperature sensor installed on the glycol line and with glycol flowing indicate that the heat pulse would lead the rise point by about 0.25 second. The rise point can reasonably be extended to any time during the data loss. Assuming the rise point started at the time of the data loss, then the heat pulse would have started at approximately the same time as the accelerometer disturbances, indicating that the high heating rate started before the bay 4 panel separated. The data indicate that the high-heating environment extended throughout bays 3 and 4.

4.8 SPACECRAFT DYNAMIC RESPONSE

At the time of the incident, spacecraft attitude control was being provided by the digital autopilot in the primary guidance, navigation, and control system. At 55:51:23 an automatic maneuver had been initiated to the attitude specified for observation of the Bennet Comet, and the spacecraft was rolling at 0.2 degree/second. All reaction control system

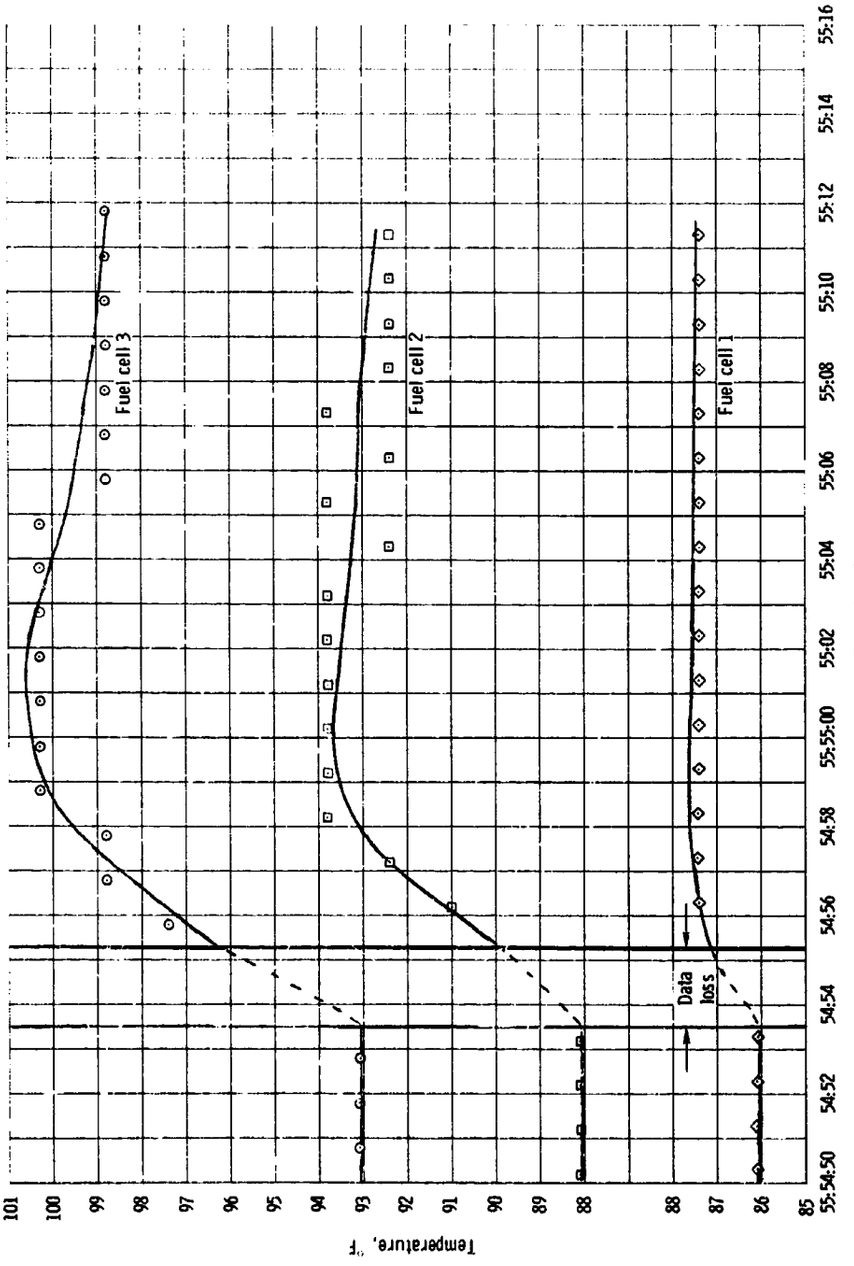

(a) Radiator inlet.

Figure 4-33. - Fuel cell glycol temperatures.

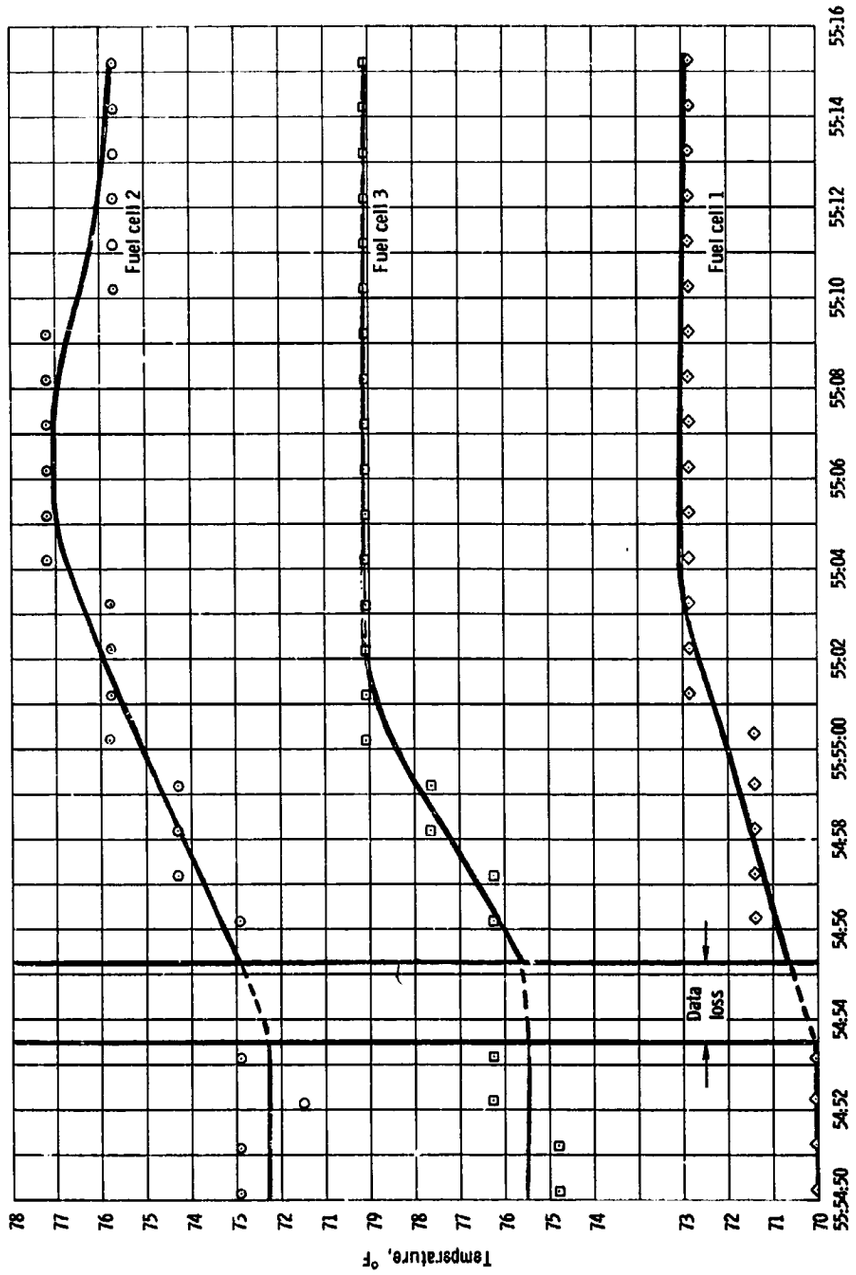

(b) Radiator outlet.

Figure 4-33. - Concluded.

quads were enabled for pitch and yaw and quads A and C for roll. No engines were firing at the time of the incident. All guidance and control system equipment was powered up except the optics.

The stabilization and control system recorded the small body rate oscillations described in section 4.6, at 0.28 second before the loss of data. When data were regained, negative rates were present in all three axes (fig. 4-34). The oscillations shown in the pitch and yaw axes on the figure are predominantly due to excitation of the first bending mode (2.7 hertz). The reaction control engine firings which occurred following resumption of data were proper for the conditions that existed. The resulting angular accelerations in pitch and roll, however, indicate that only one thruster was acting in each axis and that quad C was inoperative. The total attitude change was small (fig. 4-35).

The loss of data precludes an accurate estimation of the character of the torque applied; however, the net change in angular kinetic energy was approximately 90 ft-lb.

The inertial measurement unit accelerometers recorded a net velocity change of 0.4 ft/sec, predominantly in the vehicle Y-Z plane. An accurate assessment of the direction of the force cannot be made because the magnitude is at the one or two data bit level (0.18 ft/sec/bit). Assuming, however, that the measured velocity change was accurate and that thruster firings did not degrade the measurement, the net change in translational kinetic energy was approximately 250 ft-lb.

Venting followed the incident and attitude control was maintained automatically by the digital autopilot until the loss of main bus B when the last minus pitch thruster was disabled. Periodic attempts were made to reestablish attitude control manually using the thruster emergency coils until the thrusters were reconfigured to main A. The venting disturbance torque is shown in figure 4-36. Figure 4-37 contains a time history of network doppler data and shows the effect of venting as well as uncoupled thruster firings.

4.9 LOSS OF TELEMETRY DATA

Prior to the incident, the spacecraft was transmitting and receiving the S-band signals through the high-gain antenna, which was operating in the auto-track and narrow beam mode. Immediately before the incident, the high-gain antenna was pointing along the line-of-sight shown in figure 4-29.

At 55:54:53.57 all ground station receivers lost phase lock because of a sudden interruption of the signal. Two-way phase lock was regained

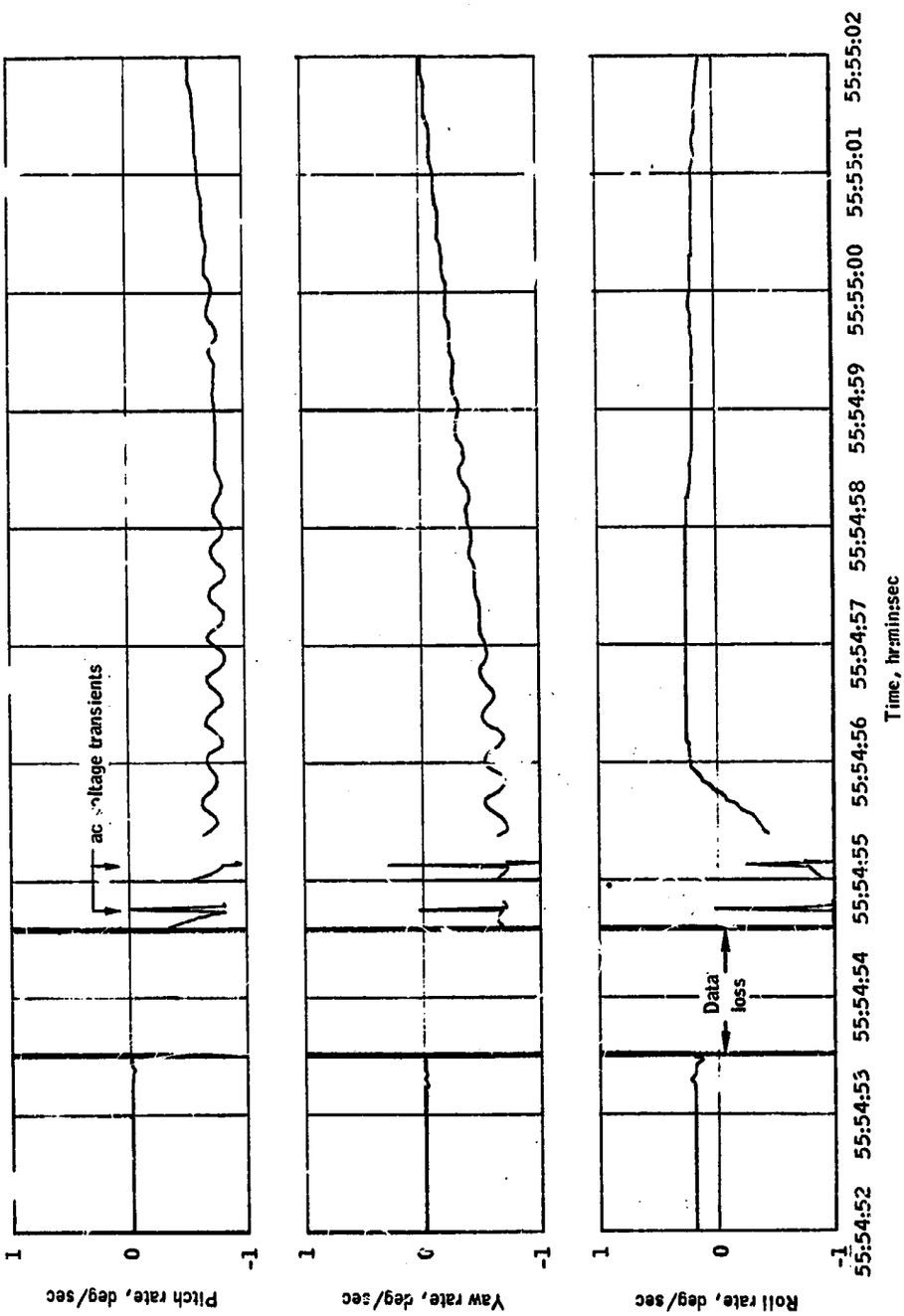

Figure 4-34.- Spacecraft dynamics during cryogenic oxygen tank 2 anomaly.

FOLDOUT FRAME 1

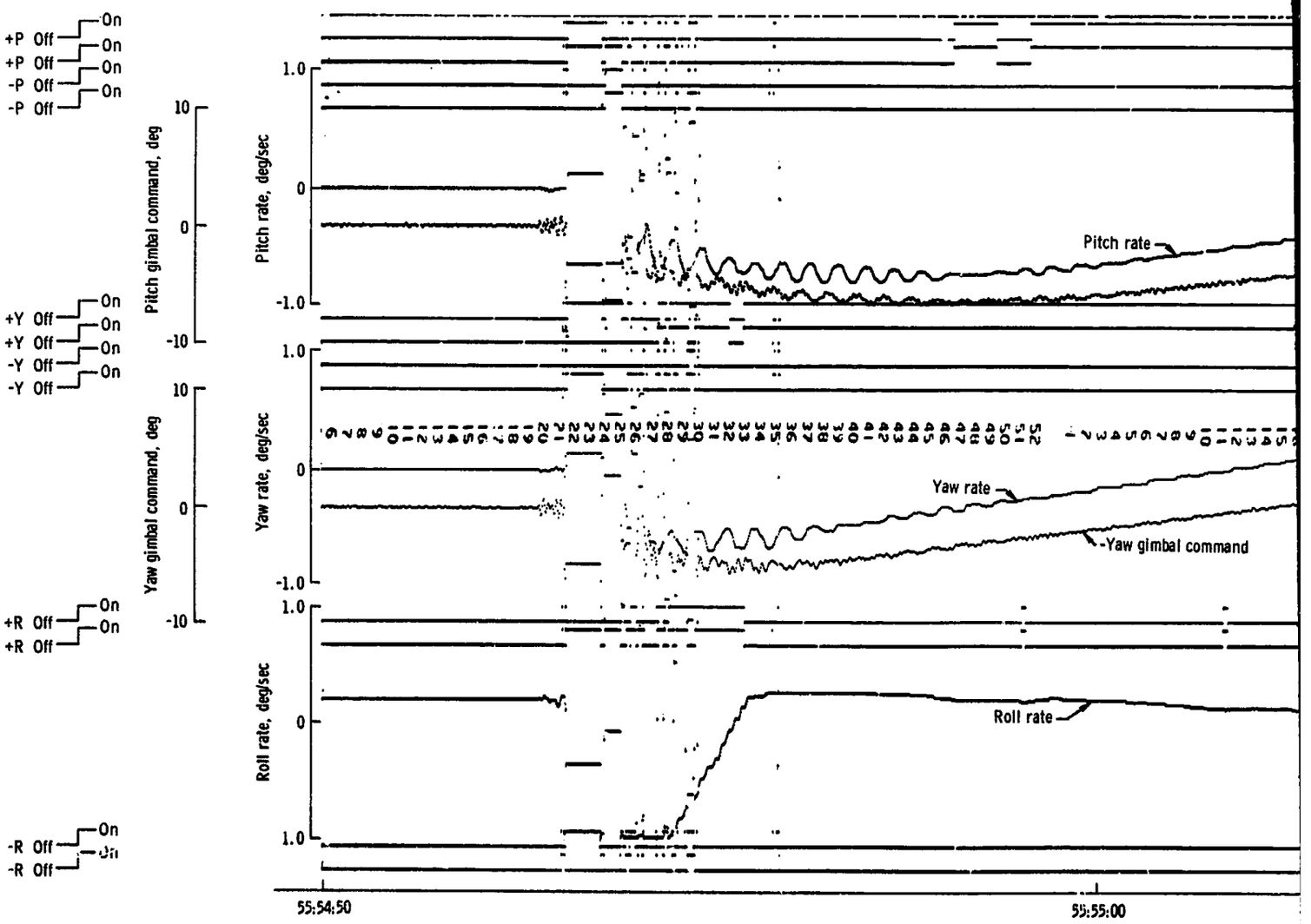

FOLDOUT FRAME 2

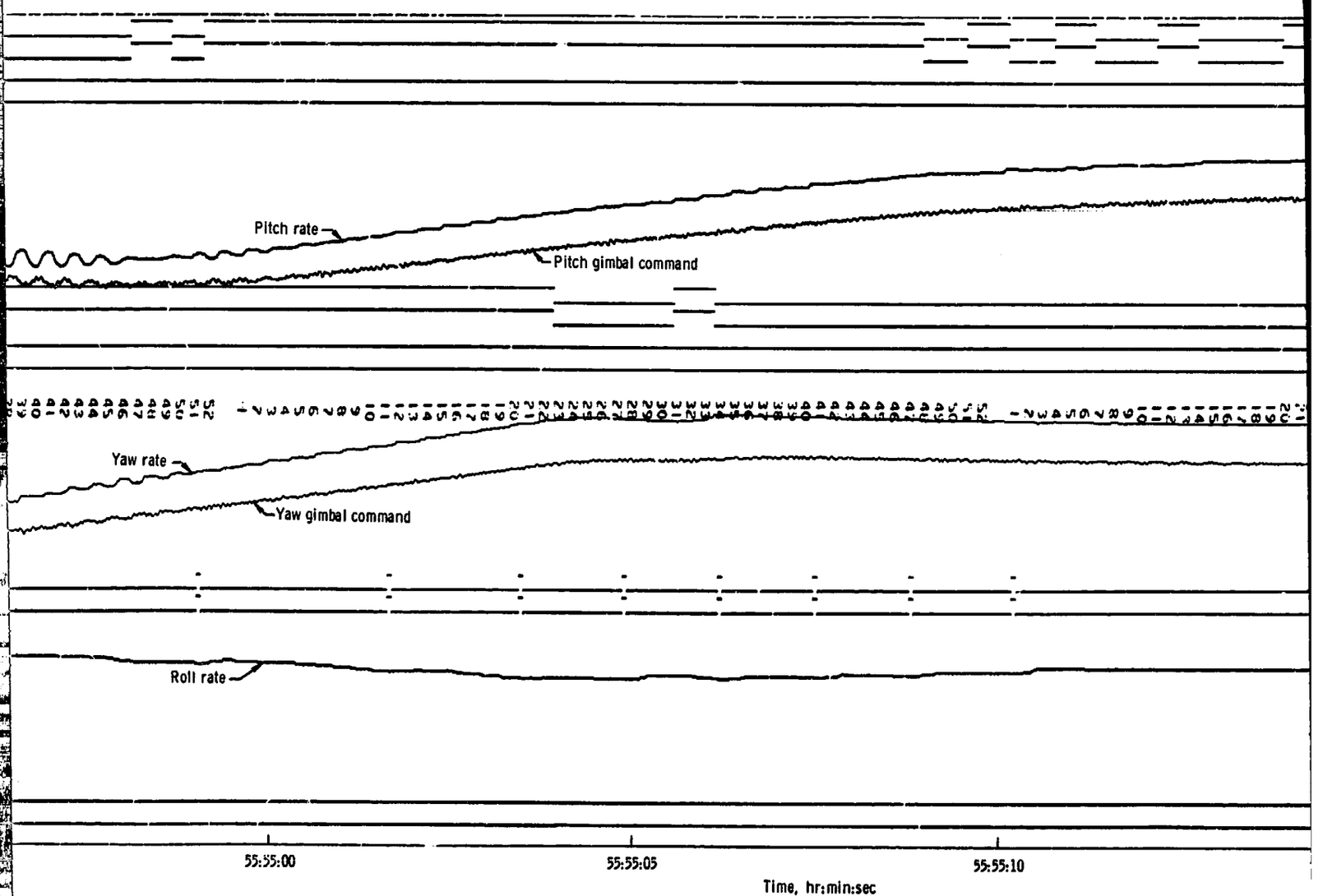

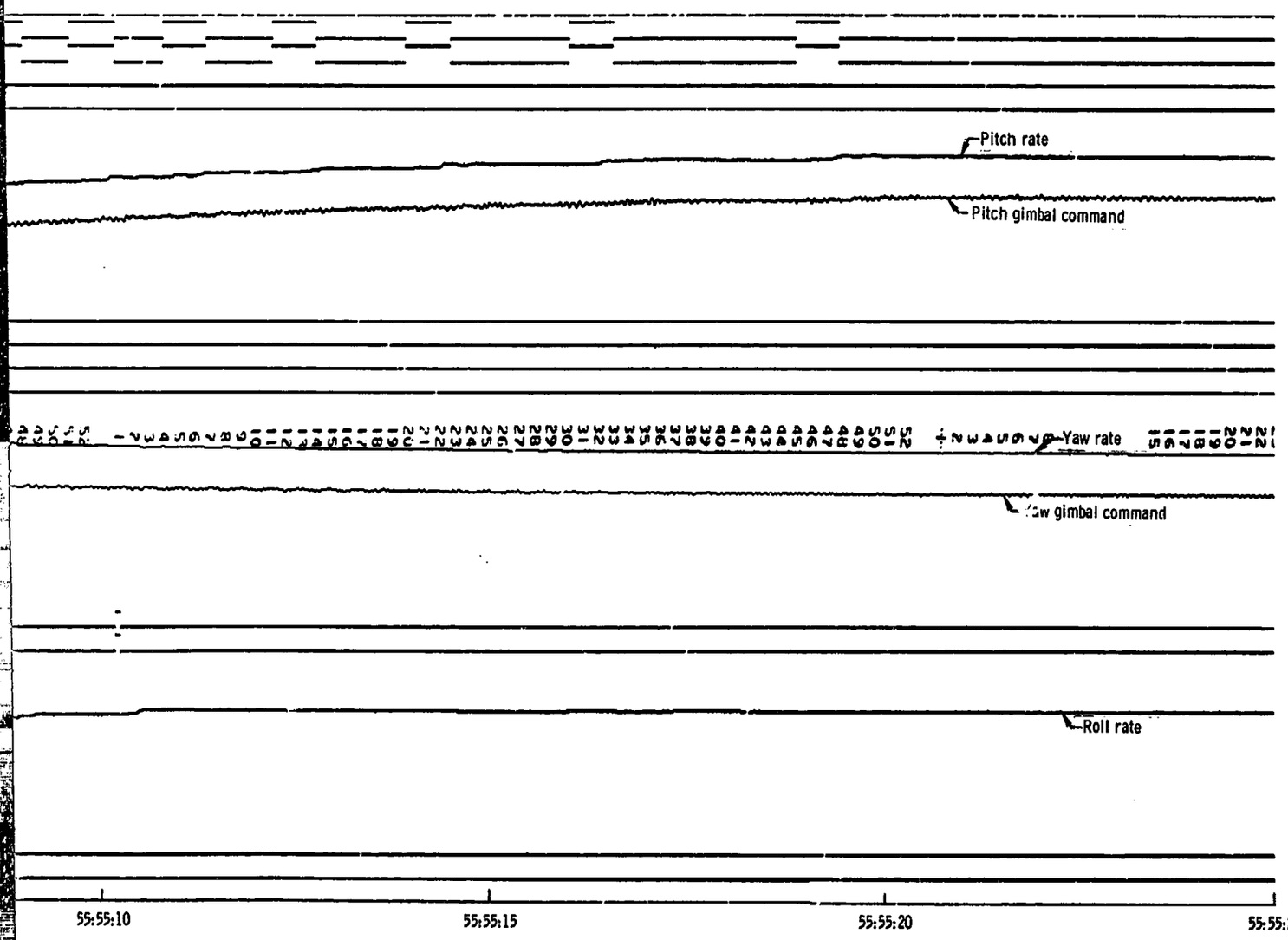

Figure 4-35. - Spacecraft dynamics during period of interest.

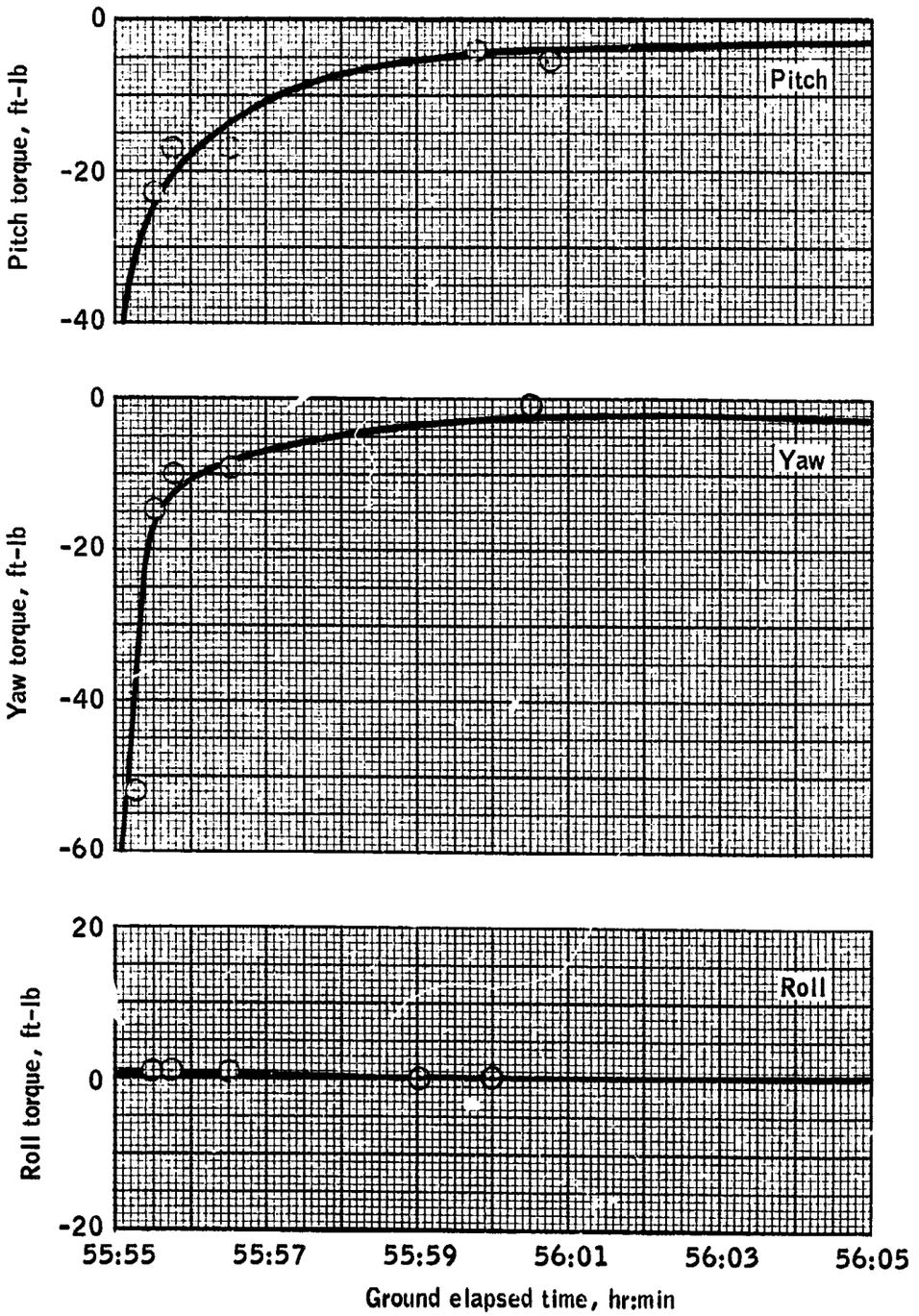

Figure 4-36.- Angular disturbances sensed by guidance and control systems.

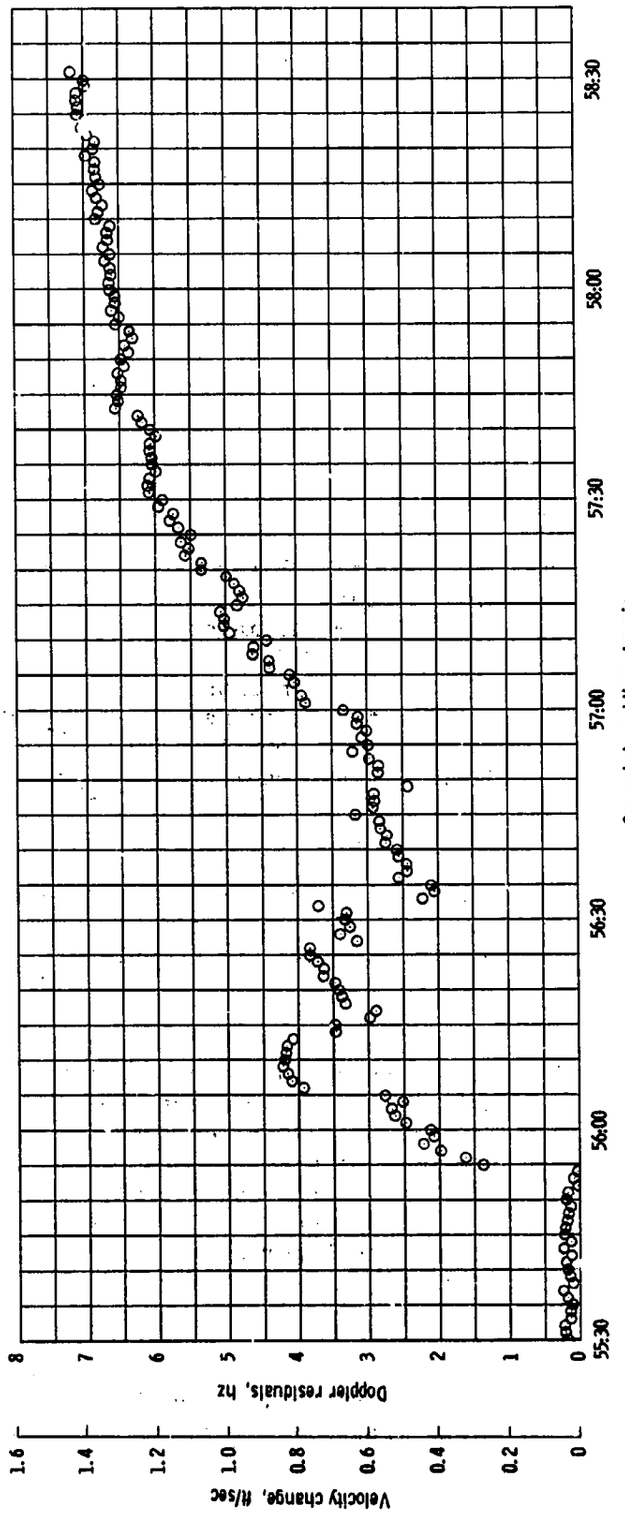

Figure 4-37.- Network doppler data during period of interest.

at 55:54:54.12. As shown in figure 4-29, the received carrier power increased to a level consistent with receipt of good quality high bit rate telemetry data through the Goldstone 210-foot antenna at 55:54:55.37.

The data indicate that the interruption of signal was caused by the physical damage to one of the four high-gain antenna dishes required for the narrow beam mode. The data also indicate that the high-gain antenna automatically switched to the wide beam mode.

4.10 LOSS OF FUEL CELL PERFORMANCE

Three fuel cells are located in bay 4 of the service module (fig. 3-2). Each fuel cell consists of a cell stack, hydrogen and oxygen control systems, a water removal system, and a thermal control and heat rejection system (fig. 4-38).

Following the incident, the fuel cell 1 regulated nitrogen pressure indication was at the lower limit of the measurement. The nitrogen regulator is internally referenced to vacuum and maintains an absolute level of the nitrogen gas over the full range of fuel cell operating conditions The regulator vents downstream pressure to maintain control of overpressure. The oxygen and hydrogen regulated pressures, which are referenced to the nitrogen system pressure, remained normal after the loss of indicated nitrogen pressure, confirming that proper nitrogen pressure was maintained by the regulator. Consequently, there was a loss of the instrumentation during the data dropout period.

About 2.5 minutes after the loss of pressure in cryogenic oxygen tank 2, the regulated oxygen pressures for fuel cells 1 and 3 decreased to nitrogen system pressure levels such that these fuel cells could no longer support a load.

The oxygen and hydrogen regulators are similar in operation to the nitrogen regulator. The regulators maintain the reactant pressure at a constant level above the nitrogen reference pressure over the full range of gas consumption — from zero flow to full power operation plus purge. The oxygen and hydrogen pressure must be maintained at a minimum of 2 psi above the nitrogen reference pressure to prevent the electrolyte solution (aqueous potassium hydroxide) from crossing the electrode interface (fig. 4-39) and causing loss of fuel cell performance. Figure 4-40 shows the pressure decay at which point the fuel cells were flooded, causing a subsequent loss of performance.

The pressure decays on fuel cells 1 and 3 were caused by closure of the fuel cell oxygen reactant shutoff valves. When the valves closed, a volume of high pressure oxygen was trapped between the reactant valves

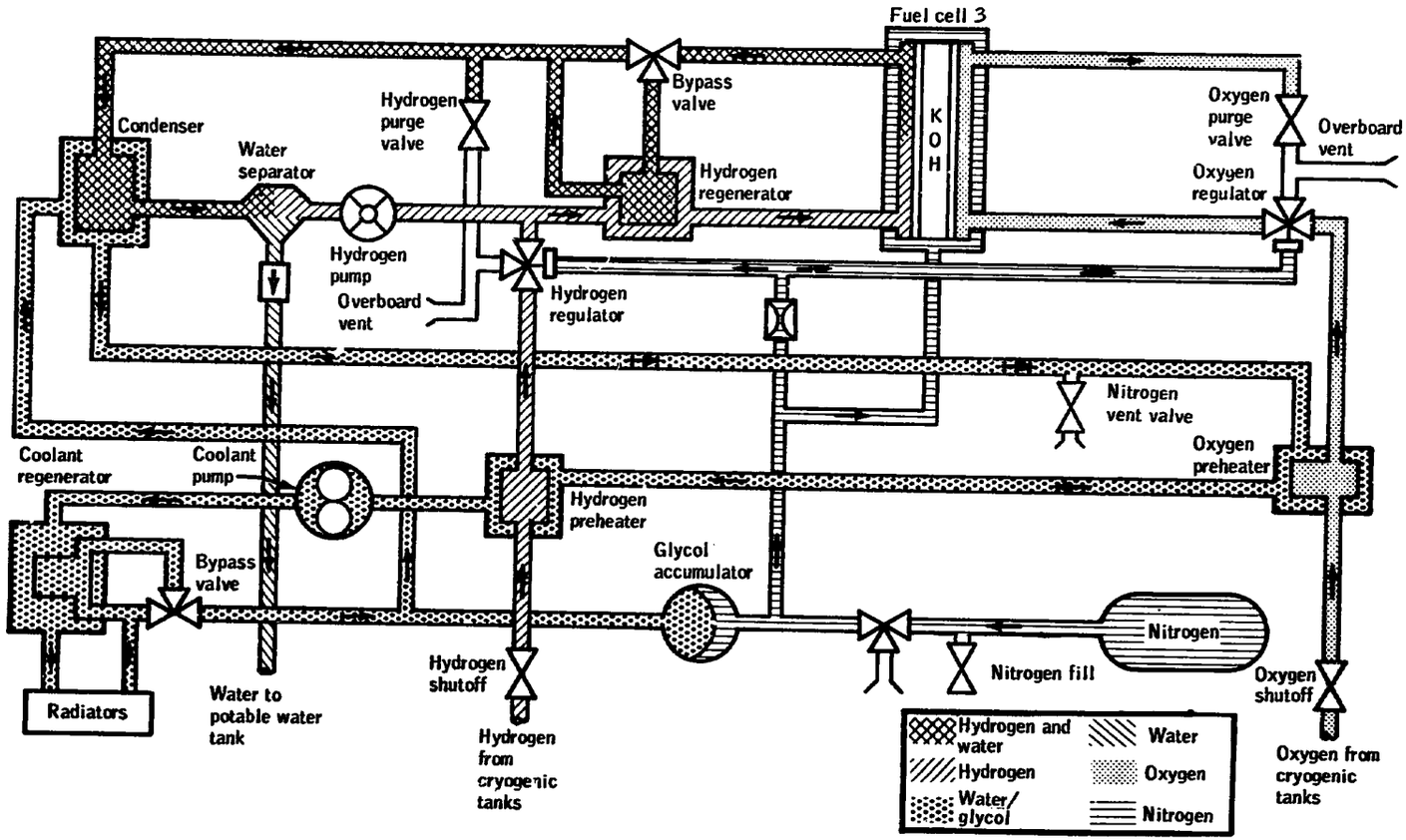

Figure 4-38.- Typical fuel cell schematic.

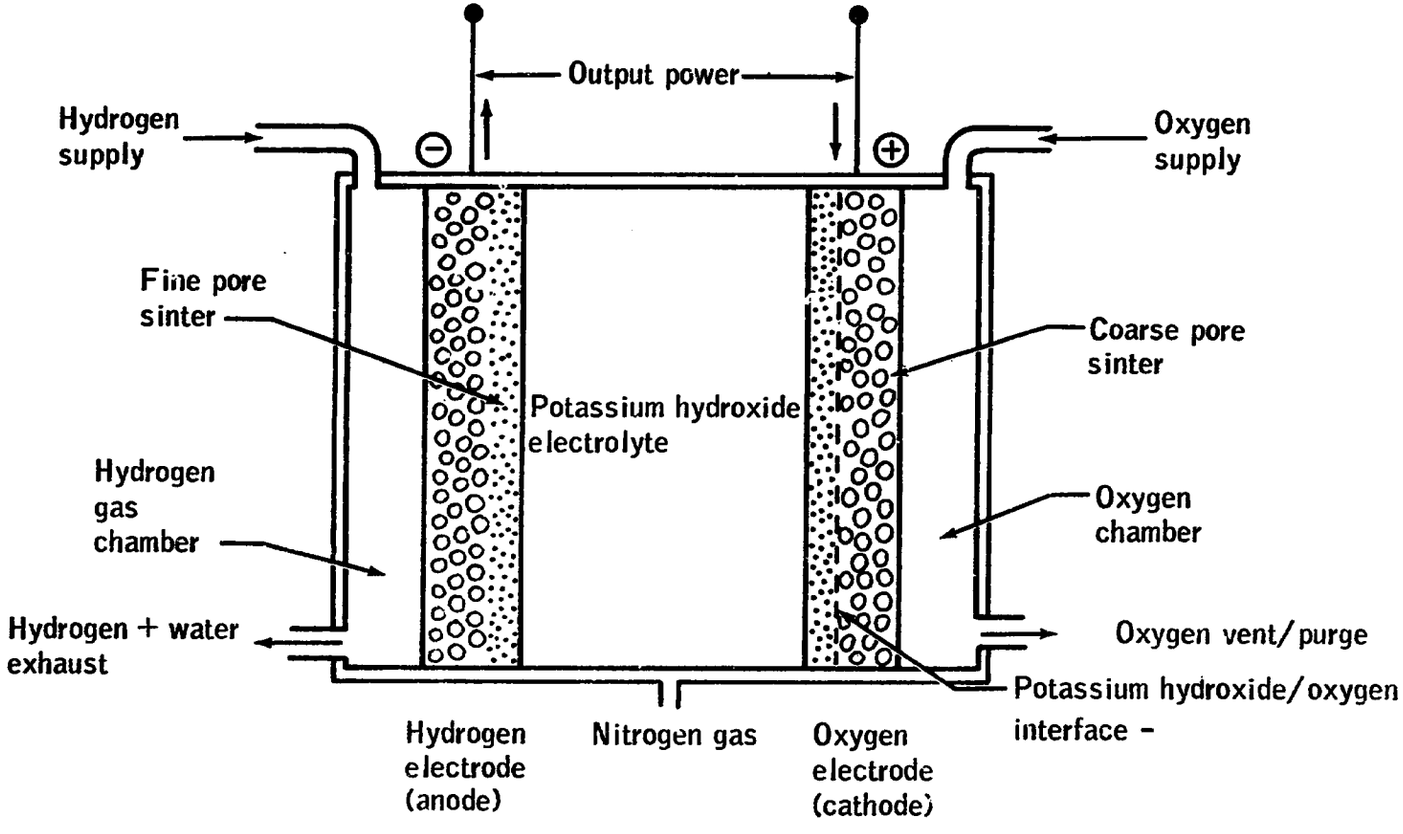

Figure 4-39.- Typical fuel cell functional diagram.

and the fuel cell oxygen regulators. This oxygen was sufficient for fuel cell operation for about 2.5 minutes, the time required to deplete the trapped supply. The agreement between the calculated and actual operating time after valve closure (fig. 4-40) verifies that fuel cells 1 and 3 were starved of oxygen and eventually could not support an electrical load.

Impact tests on the oxygen solenoid valves (fig. 4-41) show that a shock in excess of 86g for 11 milliseconds duration can be expected to cause valve closure under operating conditions.

The presence of a shock is further verified by the fact that the service module reaction control valves on quad C were closed. These valves can be switched closed at levels of 80g in 10 milliseconds. Flight experience has frequently shown a closure of one or two of the reaction control isolation valves when the service module is separated from the adapter panels; an explosive charge is used to sever the skin attachment.

The crew did not receive an indication of the shock closure of the solenoid valves since the hydrogen and oxygen solenoid valve "talkback" indicators are electrically connected in series for each fuel cell. The detection system, therefore, will show "barberpole" only when both the hydrogen and oxygen valves are closed for a fuel cell and not for closure of either valve.

Fuel cell 2 performance was normal before and immediately after the period of data loss. When fuel cells 1 and 3 were removed from the buses, fuel cell 2 assumed the total spacecraft electrical power load of approximately 60 amperes. Fuel cell 2 continued to operate normally until approximately 57 hours 46 minutes when the oxygen tank 1 pressure decayed to below the required inlet pressure of the fuel cell oxygen regulator. The oxygen regulated pressure then dropped to the nitrogen pressure level where the fuel cell could no longer sustain the load and was removed from the bus. The failure mode was identical to that experienced by fuel cells 1 and 3.

Three caution and warning alarms for fuel cell 2 hydrogen high flow rate occurred at about 56 hours and were caused by fuel cell 2 supporting the high power loads, which exceeded the 0.1617 pound per hour alarm trip level for hydrogen flow.

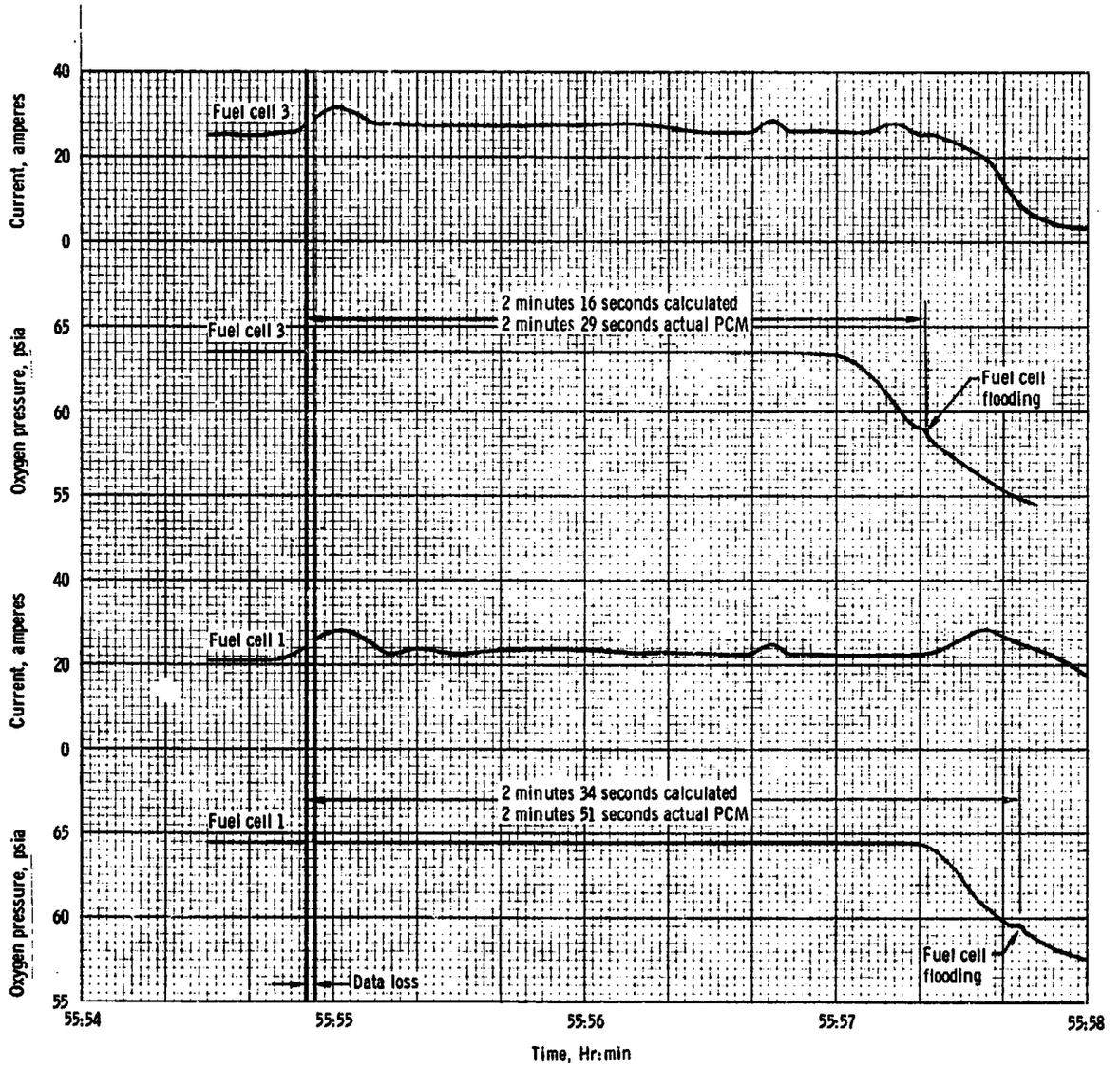

Figure 4-40. - Fuel cells 1 and 3 performance loss.

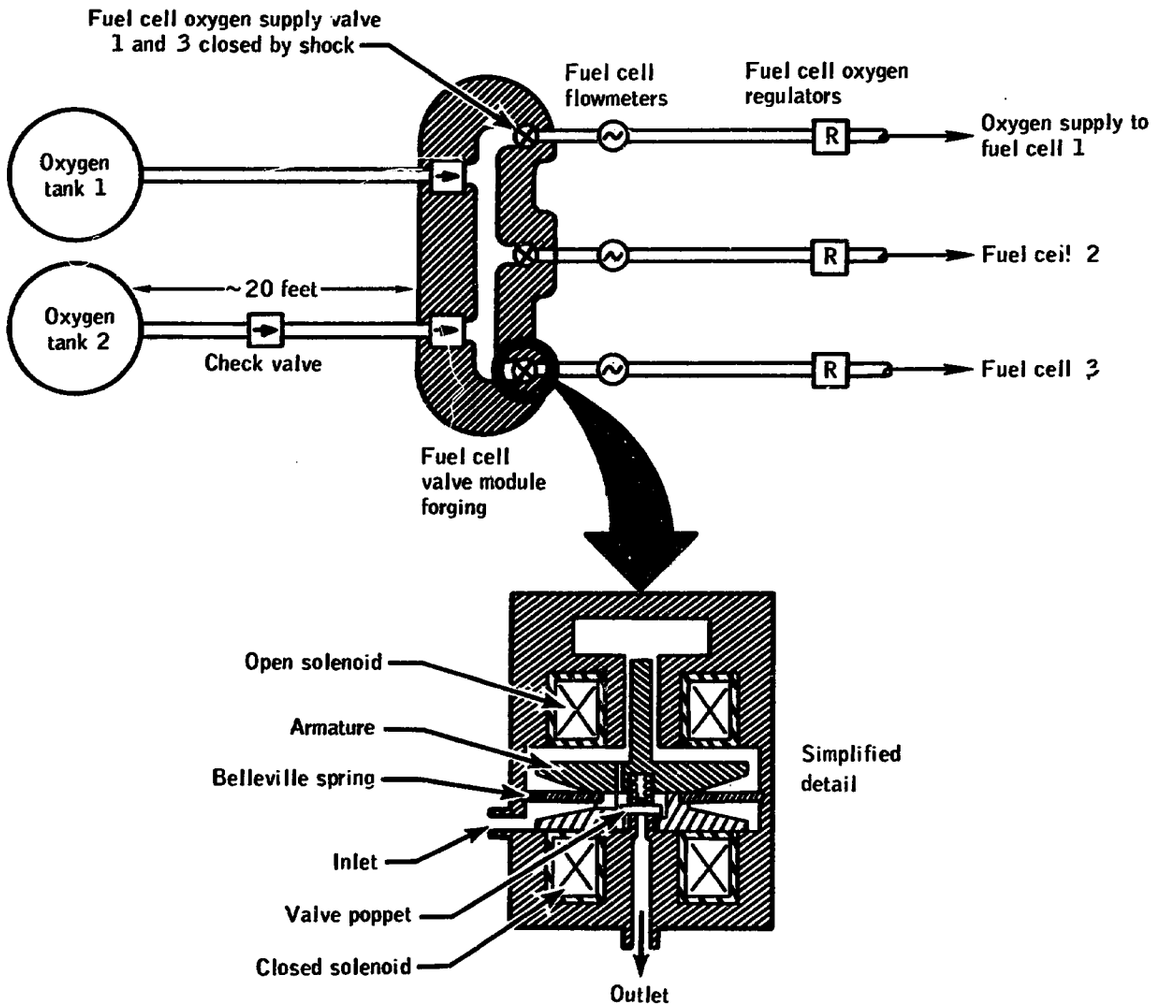

Figure 4-41.- Solenoid valves for oxygen supply.

4.11 FAILURE MECHANISM

A large number of postulated mechanisms were examined, and the scope of the review is reflected in table 4-II. Many of the potential mechanisms were quickly eliminated by comparing the end result, or the reaction rate produced by the mechanism, against the observed flight data. Others were eliminated on the basis of data from the literature or from tests that showed the mechanism to be a second or higher order effect. Of the mechanisms listed in the table as "possible," the one that satisfies the flight data is initiation of combustion in the tank by electrical shorts. The association of fan energization, the electrical shorts at the start of pressure rise, and the availability of sufficient electrical energy in the fan circuit to cause ignition of the polytetrafluoroethylene led to the fan motors and power leads being the most likely point of ignition.

Electrical power for the fans, heaters, and quantity probe system is provided through a 24-pin electrical connector, which is the electrical and mechanical interface with the cryogenic oxygen volume. Seventeen wires and the shielded cable are soldered to the connector, and these wires extend through approximately 32 inches of conduit coiled in the upper cap of the vacuum jacket and enter the pressure vessel through the boss about 5 inches from the temperature sensor. The conduit is made of Inconel X-750 (AMS 5582). Each wire is insulated with color-coded polytetrafluoroethylene insulation about 10 mils thick. Table 4-III lists the materials in the connector and conduit. In addition, the wire bundles for various systems are enclosed in heat-shrinkable type polytetrafluoroethylene sleeving (0.012 inch thick). A total of about 0.1 pound of polytetrafluoroethylene insulation is present in the electrical connector and conduit and when totally combusted would yield about 195 Btu of energy.

The fan wiring leads consist of two harnesses of four wires each for the two 3-phase fan motors. Wires (MIL-W-16878, type E) are 26-gage nickel and are coated with 0.010-inch polytetrafluoroethylene insulation. Also, each harness of four wires is covered in some regions with a polytetrafluoroethylene sleeve of approximately 0.012-inch thickness. Wire runs of the two fan harnesses are as indicated in figure 4-42 and are identical, except that the lower fan harness is routed through a tube in the heater assembly.

The fan motor power leads internal to, and near, the heater assembly are extremely vulnerable to heat damage in abnormal operations. This has been demonstrated dramatically in a test employing approximately 8 hours of continuous heater operation. The insulation degradation caused in a test simulating the detanking cycle used on oxygen tank 2, (discussed in section 5.0) is seen in pictures of the wiring which failed (fig. 4-43).

TABLE 4-II.- INITIATION MECHANISMS

Mechanism	Significant Data	Assessment[a]
Fan Motor Assembly and Leads (Electrical)		
Ohmic heating of field coils (stalled rotor)	Ignition unlikely based on low pressure 1 g test data and low power input (30 watts total per motor).	Unlikely
Continuous shorts (in leads or coil)	Ignition possible based on hot wire ignition test data. Can get 1 to 2 amps through fuse.	Possible
Intermittent shorts (in leads or coil or to housing)	Sufficient energy available from inverter to ignite insulation (North American Rockwell and Manned Spacecraft Center test).	Possible
Fabrication and assembly error	Both motors passed preflight room temperature tests August 1966. Would require degradation and failure after extended period of normal usage. Data included elsewhere in the report.	Unlikely
Fan Motor Assembly and Leads (Mechanical)		
Loss of fan parts at high RPM (impact or friction ignition)	Loss of fan unlikely (self-locking nut and square shaft). Parts considered as contaminants.	Unlikely
Overheated bearing ignites Rulon A retainer	Ignition temperature 463° C at 2000 psi gaseous oxygen. Low energy source (motor torque 0.9 in-oz.) limits energy input into bearing. When bearing seizes, becomes stalled rotor (covered separately).	Unlikely
Rotor or fan blade contacting adjacent structure (friction ignition)	Ignition of aluminum possible. Preflight checkout showed no problem. No cause for occurrence in flight.	Unlikely
Heater and Controls (Electrical)		
Element shorted to sheath	Heater not powered at time of incident. Heater operation normal in both tanks prior to tank incident (cryogenic data).	Unlikely
Leads shorted to ground Intermittent shorts (sparking)	Heaters not powered at time of origin of incident. (Verified by detailed review of current tank pressure data.)	Unlikely

TABLE 4-II.- INITIATION MECHANISMS - Continued

Mechanism	Significant Data	Assessment[a]
Heater and Controls (Electrical) - Continued		
Inadvertent operation of heater	Flight data (current) voltage shows no indication of inadvertent operation. Inadvertent operation would not account for energy release in tank unless combined with chemical reaction.	Unlikely
Oxygen in thermal switch (ignited by spark or impact)	Previous operation normal and switch in closed position at time of event.	Unlikely
Heater and Controls (Mechanical)		
Impact Friction Shock wave	Requires impact or energy source from some other event.	Unlikely
Material yielding Fracture	No failure or loading mechanism in this time period which can be explained by flight data.	Unlikely
Quantity Gage Assembly (Electrical)		
Short between plates, and between plates and ground	Off scale data could confirm short between plates. Maximum power input less than 7.35 millijoules Insufficient data on energy required to ignite insulation. No correlation with flight voltage transients.	Unlikely
RF heating	Insufficient energy input. Analyzed by North American Rockwell to be 350 nanowatts maximum.	Unlikely
Quantity gage plate lead short to heater lead	No power to heater (not on) confirmed by main bus current data. Maximum power input less than 7.35 millijoules from probe. Insufficient data on energy required to ignite.	Unlikely
Temperature transducer short	Flight data indicate normal function after initial pressure rise in tank 2. Maximum energy input is less than 4 microjoules.	Unlikely

TABLE 4-II.- INITIATION MECHANISMS - Continued

Mechanism	Significant Data	Assessment[a]
Quantity Gage Assembly (Mechanical)		
Impact Friction Shock wave	Requires prior event, not associated with gage, for energy source.	Unlikely
Yielding Fracture	No loading mechanism. Consistent with data.	Unlikely
Pressure Vessel (Electrical)		
Ohmic heating to produce overpressure	No sustained high currents, low power. Heater and fan leads could touch vessel. Heater leads not powered.	Unlikely
Spark discharge to pressure vessel	Same as above.	Unlikely
Pressure Vessel (Mechanical)		
Impact	Impact source not identified.	Unlikely
Friction	Friction source not identified.	Unlikely
Fracture	Vessel intact after event initiation.	Unlikely
Yielding	Below yield stress when event initiated.	Unlikely
Shock wave	Shock source not identified.	Unlikely
Vacuum Jacket and Associated Equipment (Electrical)		
Ohmic heating of vacuum jacket or pressure vessel	No internal current sources except vac-ion pump. No continuous high currents, no indication of external arcing possibility.	Unlikely
Vac-ion pump failure resulting in sparking and ignition of material	Requires oxygen leakage from tank to cause difficulty. Vac-ion pump turned off prior to launch.	Unlikely
Vacuum Jacket and Associated Equipment (Mechanical)		
Impact Friction Fracture Yielding	Oxygen required, not available unless leak or failure occurred.	Unlikely
Flow from pressure vessel leak causing ignition of aluminized Mylar	Long exposure of Mylar to liquid oxygen increases its impact sensitivity and degree of reactivity. Impact threshold level decreases and the reactivity progresses from charring to the exposive state. Aluminized Mylar unacceptable in liquid oxygen impact.	Possible

TABLE 4-II.- INITIATION MECHANISMS - Concluded

Mechanism	Significant Data	Assessment[a]
Other Possible Causes		
Foreign material in tank		
a. Lubricant and glass beads	Found on ground support equipment filter after first pad fill.	Possible
b. Rivet or rivet pin	Oversize rivet hole in quantity gage.	
c. Quantity gage button spacers	Flow stoppage during detanking.	
d. Inadvertent substitution of titanium for steel	Identical size and shape parts for oxygen tank and hydrogen tank. Same basic part number, dash number different.	
e. Broken safety wire	Twisted wire on Beech motors and filter.	
Tank electrical connector failure. (Bad connection resulting in spark ignition.)	AC current anomalies could be related. Wire insulation is available fuel.	Possible
Ionization due to cosmic radiation (resulting in spark discharge at quantity probe).	Solar events which occurred during flight were after the event. Very high voltage required for dielectric breakdown of gas.	Unlikely
Gaseous fuels (such as hydrogen) produced by metabolism of microorganisms	Nutrients not available. Metabolic rate near zero at low temperature. Aerobic species are not known which produce oxidizable products.	Unlikely
Triboelectric charging of tank interior causing spark ignition	Tank and shell are at vehicle potential.	Unlikely
External plumbing problems	Liquid oxygen flowing over pressure transducer can cause apparent pressure increase. Temperature flight data and probe behavior cannot be explained. Bay blow-out questionable.	Unlikely

[a]Unlikely: Energy source unlikely to produce observed flight data.
Possible: Energy source possibly could produce flight data-detailed analysis performed.

TABLE 4-III.- MATERIALS IN CONNECTOR AND CONDUIT

Service	Number of wires	Wire size (AWG)	Material
Heater	4	20	Silver plated copper, polytetrafluoroethylene insulated
Quantity probe	1	20	Nickel - polytetrafluoroethylene insulated (outer probe)
	1	20	Nickel - polytetrafluoroethylene insulated (inner probe)
Temperature sensor	4	22	Nickel - polytetrafluoroethylene insulated
Motors	8	26	Nickel - polytetrafluoroethylene insulated
Sleeve			Heat shrinkable polytetrafluoroethylene tubing
Connector			Inconel with gold plated pins
Solder			60 percent tin, 40 percent lead

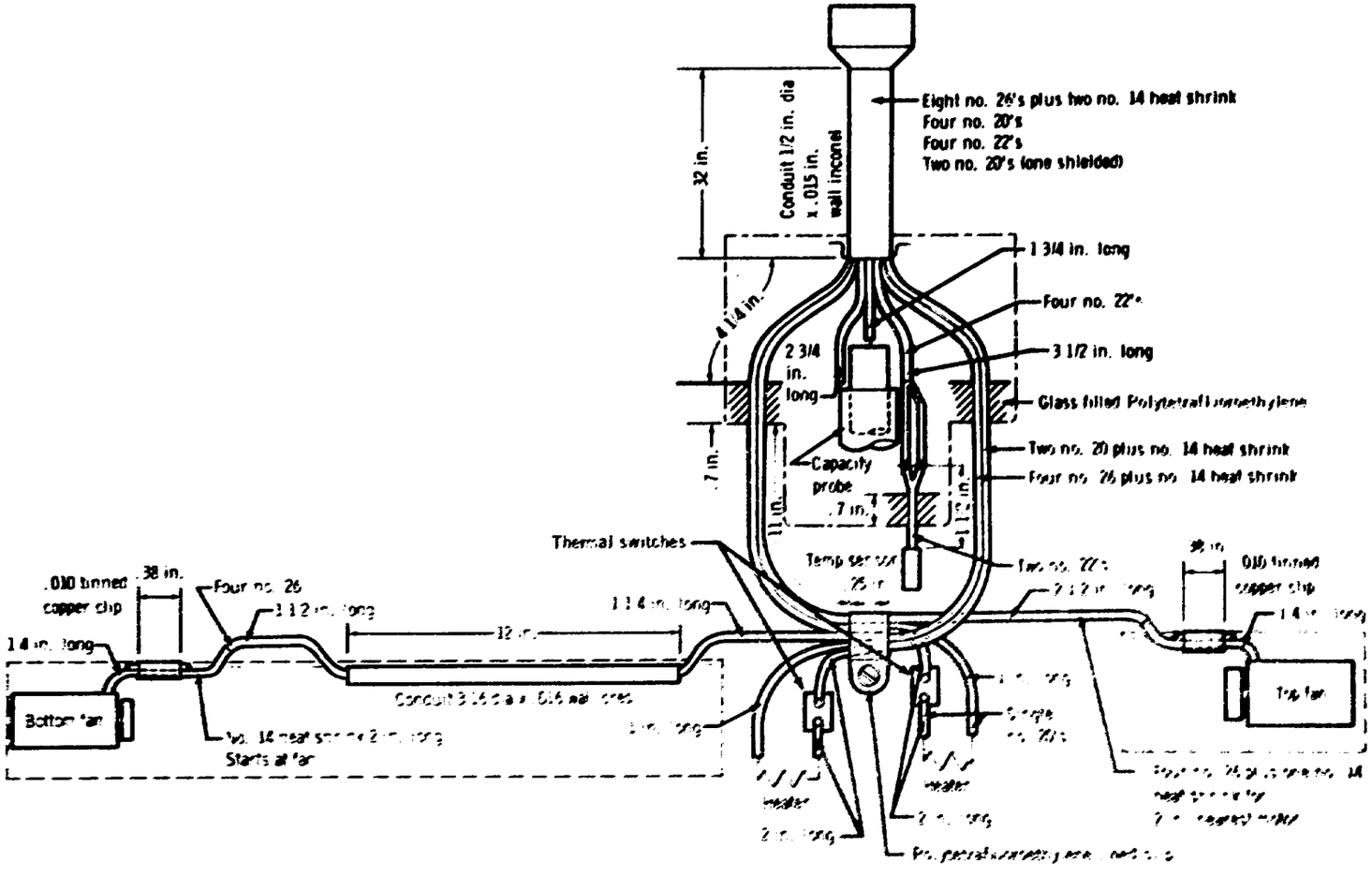

Figure 4-42.- Wiring distribution within cryogenic oxygen tank.

Figure 4-43. - Fan motor wire damage from heater tests.

This test showed that insulation will be severely damaged by the abnormal heater operation so that numerous locations for electrical shorts or arcs are available when the fan circuits are powered.

By this mechanism, an arc ignition could occur in these leads. The maximum electrical energy available in the fan motor wiring during the first short is about 160 joules. Tests confirm that the ignition energies of this material by a spark source is less than 1 joule. The rate of propagation has been shown by test to be greatly affected by flow and gravitational conditions in the tank (zero-g rate is less than one-g rate). As a result, it is difficult to assess actual propagation at the time of the failure. The 14-second plateau in the pressure-time flight data could be due to partial blocking or slowing of the flame front as the flame propagates to a grommet and must penetrate a thicker, better thermally-sinked component. Other barriers to propagation are also possible.

The total energy available from complete combustion of the wire insulation was determined by estimating the weight of the wire insulation and sleeve material and using literature data on the heat of combustion of polytetrafluoroethylene (2100 to 2200 Btu/lb). These estimates are summarized in table 4-IV. Combustion of wire insulation will furnish sufficient thermal energy for the process requiring minimum energy for the tank pressure increase as described in section 4.3.

Tests have shown flame propagation into the conduit region will cause rapid degradation and failure of pressure integrity. It is also significant that this is the only region where the wire insulation comes in close proximity to the pressure shell. A test has shown that ignition of the wire insulation at the electrical connector end resulted in very rapid failure of the conduit with little pressure or temperature response back in the simulated pressure vessel. A test with ignition outside the conduit and propagation along wire insulation into the conduit caused very rapid failure of the conduit. Additionally, a "torch" effect enlarged the opening as a result of melting or burning of the metal in the conduit tank interior region. This latter effect could explain the rapid loss of pressure from tank 2 as well as other higher order effects.

TABLE 4-IV.- HEAT AVAILABLE FROM WIRE INSULATION

Location	Heat available from wire insulation (Btu)
Zone 1*	195
Zone 2**	38.6
Zone 3***	34.4

*Zone 1 - Wire insulation in conduit from connector to tank-conduit interface.

**Zone 2 - Wire insulation from tank-conduit interface to lowest portion of upper polytetrafluoroethylene - 25 percent glass probe insulator.

***Zone 3 - All other wire insulation.

PRECEDING PAGE BLANK NOT FILMED

5.0 PREFLIGHT CONTRIBUTING EFFECTS

A comprehensive review of the history of cryogenic oxygen tank 2 was made to determine whether an unfavorable condition could have existed prior to launch. This review included test records, materials review dispositions, and failure reports. No positive indication of any unfavorable conditions prior to shipment could be found in the testing or inspections conducted. However, an abnormal condition was found in the prelaunch detanking procedure which is discussed in 5.1.

In addition to the review discussed, a special review and demonstration of the assembly methods used to install the wiring, fans, heater assembly, and quantity probe was made by the vendor for this investigation. The installation procedures for the heater, fan, and probe wiring were found to be critical for several areas where routing damage would not be visible on the assembled product. However, this condition most likely did not contribute to the ultimate loss of the tank pressure in flight.

A detailed assessment was also made of the incident where the oxygen shelf hoist assembly failed during the factory removal of the tank shelf from the Apollo 10 spacecraft (fig. 5-1). Analysis and test show that the maximum shock upward would be about 7 g's, and the maximum shock downward would be about 15 g's. Analytically, the components within the tank would be expected to withstand 100 g's shock. Consequently, this condition is not believed to have contributed to the ultimate failure of the tank in flight.

The condition which most probably led to the failure, occurred during the special detanking procedures used after the countdown demonstration test.

The cryogenic oxygen tank 2 could not be off loaded after the initial filling during the countdown demonstration test using the normal procedures. The problem resulted from loose or misaligned plumbing components in the dog-leg portion of the tank fill path (fig. 5-2). Allowable manufacturing tolerances are such that the tank may not be detanked normally under these conditions. A test has verified this fact. The condition of loose plumbing in the probe assembly, which existed in the tank before the detanking, was judged to be safe for flight in every aspect.

After numerous attempts with gaseous oxygen purges and higher expulsion pressures in an attempt to remove the fluid, the fluid was boiled off through the use of tank heaters and fans, assisted by pressure cycling. The sequence of detanking is shown in figures 5-3 and 5-4. The heater-on time was about 8 hours. It was thought that no damage would be sustained by the tank or its components because of the protection afforded by the internal thermal switches.

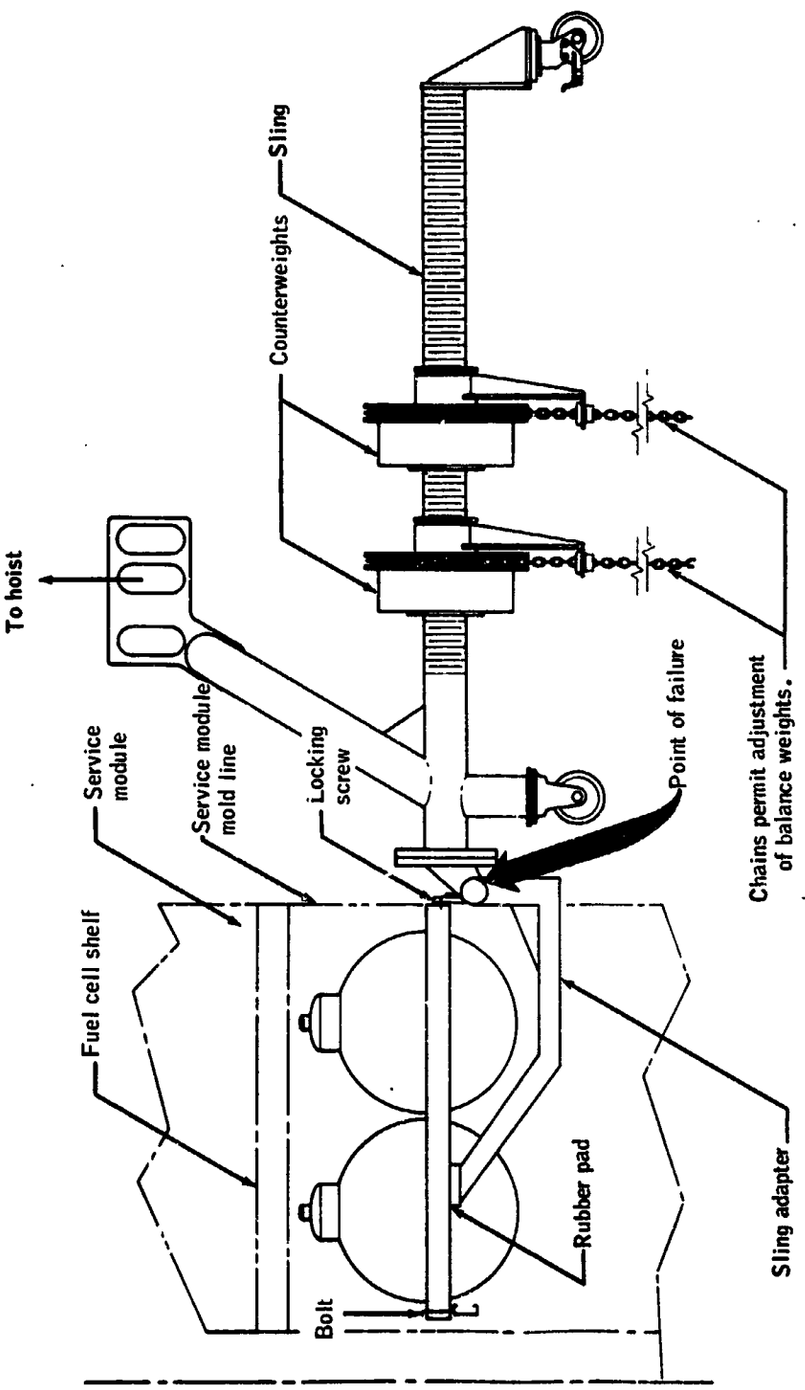

Figure 5-1.- Oxygen shelf and hoist assembly.

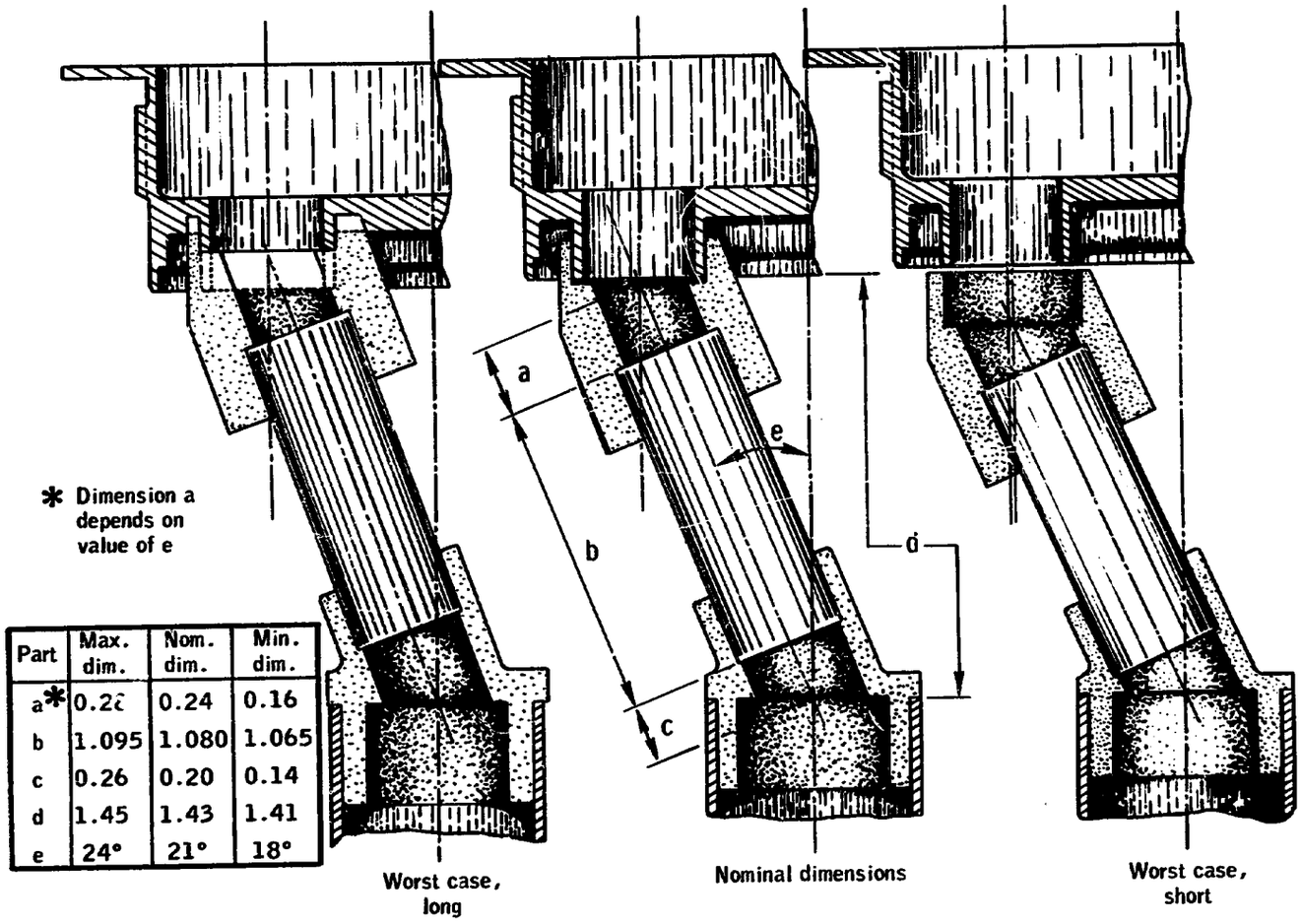

Part	Max. dim.	Nom. dim.	Min. dim.
a*	0.28	0.24	0.16
b	1.095	1.080	1.065
c	0.26	0.20	0.14
d	1.45	1.43	1.41
e	24°	21°	18°

Figure 5-2.- Manufacturing tolerance study.

The thermal switches, which normally open at about 80° F, show no sign of operation from the heater voltage data. Inflight, these switches have not operated due to the temperatures in the tank. Further, the switches in the past have not operated under a load on the ground, and they were not designed or tested for this condition.

In the case of Apollo 13, the use of the heaters to assist in detanking required the switches to open under load. This is the first time the switches were operated with 65 V dc and 6 amperes which is twice the normal flight operating conditions for each heater. Tests show that opening the switches under these ground power conditions will fuse the contacts closed at the instant of power interruption (fig. 5-5). Tests have verified that when the heaters are on for the duration experieced during prelaunch operations (approximately 8 hours), the fan motor wire insulation is severely degraded (fig. 4-43).

Wiring can be damaged within a couple of hours, with the heaters being "on" continuously as evidenced by the temperature on the heater assembly (figs. 5-6 and 5-7).

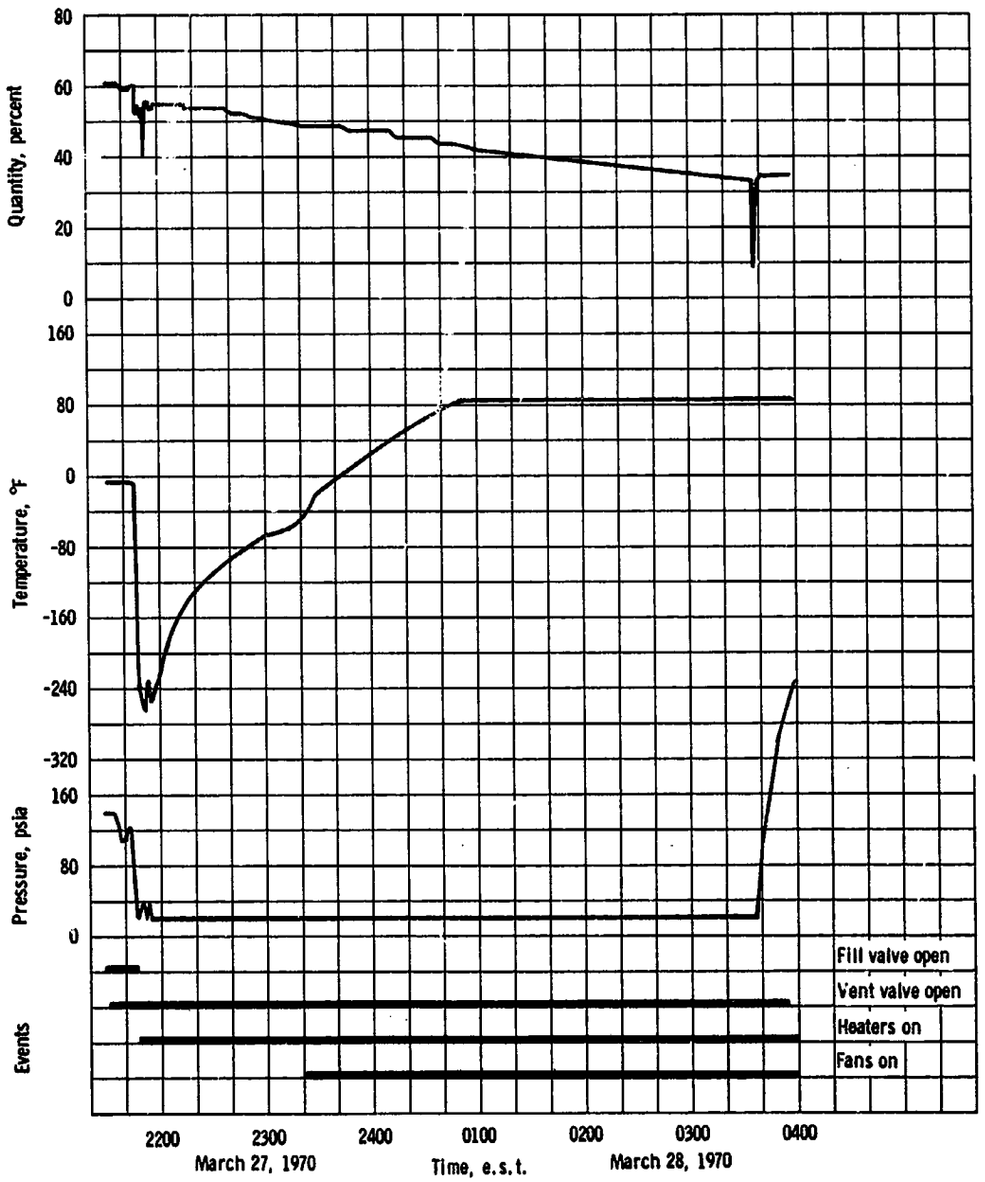

Figure 5-3. - Characteristics of oxygen tank 2 detanking using fans and heaters (CDDT).

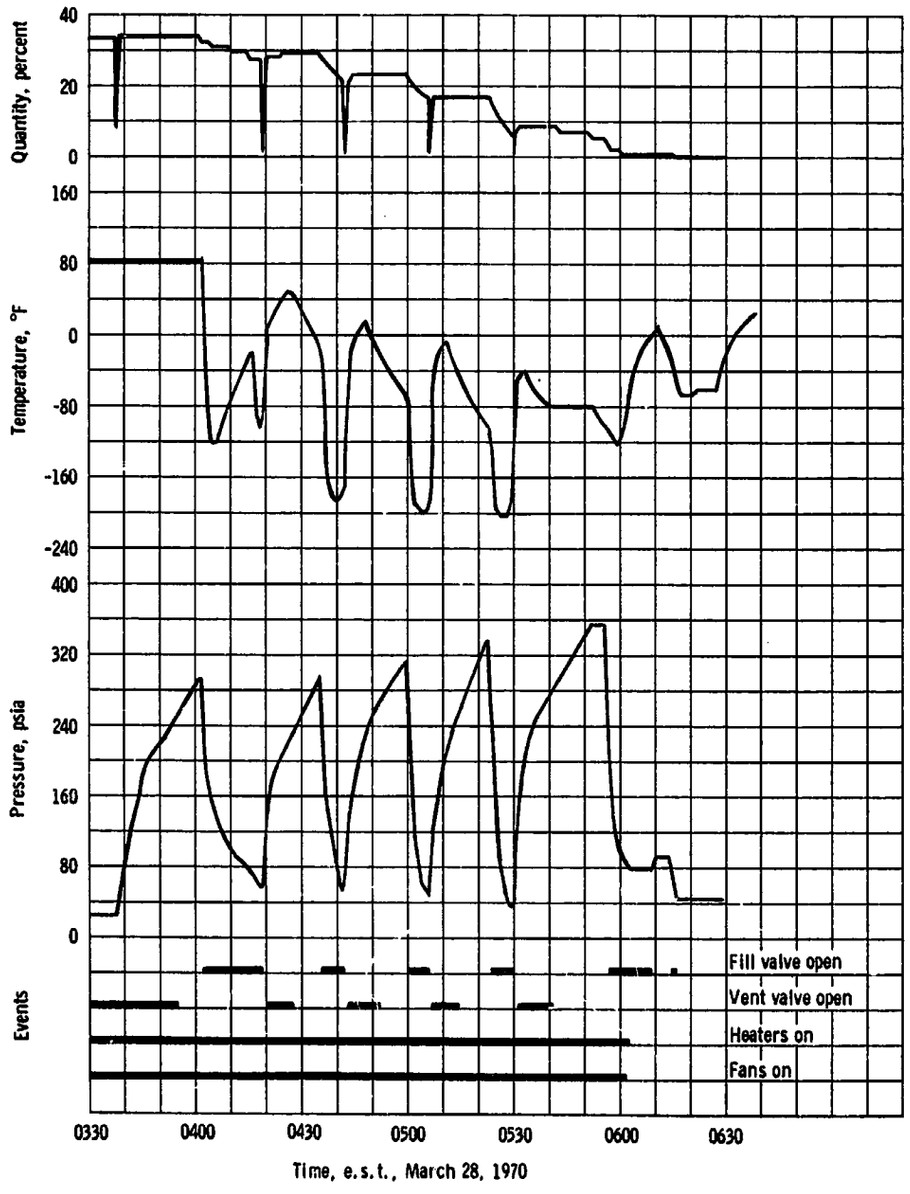

Figure 5-4. - Characteristics of oxygen tank 2 detanking using fans, heaters, and GSE pressure (CDDT).

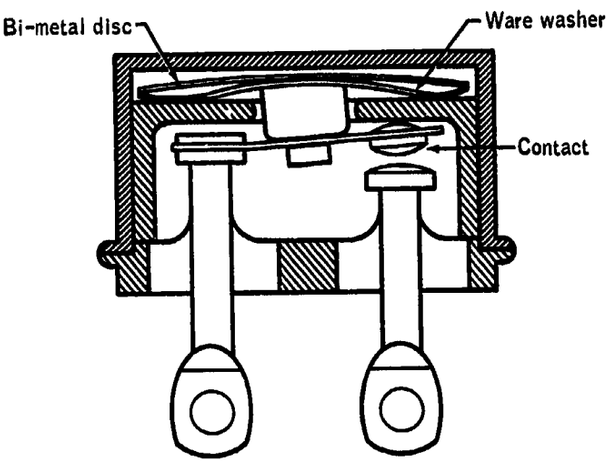

(a) Switch cross section.

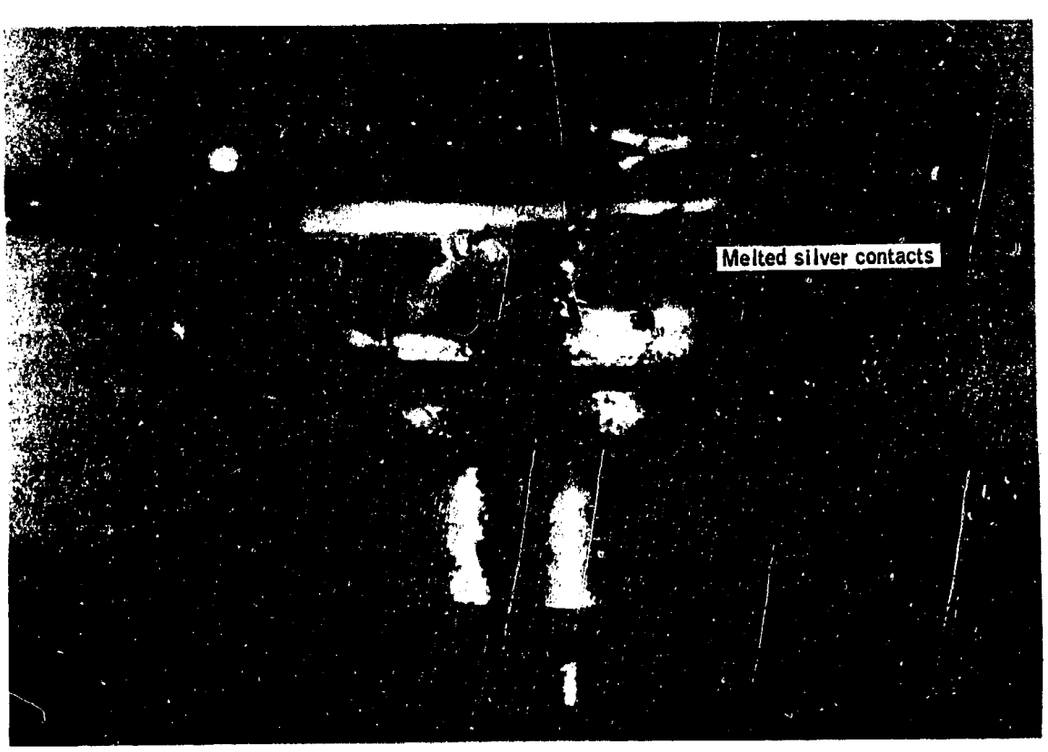

(b) Welded contacts after test.

Figure 5-5.- Master thermal switch.

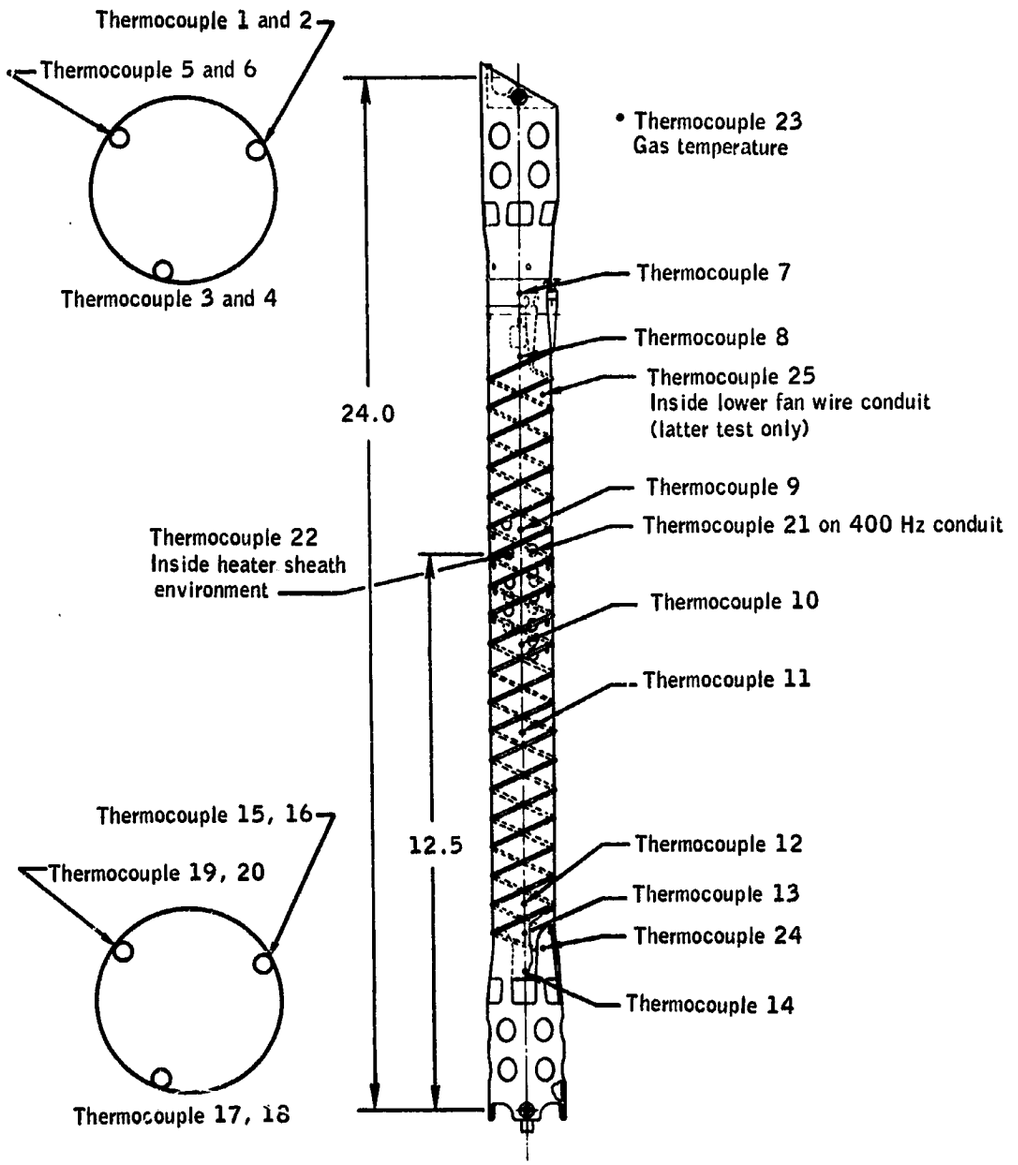

Figure 5-6.- Heater/fan temperature sensor locations

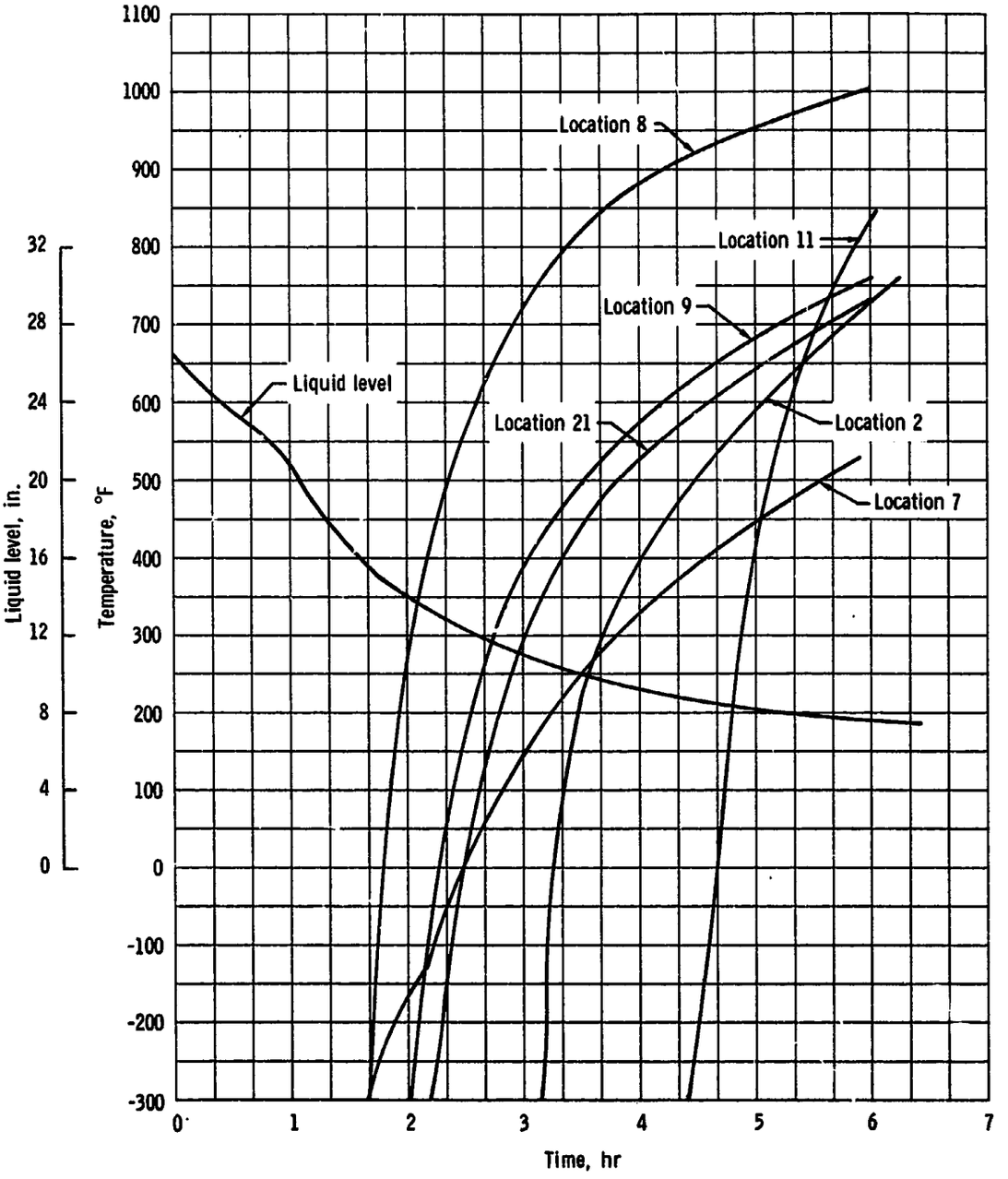

Figure 5-7. - Heater/fan typical test results.

6.0 CONCLUSIONS

The analysis of the data and results of special tests associated with the incident leads to the following conclusions.

1. The detanking problem which occurred during the countdown demonstration test resulted from loose or misaligned fill-line plumbing components within the tank. This condition was not the direct cause of the anomaly, but did result in the use of a special detanking procedure following the countdown demonstration test.

2. Both heater thermal switches failed closed from heater operation during the special detanking. The failed switches allowed continuous heater power to be applied, and led to severe damage of the insulation on the power wires leading to a fan motor.

3. The failure of the thermal switches was caused by an incompatibility between the capacity of the switches and the voltage used from the ground power supply.

4. A fire was started by electrical short-circuits in the wiring to the fan motors inside oxygen tank 2 shortly after the fan circuits were energized for the seventh time.

5. Burning of the insulation proceeded for about 80 seconds before reaching the pressure vessel electrical conduit; through which all electrical tank wiring passes. The heat of the burning caused failure of the Inconel conduit first, and ultimately led to the failure of the vacuum dome and separation of the bay 4 structural panel.

6. The internal component design of the tank lends itself to possible damage which can go undetected. Further, the plumbing parts have tolerance allowables which can build up to prevent normal detanking.

7. The design of the warning system for indicating the position of the reactant valves to the fuel cells does not allow detection of individual valve closures to any fuel cell, a condition which existed during this incident.